EVALUATION OF AN ELECTRONIC PRESSURE SENSOR FOR TIBIO-FEMORAL CONTACT PRESSURE MEASUREMENT

by

Brandon Dale Marshall

Bachelor of Science in Mechanical Engineering, Clemson University, 2010

Submitted to the Graduate Faculty of

Swanson School of Engineering in partial fulfillment

of the requirements for the degree of

Master of Science in Mechanical Engineering

University of Pittsburgh

2014

UNIVERSITY OF PITTSBURGH

SWANSON SCHOOL OF ENGINEERING

This thesis was presented

by

Brandon Dale Marshall

It was defended on

November 12, 2014

and approved by

Patrick J. Smolinski, Ph.D., Associate Professor,

Department of Mechanical Engineering and Materials Science

William S. Slaughter, Ph.D., Associate Professor,

Department of Mechanical Engineering and Materials Science

Mark C. Miller, Ph.D., Associate Research Professor,

Department of Mechanical Engineering and Materials Science

Thesis Advisor: Patrick J. Smolinski, Ph.D., Associate Professor,

Department of Mechanical Engineering and Material Science

EVALUATION OF AN ELECTRONIC PRESSURE SENSOR FOR TIBIO-FEMORAL CONTACT PRESSURE MEASUREMENT

Brandon Dale Marshall, M.S.

University of Pittsburgh, 2014

The purpose of this study was to evaluate K-Scan electronic pressure sensor model K-4000 (K-Scan; Tekscan, Inc., Boston, MA, USA) for use in the human knee joint to assess the effect that anatomic double-bundle ACL reconstruction has on tibio-femoral contact pressure. The sensor was used to measure static pressure when 1000N of axial loading was applied to the knee joint using a materials testing machine. This study also considered the calibration of the sensor. Three methods of calibration were investigated: pressurized bladder, materials testing machine, and polyurethane rollers. Calibration data from the materials testing machine was used in this study because it was the only method able to calibrate the sensor for the widest pressure range.

Twelve fresh, frozen cadaveric human knees were used for this study. Double-bundle ACL reconstruction was performed arthroscopically using hamstring grafts. Three different graft fixation tensions were used: i) AM/PL: 30N/10N, ii) AM/PL: 10N/30N, iii) AM/PL: 40N/40N. Each knee was tested with 1000N of axial loading 0, 15, 30, and 45 degrees of flexion at the intact state and each of the reconstructions, and pressure readings were taken with the sensor for each test. The results of this study found that double-bundle ACL reconstruction did not

significantly change the peak contact pressure, location of peak pressure, and location of center of pressure of the intact knee during 1000N of axial loading. This study also found that there was no significant change in peak contact pressure, location of peak pressure, and location of center of pressure during ACL graft fixation (without loading).

TABLE OF CONTENTS

LIST OF TABLES

LIST OF FIGURES

PREFACE

I would like to thank my thesis advisor, Dr. Patrick Smolinski, for the time and guidance he has given me throughout this study and write-up. I would also like to thank Junjun Zhu and Monica Linde-Rosen for their help with this study. Lastly, I would like to thank Dr. James Chang, who was the orthopedic surgeon and scholar that performed the ACL reconstructions in this study.

1.0 INTRODUCTION

Measuring contact area and pressure between two surfaces in the human body is an ongoing research area in the field of biomechanics. Some applications include the contact between a material surface and human skin, the contact between two articulating joints, orthopedic implant evaluation, and between teeth. Contact pressure between two surfaces can typically be measured using two methods: pressure sensitive film and piezoelectric pressure sensors. Pressure sensitive film has been used since the 1970's and 1980's to measure joint contact area and pressure. However, the development of computers in the 1990's has led to the creation of piezoelectric pressure sensors that can be used to measure contact area, force, and pressure between two adjacent surfaces that are in contact.

The first commercial piezoelectric pressure measurement system was marketed by Tekscan, which developed the I-Scan pressure mapping system (I-Scan; Tekscan, Inc., Boston, MA, USA). This pressure mapping system can be used to measure the contact area and pressure between two surfaces, and consist of a USB handle, data acquisition and analysis software, and electronic pressure sensors. While the manufacturer has developed many types of electronic pressure sensors that are compatible with their pressure mapping system, each designed for a specific purpose, the K-Scan sensors (K-Scan; Tekscan, Inc., Boston, MA, USA) are a range of sensors that have been designed for human joint analysis. These sensors have been designed to

be placed between articular cartilage in human joints in order to measure contact pressure and area.

1.1 OBJECTIVES

The purpose of this study was to evaluate K-Scan electronic pressure sensor model K-4000 (K-Scan; Tekscan, Inc., Boston, MA, USA) for use in the human knee joint to assess the effect that anatomic double-bundle ACL reconstruction has on the tibio-femoral contact pressure. The outcome will provide insight into the calibration and use the sensor to measure tibio-femoral contact pressure under static axial loading.

2.0 BACKGROUND

2.1 PRESSURE SENSORS

Pressure sensors come in a range of shapes, sizes, pressure ranges, and spatial resolutions, where these specifications are given according to the sensor model. These measure the interface pressure between two surfaces. The row-column intersection of the sensor form sensing elements, or cells. The software displays the pressure of each cell in real-time, that when viewed together forms a pressure profile of the surfaces that are in contact.

2.1.1 Sensor

The K-4000 (K-Scan; Tekscan, Inc., Boston, MA, USA) sensor has been used to collect the data that will be presented in this study. Figure 1 shows a diagram of the sensor, which is 0.1 mm thick, flexible, and has two independent pressure sensing regions [32].

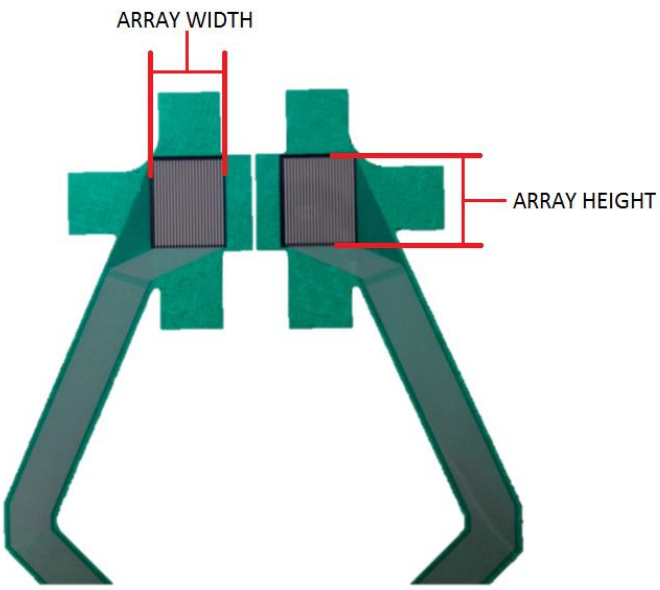

Figure 1. K-4000 (K-Scan; Tekscan, Inc., Boston, MA, USA) pressure sensor

The sensor has two independent sensing regions, also called arrays, which are identical. The array height is 33.0 mm, and the array width is 27.9 mm. There are 22 columns and 26 rows in each array, giving a total of 572 cells in each array and 1044 cells in the entire sensor. The width of each of the array columns is 0.8 mm, and the width of each of the array rows is 1.3 mm [32]. The sensors are made up of two flexible polyester sheets, and have electrically conductive material printed on the inside of the sheets. The conductive material on the inside surface of one of the polyester sheets forms columns, while the other forms rows. A piezoresistive ink is printed over the columns and rows, and an array is formed when the two sheets are laminated together. The intersection of columns and rows forms a sensing element, or a cell. Since the cell only consists of the column-row intersection, not the entire array area is active [33]. The sensor cannot detect the pressure applied to the empty regions that surround the active intersections.

There are two properties that describe the spatial resolution of the sensors: cell spacing and cell density. The spacing of each of the array columns, which refers to the spacing between

the center of one cells column and its neighbor, is 1.3 mm, and the spacing of each of the array rows, which refers to the spacing between the center of one cells row and its neighbor, is 1.3 mm [32]. The smaller the spacing, the more cells will be located in the sensor and the higher the spatial resolution of the sensor will be. The sensor's cell density is 62.0 cells per cm^2 [32]. Higher spatial resolution will allow the sensor to detect smaller changes in contact pressure, more accurately determine contact locations, and more defined pressure profiles.

2.1.2 Sensor Specifications

The manufacturer inspects 100% of the pressure sensors that they manufacture to make sure that the meet the company's established specifications [35]. The published specifications on their pressure sensors are valid for all of their electronic sensors, and are given below.

2.1.2.1 Accuracy and Repeatability

Repeatability is the measure of the sensor to produce the same output when pressure applied to the sensors under the same conditions. Accuracy is the measure of the sensor to produce the output that is close to the true value of the pressure which is applied to the sensors. The sensors have a repeatability of ± 3.5% and an accuracy of ± 10% [35].

2.1.2.2 Linearity

The pressure mapping system uses an 8-bit analog to digital converter that has an output range of 0 - 255 to linearize the output into digital output. The sensors have a linearity of ± 3% [35].

2.1.2.3 Hysteresis

Electronic pressure sensors, as most other measurement devices, can experience the effects of hysteresis. Hysteresis occurs when there is a difference in the sensors output during loading and unloading. The effects of hysteresis are minimal for applications that experience small changes in pressure, and when pressure is either only increased or decreased. Applications that have pressure both increasing and decreasing many be subject to error introduced by hysteresis.

2.1.2.4 Drift

Drift is the change in a measurement devices output when a constant pressure is applied to it over time. Drift needs to be taken into account during the calibration of the sensor. This can be achieved by calibrating the sensor in a similar time frame that the sensor would be expected to be used for. The sensors drift is given as 5% per log time [35].

2.1.2.5 Temperature Sensitivity

The output of the sensor will vary when the sensor is subject to different temperatures. The operating temperature of the sensors is -40°C to 60°C [35].

2.1.2.6 Lag Time

The lag time of the sensor is the time that elapses between when pressure is applied to the sensor and when the corresponding signal is read by the system. The lag time of the sensors is 5µsec [35].

2.1.3 Data Acquisition Hardware

Figure 2 the pressure mapping system, which consists of the USB handle, data acquisition and analysis software, and sensors. The USB handle is connected to a computer with a Window's operating system (Windows; Microsoft Corporation, Redmond, WA, USA) compatible.

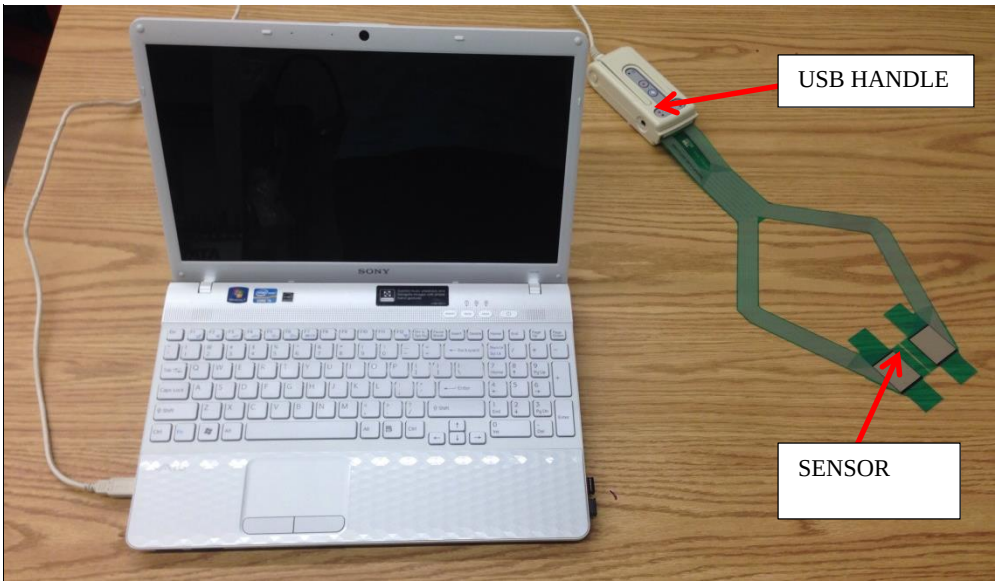

Figure 2. Pressure mapping system

2.1.4 Pressure Range

The pressure mapping system uses an 8-bit analog to digital converter that has an output range of 0 - 255. Thus, a calibration is needed to convert the digital output, or raw output, of each cell into pressure. Once the raw output reaches 255, the sensor becomes saturated so that increasing the applied pressure will no longer produce an increase in raw output. The manufacturer

publishes their sensors standard pressure ranges along with their specifications. The upper value of their sensors pressure range is 80% of the maximum pressure that the sensor can measure, and the lower value is 1.2% of the maximum pressure that the sensor can measure and is also the minimum pressure that the sensor can be used at. The resolution of the sensor is the smallest change in pressure that the sensor can detect, and is given as 0.4% of the upper value of the pressure range [33].

In order to produce raw output, the circuitry in the USB handle measures the change in resistance of each cell when a pressure is applied to the sensor by limiting current flow to one particular cell at a time. The resistance of a cell is highest when no pressure is applied to it, and the resistance of each cell in the array is the same when no pressure is applied to the array [34]. The USB handle can adjust the resistance of each cell of the array when no pressure is applied to it, which means that the effective pressure range of the sensor can be changed. The sensor has 8 pressure ranges, and each corresponds to a pressure sensitivity setting. A unique calibration is needed for each of the sensitivity settings because the resistance of each setting will be different. The pressure sensitivity settings available in the software for the sensor are (listed in order of increasing pressure range): High2, High1, Mid2, Mid1, Default, Low3, Low2, Low1, and Low.

The standard pressure ranges that are listed are intended to give an indication of the types of applications the sensor model can be used for, and are established using a specific sensitivity settings. The sensor's standard pressure ranges are listed as: i) 0.155MPa to 10.343MPa with a resolution of 0.0517MPa, ii) 0.931MPa to 62.055MPa with a resolution of 0.310MPa, iii) 1.034MPa to 68.950MPa with a resolution of 0.345MPa [32]. However, the sensitivity settings that these pressures correspond to are not listed and represent three of the nine available sensitivity settings.

2.1.5 Sensor Output

Since the intersection of rows and columns in the array form an active sensing area, or cell, the entire sensor is not active, as shown in Figure 3. In order for the sensor to have output over its entire area, the output of the active area of the sensor is extrapolated by the software to the inactive regions that surround it. The cells output will be extrapolated halfway into the empty space between itself and its neighboring cell on each side, unless it is at the end of the array where there are no neighboring cells. Therefore, the cells output effectively encompass the active region, and some of the inactive region. However, extrapolating the output from the active areas to the inactive areas can cause error in the computation of contact area and pressure. The magnitude of this error is related to the sensors spatial resolution. Figure 3 shows the output of sensor using the software where the output of the sensor covers the sensors entire area.

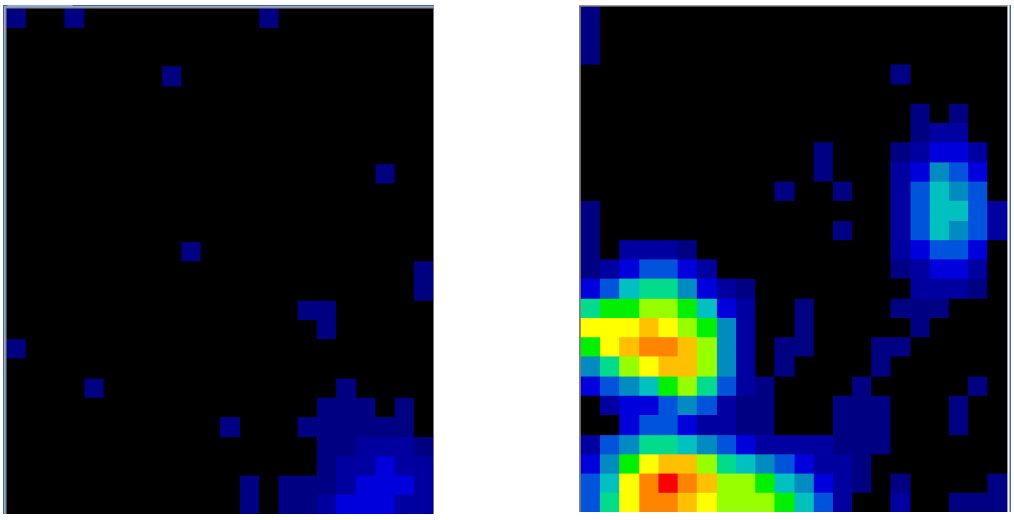

Left pressure sensing region **Right pressure sensing region**

Figure 3. Sensor output in the software

The raw output of the sensor, once calibrated, can be used to calculate the pressure applied to each cell in the sensor. The pressure across each cell can be converted to force, which is directed through the center of the cell. Since the output from the active region is extrapolated to the inactive region, pressure calculations are based on the effective region of each cell, and conversion from pressure to force would be based on the total effective area (area of the active and inactive region). The contact area can be calculated by the total number of cells that have non-zero output. From the calculation of total force and average pressure for each cell, the total force passing through each side of the sensor and the average pressure acting on the active cells of each side of the sensor can be calculated. The peak force and peak pressure on each side of the sensor can also be calculated.

2.1.6 Contact Surfaces

Shear stress can confound the sensor's output and reduce the life of the sensor. Since the sensor is made of a thin and flexible material, shim stock can be placed over the sensor for protection in applications where shear force is present. The shim stock will minimize the effects of shear stress on the sensor, which will give more repeatable output and protect the sensor from wear [35]. However, placing shim stock over the sensor can alter the contact mechanics of the surfaces, and may not be appropriate for all applications.

2.1.6.1 Contact Surface Curvature

The curvature of the contact surfaces where the sensor is used will affect the way that the sensor measures the pressure applied to its sensing area. While the sensors can be placed around objects with large radii of curvature in relation to the size of the sensor because the sensors are

thin and flexible, objects with small radii of curvature could introduce the effects of bending to the sensor by causing the sensor to bend upward, or downward, thus creating shear stress [35].

2.1.7 Software Settings

The software has many settings that allow the user to capture pressure readings for a wide range of applications. The software can be used to capture both static and dynamic pressure readings. Static pressure readings are taken when only the spatial distribution of pressure is sought, and dynamic readings are taken when a time history of the pressure is sought. Static pressure will be the focus of this study; therefore, the details of the dynamic case will not be discussed in full detail.

2.1.7.1 Averaging Function

The software has an averaging capability where each cells raw output is modified to reflect the value of the neighboring cell's output. Figure 4 shows a group of nine cells, where raw output of cell X1 will be modified to reflect the value of its neighbors. The benefit of using an averaging function is that it creates smoother output that is less susceptible to spikes in individual cells, which could be the result of damaged cells [35]. This is convenient for many applications where the output would not be expected to spike dramatically across the sensor.

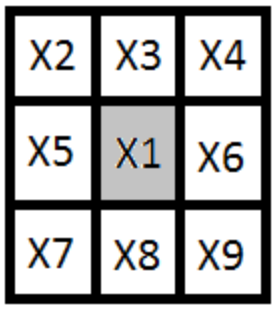

Figure 4. The averaging function of cell output

There are two averaging functions in the software. The first averaging function modifies the raw output of cell X1, as shown in Figure 4, to reflect the value of its neighbors, even if cell X1 has a value of zero. Therefore, this averaging function can result in an increase in total contact area, and is given by Equation 2.1 [35].

$$X_{avg} = \frac{\frac{X2+X4+X7+X9}{2}+X3+X5+X6+X8+X1}{7} \tag{2.1}$$

The second averaging function also modifies the raw output of cell X1, shown in Figure 4, to reflect the value of its neighbors. However, it does not include the neighboring cells that have zero output. Therefore, this averaging function does not result in an increase in the total contact area, and is given by Equation 2.2 [35].

$$X_{avg} = \frac{\frac{X2+X4+X7+X9}{2}+X3+X5+X6+X8+X1+X1}{8} \tag{2.2}$$

The averaging function that does not result in an increase in contact area, given in Equation 2.2, was used in this study. This averaging function was selected because it does not

result in an increase in contact area. If an averaging function will be used for a given application, then the same averaging function also needs to be used during the calibration process since it affects the way that the sensor calculates the pressure that is applied to each cell. The software will repeat the above mentioned process whenever one of the averaging functions is selected for each cell in the sensor, unless the cell is located on the border of the sensor.

2.1.8 Sensor Selection

The sensors come in a range of shapes, sizes, pressure ranges, and spatial resolutions, where these specifications are specified by the sensor model. In order to select the correct sensor for the application from the manufacturers sensor catalog, the user will have to have an estimate of the size of the sensor that will be needed, the peak pressure range that will be expected, and the spatial resolution that will be required for the pressure profile. The sensor needs to be selected according to the expected peak pressure, and not the average pressure or total pressure, which will be applied to the sensor. The sensor used for this study was selected because it was designed to be used in the human knee joint, where it has two separate sensing regions, or arrays, that can be placed under each condyle in the knee. The expected tibio-femoral peak pressure of a knee with an intact ACL has been found to be around 4-6 MPa in previous studies [26,1].

2.1.9 Calibration

Calibration needs to be performed so that the raw output of each cell can be converted into pressure. The calibration process involves applying known pressures to the sensor's array so that the relation between the raw output of each cell and the pressure applied to the sensor array can

be determined. Since the sensor is composed of many different cells, a relation between the output of each cell and the pressure applied to the cell need to be determined.

2.1.10 Software Calibration Function

The sensor's software has built in functions that allow the recording of calibration data which can be applied to the raw output of a recording in real time, or once the recording has been taken and saved. The software has a two point linear calibration function and a two point power law calibration function for use with static pressure. For both calibration functions, the pressure readings should be taken near the beginning and near the end of the pressure range that will be tested [35]. However, Brimacombe et. al found that the software's power law calibration function is more accurate than the linear law calibration function [7]. The software also has a dynamic calibration for use with dynamic pressures; however the dynamic case will not be the focus of this study.

2.1.10.1 Equilibration Function

A typical electronic pressure sensor may be composed of over a thousand cells. The sensor used in this study has 572 cells on each of the two active sensing areas, giving a total of 1144 cells in the sensor [32]. The individual response of each of the cells can vary slightly as a result of the manufacturing process. Damage and wear to the cells of the sensors matrix can also cause the individual response of each cell to vary [35]. The uniformity of the sensors response can be measured by applying a known uniform pressure to the sensor. The software has an "equilibration" function that can be used to compensate for variations in cell response at a

particular uniform pressure. The equilibration function can equilibrate the sensor at up to ten points over the pressure range over which the sensor is calibrated [35].

2.1.10.2 Tare Function

The software has a tare feature that is part of the calibration function, which modifies the calibrated output to correct for residual pressure which is often referred to as the "offset pressure" that is initially present on the sensors matrix [35]. The tare function is not applied to the raw output but instead during the software's calibration. The limitation of the tare function is that it can only be used if the user opts to use the software's calibration. The function can also be used to subtract out the effects of hardware that is used to fix the sensor in place [35].

2.1.11 User-defined Calibration

While the software has a built in calibration function, the sensor can also be calibrated outside of the software because the output of the sensor can be exported as an array in an ASCII file which can be imported into a programing environment, such as Matlab (Matlab; MathWorks, Natick, MA, USA), for analysis. However, most studies have used the built in calibration in the software [7]. Calibrating the sensor outside of the software offers the user greater control over the calibration. For example, if the user wanted to perform a linear calibration, the user would be able to create more than a two point calibration. Being able to incorporate more than two points into the calibration will also allow the user to verify if the output of the system behaves according to the type of equation that they will use for the calibration, for example linear, power, etc., over the entire range of pressure that the sensor is calibrated over. Brimacombe et. al have shown that greater accuracy in calibration can be achieved by using user-defined calibration

versus using the software's two point calibration [7]. Papaioannou et. al has shown that when using a user-defined calibration for each individual cell of the sensor, the output of each cell as a function of the applied pressure can be fitted with a power trend line [29].

The manufacturer recommends that the sensors be exercised, or conditioned, before each use and/or calibration by loading them three to five times. Furthermore, they recommend that the sensors are loaded at a load that would produce a pressure of about 20% greater on each cell than would be expected during the actual application, and that the material used during the conditioning is of a similar stiffness to the material that will be used for loading. Conditioning helps to reduce the effects of drift and hysteresis, and is necessary to be done before the first time that a sensor is used [35].

2.2 JOINT CONTACT PRESSURE MEASUREMENT

The ability of the electronic pressure sensors to measure dynamic pressure is a significant improvement over the long established method of measuring joint contact pressure and area, which is the Fuji Prescale Film Pressure Measuring System (Fuji Photo Film Co. Ltd., Tokyo, Japan). This is a pressure indicating film which was first applied to biomechanics in 1980 by Fukubayashi and Kurosawa to measure contact area and pressure, and produce contact distribution patterns in the knee for static loads [17]. The film is composed of pressure sensitive ink bubbles and indicates applied pressure by red color density. The red color density can be compared to the color density of known pressures which allows the pressure that was applied to the film to be calculated.

The development of computers in the 1990's has led to the creation of piezoelectric pressure sensors that can be used to measure contact area, force, and pressure between two adjacent surfaces that are in contact. The first commercial piezoelectric pressure measurement system was marketed by Tekscan, which developed the I-Scan pressure mapping system (I-Scan; Tekscan, Inc., Boston, MA, USA). These electronic pressure sensors have been used to measure contact pressure in a wide-range of bioengineering applications. Some applications include the contact between a material surface and human skin, the contact between two articulating joints, orthopedic implant evaluation, and between teeth. The performance of electronic sensors has been evaluated by many studies. Bachus et. al compared the accuracy of a Tekscan sensor (K-Scan; Tekscan, Inc., Boston, MA, USA) to Fuji film (Fuji Photo Film Co. Ltd., Tokyo, Japan), and found that the pressure film has a comparable accuracy to the electronic pressure sensors [2]. D.R. Wilson et. al reported similar results [37]. Fregly and Sawyer reported that the discretization error for Tekscan's K-Scan sensors (K-Scan; Tekscan, Inc., Boston, MA, USA) was around 1 – 4 % when measuring peak pressure [16]. Otto et. al showed that the output of the sensor is subject to the effects of drift, and that the output of the sensor due to static loading can decrease as much as 30 % over a ten minute period [27].

However, using an electronic pressure sensor in applications such as measuring the contact between two articulating joints, as was done in this study, will lead to various considerations before using the sensor. According to Brown et. al, the sensor will have to be calibrated for the pressure range that it is intended to be used for, which means that this pressure range needs to be determined [8]. The sensor will also have to be inserted into the joint, and fixed into place so that it does not move during testing to reduce damage from shear as well as to preserve the placement of the sensor in the joint [30]. Since calibration of the sensor directly

inside of the joint (in-situ) is generally not feasible, the sensor has to be calibrated externally under conditions chosen to best replicate the application that the sensor will be used for [30]. The elastic modulus of the material that the sensor will be calibrated with needs to be similar to the application that the sensor will be used with since the elas of the sensor depends on the elastic modulus of the material that it is compressed between [19]. Brimacombe et. al has shown that user-defined calibrations are more accurate than using the calibration functions that are built into the sensors software, since under-defined calibrations can be tailored to the sensor being used, the pressure ranges needed, the interface materials, etc. [6].

Many different studies have reported using electronic pressure sensors to measure joint contact pressure. Rudert et. al used a custom designed Tekscan sensor (K-Scan; Tekscan, Inc., Boston, MA, USA) for measurement of dynamic contact pressure in the human cadaveric hip joint [30]. The pressure sensor was designed to measure pressure from 0 – 20 MPa, which is the expected pressure range established by previous studies of contact pressure in the hip, and the sensor has the shape of an annulus. The sensor was calibrated by being placed between two aluminum platens in a materials testing machine. Three different types of upper platens were used: a flat aluminum platen, a flat aluminum platen lined with a 1mm thick layer of 90A polyurethane, and a conical platen lined with a 1mm thick layer of 90A polyurethane (the platens were lined with polyurethane to simulate contact of cartilage).

The average stresses were calculated from the applied load divided by the contact area of the upper platens, and the average raw output of the sensor was calculated. The sensors response to applied pressure was modeled by a second-order polynomial. The results showed that the response of the sensor to loading under the flat platen and the conical platen are virtually identical when they are both lined with polyurethane. However, the response of the sensor to

loading under the flat platen without a polyurethane lining was lower than the response of the sensor to the flat platen with a polyurethane lining. Thus, the sensors performance was not affected by the curvature of the platens, but the sensors performance was effected by the material that made contact with the sensor. Rudert et. al recommends that the user recalibrate the sensor, as necessary, due to degradation of the sensor during biomechanical testing. The sensor needs to be recalibrated when the total output of the sensor decreases over the duration of testing. They also recommend applying petroleum jelly to lubricate the sensor when it is used in testing to help prevent damage to the sensor.

Paci et. al used a Tekscan K-6900 sensor (K-Scan; Tekscan, Inc., Boston, MA, USA) to measure the medial compartment contact pressure with release of the type I anterior intermeniscal ligament in human cadaveric knees, where the skin on the knee was left intact during testing [28]. The sensors were inserted through a small incision below the menisci, which was large enough to insert the sensor without damage, and the sensor was sutured to anchors placed in the tibia. They reported using a new sensor for each knee, and calibrated each sensor with three loads, which were not specified, to obtain a three-point non-linear calibration. Axial loading of 1000 N was selected for axial loading to prevent damage to the sensor (the amount of loading that would cause damage to the sensor was not specified), and it is comparable to the loading used in other studies.

Seitz et. al used a Tekscan sensor (K-Scan; Tekscan, Inc., Boston, MA, USA) to measure the effect of partial meniscectomy on contact pressure in human cadaveric knees, where the skin, fat, muscles, and ligaments were removed from the knee for testing [31]. The sensors were inserted by distracting the joint, and the sensors were placed so that they were beneath the whole menisci. The sensors were calibrated in a materials testing machine, between two platens.

Seven points of loading were defined for calibration: 0.25, 0.5, 1, 2, 4, 7 and 8 MPa. To account for the time dependent behavior of the sensors, they used the mean values of output of the sensor that occurred for the first minute that the known pressure was applied to the sensor (the sampling rate was 5 Hz). They reported using a power law for calibration, to establish the relationship between applied pressure and the output of the sensor.

Wilharm et. at used the Tekscan K-4000 sensor (K-Scan; Tekscan, Inc., Boston, MA, USA) to measure retropatella contact pressures in human cadaveric knees [36]. A layer of film was placed over the sensor to protect it from the effects of shear when it was placed in the knee. Ten knees were tested, and placed in a test fixture which was mounted in a materials testing machine. Twelve loading cycles were conducted, with consistent loading placed on the fixture by the materials testing machine during each loading cycle. The results showed that measurements of total output by the sensor decreased from between 1-2 % between each successive loading cycle. The decrease was attributed to the degradation of the sensor during loading.

Lee et. al used the Tekscan K-4000 sensor (K-Scan; Tekscan, Inc., Boston, MA, USA) to measure the effects that serial medial meniscectomies had on tibio-femoral contact pressure in human cadaveric knees, were the skin, fat, muscles, and patellar were removed prior to testing [23]. The sensors were inserted below the menisci by creating small anterior and posterior capsules in the medial and lateral compartments. The specimens were fixed in a testing fixture, which was mounted onto a materials testing machine. Because the skin, fat and muscles had been removed, the condyles could were positioned in the testing fixture to allow joint compression to be applied evenly. 1800 N of axial loading was used for testing. A new sensor was used for each specimen, and was calibrated and conditioned immediately before testing.

The sensors were conditioned by subjecting them to three cycles of 2800 N of axial loading applied to the sensor between the platens of a materials testing machine. A two point power law calibration using the sensors software was performed with 700 N and 2100 N of loading captured between the platens of the materials testing machine.

Bedi et. al used the Tekscan 4010N sensor (K-Scan; Tekscan, Inc., Boston, MA, USA) to measure the effects that radial tear, repair, and partial meniscectomy of the medial meniscus had on tibio-femoral contact pressure in human cadaveric knees, where the skin, fat, muscle, and patellar were removed prior to testing [4]. The sensors were inserted below the medial meniscus by making one centimeter incisions in the meniscotibial ligaments anteriorly and posteriorly, allowing the sensor to be passed beneath the meniscus, and to be flush with the tibial plateau without detaching the meniscotibial ligaments or meniscofemoral ligaments. The sensor was secured in the knee using sutures placed through the insertion site of the anterior cruciate ligament and the tissues surrounding the knee capsule.

Brady et. al used the Tekscan K-4000 sensor (K-Scan; Tekscan, Inc., Boston, MA, USA) to measure the effects of initial graft tension on the tibio-femoral contact pressure after ACL reconstruction using a patella tendon graft in human cadaveric knees [5]. The sensor was calibrated in-situ inside of a knee, with an unused sensor. The knee was placed in a testing fixture mounted on a materials testing machine. Once the knee was fixed, the flesh was removed and the ligaments were released, and then the lateral condyle was sawed off. Then one side of the sensor was placed below the medial meniscus, through an incision on the anterior side, and held in place with a hemostat clamped to the tab on the side of the sensor. The sensor was preconditioned five times before use, according to the manufactures recommendations [35]. A two point power law calibration was performed using the sensors software, at 50 N and 165 N.

Fleming et. al used the Tekscan K-4000 sensor (K-Scan; Tekscan, Inc., Boston, MA, USA) to measure the tibio-femoral contact pressure during initial graft tensioning during ACL reconstruction in human cadaveric knees [15]. They also calibrated the sensor inside the knee using the methods described by Brady et. al.

D.C. Wilson et. al used the Tekscan K-6900 sensor (K-Scan; Tekscan, Inc., Boston, MA, USA) to measure lumbar spine facet pressures [38]. Two different methods of calibration using the sensors software were examined: linear calibration using one point, and power law calibration using two points. The sensor was calibrated to be used with 0, 50, and 100 N of axial loading. The sensor was placed between the platens of a materials testing machine for calibration. For the linear calibration, 80 N of loading was placed on the sensor by the materials testing machine. For the power law calibration, 20 N and 80 N of loading was placed on the sensor. The results of the experiment showed that the peak pressure using the linear calibration method was 30 % lower than the peak pressure using the power law calibration.

D.C. Fitzpatrick et. al a Tekscan sensor (K-Scan; Tekscan, Inc., Boston, MA, USA) to measure contact stress of posterior malleolus fractures in human cadaveric ankles [14]. They reported calibrating the sensor to pressure ranges established by previous comparable studies, which was 0 – 20 MPa, and chose to report the 90^{th} percentile stress, rather than the peak stress, in order to account for sensor crinkle in the joint as well as sensor (the rational of choosing this was not specified), and chose their axial loading to be one times body weight to avoid degradation of the sensor at higher loads (the amount of loading that would cause degradation of the sensor was not specified). McKinley et. al used a custom designed Tekscan sensor (K-Scan; Tekscan, Inc., Boston, MA, USA) to measure instability-associated changes in contact pressure in human cadaveric ankles during motion [25]. The sensors were calibrated at a 132Hz

(sampling rate) using a dynamic load, on a cell-by-cell basis, by applying a uniform pressure to the sensor (the method of applying the uniform pressure was not specified).

Mazzocca et. al used the Tekscan K-4205 sensor (K-Scan; Tekscan, Inc., Boston, MA, USA) to measure the effect on contact pressure that four common arthroscopic rotator cuff repair techniques have over time in human cadaveric shoulders [24]. They reported that the sensor was calibrated to a pressure range consistent with previous rotator cuff tear studies. They verified the accuracy and repeatability of the sensor by conducting a pilot study to verify that the sensor produced consistent and correct output, once calibrated, when a 5 N and 100 N load were placed on the sensor. They also performed a drift test, in both tension and compression, to evaluate the sensors output over time. They found that in 60 minutes, a load of 10 N applied by a materials testing machine varied 4.69 % in tension and 5.85 % in compression.

2.3 ANATOMY OF THE KNEE JOINT

The ligaments in the knee joint form a complex system that works to guide the motion of the knee [22]. The knee joint is shown in Figure 5, which is a figure taken from Gray's Anatomy. The four major ligaments of the human knee joint are the Anterior Cruciate Ligament (ACL), Posterior Cruciate Ligament (PCL), Medial Collateral Ligament (MCL), and Lateral Collateral Ligament (LCL) [22].

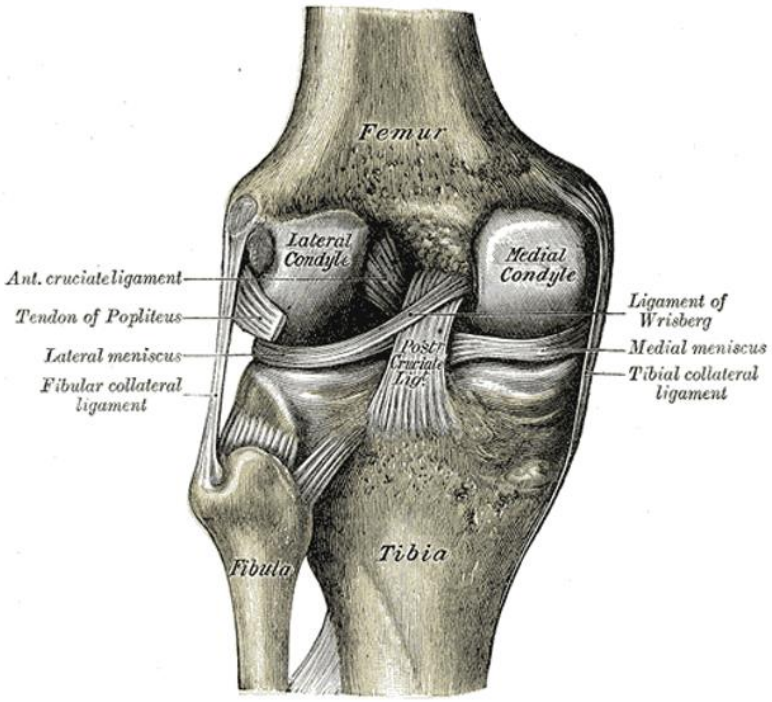

Figure 5. Posterior view of left knee joint at full extension [18]

The meniscus works to disperse the weight from the body over onto the tibia [20]. The meniscus also works to reduce friction during motion of the femur on the tibia during flexion and extension of the knee [10]. The meniscus attaches to various ligaments in the knee joint: the transverse ligament connects the anterior horn of the lateral meniscus to the anterior horn of the medial meniscus, the menisco-tibial ligaments (also called the coronary ligaments of the knee) connect the inferior edges of the menisci to the tibia, and the menisco-femoral ligaments (also called the ligaments of Humphrey and Wrisberg) connect the posterior horn of the lateral meniscus to the lateral aspect of the medial femoral condyle [18]. The meniscus is shown in a disarticulated joint in Figure 6, which is a figure taken from Gray's Anatomy.

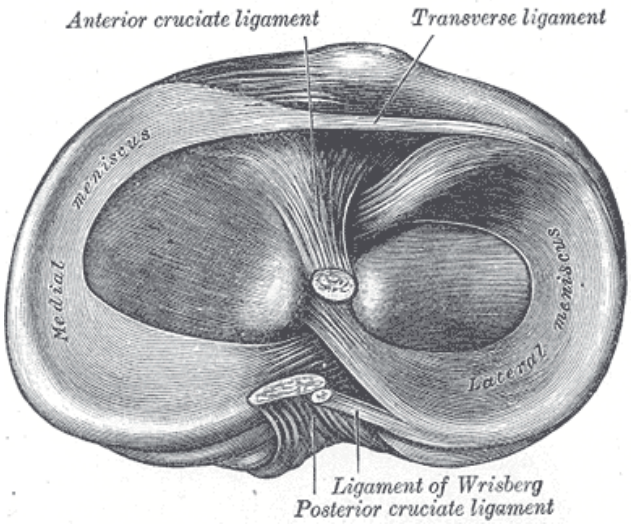

Figure 6. Disarticulated left knee joint showing the meniscus [18]

2.3.1 ACL

The ACL attaches to the femur and the tibia. The ACL is thought by some to consists of two bundles, which are named according to their insertion sites on tibial plateu: the anteromedial bundle (AM) and posterolateral bundle (PL). The purpose of the ACL is to help stabilize the knee joint and guide knee motion by limiting anterior tibial translation (ATT), varus-valgus and axial tibial rotations, and knee hyperextension [39]. The ACL may be damaged when it is overload during sports injuries, accidents, etc. The ACL can be damaged in varying degrees, and will often require surgical reconstruction due to its avascular nature. However, surgical reconstruction may alter the femoral condyle's alignment with respect to the tibia. This may change the contact between the femoral condyles and the tibia, and combined with the resulting change in laxity of the knee due to reconstruction, may lead to abnormal motion of the knee that may injure articular cartilage and contribute to the development of osteoarthritis [11].

2.3.2 ACL Reconstruction

Approximately 60,000 to 175,000 cases of ACL reconstruction are performed in the United States each year, making it one of the most common athletic injuries [40]. Reconstruction is referred to as anatomic if the position of each graft matches the position of the insertion site of the native ACL. Generally, ACL reconstruction can be broken down into two categories: single-bundle and double-bundle reconstruction. In single-bundle ACL reconstruction, the native ACL is replaced with a single ACL graph. Historically, single-bundle has been the most popular form of ACL reconstruction. However, studies have shown that while single-bundle ACL reconstruction is effective in restoring the restraint to anterior tibial translation, single-bundle ACL reconstruction is ineffective in restoring the rotational laxity of the knee [9]. In double-bundle ACL reconstruction, the native ACL is replaced with two ACL graphs. Biomechanical studies have shown that the insertion of the second bundle can better restore the rotational laxity of the knee than single-bundle reconstruction [39]. In both single-bundle and double-bundle ACL reconstruction, there is no agreement in the clinical community over the graft fixation tensions that will best restore the laxity of the knee.

3.0 EXPERIMENTAL METHODS

3.1 EXPERIMENTAL PROTOCOL

3.1.1 Cadaveric Specimens

The experimental protocol that was used for this study was approved by the University of Pittsburgh. Fifteen frozen fresh cadaveric human knees were used for this study. Three knees were dislocated during testing and were excluded. The remaining twelve (n=12) knees which made up the study consisted of eleven males and one female, with an average age of 60.7 years. The knees were defrosted at room temperature twenty four hours before they were used for testing. The knees were inspected arthroscopically before testing to exclude the possibility of osseous abnormalities that would damage the sensor. To fix the knees during testing, the ends of the femur and tibia were scraped of flesh and potted with an epoxy compound using a cylindrical mold (Bondo; 3M, Saint Paul, MN, USA) before testing. All preparation and reconstructions of the knees was performed by the same orthopedic surgeon.

3.1.2 ACL Reconstruction

Double-bundle ACL reconstruction was performed arthroscopically using hamstring grafts by an orthopedic surgeon. Double-bundle ACL reconstruction replaces the native ACL with two grafts: AM graft and PL graft. Since the reconstruction is anatomic, the two tunnels for the grafts are drilled through the native ACL's insertion sites. Once the tunnels are drilled, the grafts are fixed with a post to the tibia. Three different graft fixation tensions were used: i) AM/PL: 30N/10N (referred to as "Recon 1"), ii) AM/PL: 10N/30N (referred to as "Recon 2"), iii) AM/PL: 40N/40N (referred to as "Recon 3"). For each reconstruction, the PL bundle was fixed first with the knee at 0 degrees (full extension), and then AM bundle was fixed at 30 degrees. The order that the three ACL reconstructions were performed in the knee was randomized for each specimen.

3.1.3 Sensor Placement

The sensor was placed below the meniscus in the knee joint. In order to get the sensor into the knee, the joint capsule and the menisco-tibial ligaments were cut anteriorly, as shown in Figure 7. The meisco-tibial ligaments were also cut posteriorly so that the sensor could be pulled through the knee joint.

Figure 7. Sensor placed in the knee compartment through the anterior incision

Because the tibial-meniscal compartment is narrow, the tabs around the sensor were removed. Once the tabs were removed from the sensor, small holes were punched along the top and bottom of each side of the sensor so that the sensor could be sutured into place, as shown in Figure 8. The sensor was sutured arthroscopically to the soft tissue surrounding the meniscus, which consists of the joint capsule and ligaments that connect to the meniscus in the knee. The sensors were sutured into place so that they would not move around during knee flexion. By keeping the sensor in place, a better comparison can be made between the data collected at different states within the same knee (Intact, Recon 1, Recon 2, and Recon 3). The sensor was left sutured in the knee during ACL reconstruction.

Figure 8. Sensor prepared for insertion into the meniscal compartment of the knee joint

Figure 9 shows a disarticulated left knee, where the placement of the sensor can be seen, as well as the two bundles of the ACL, where the AM bundle is colored blue and the PL bundle is colored red.

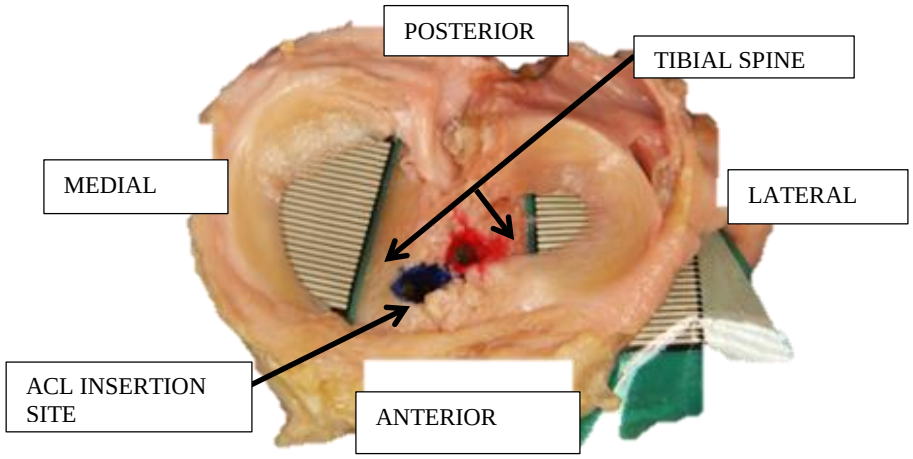

Figure 9. Disarticulated left knee joint showing sensor placement

Since the morphology of each knee is different, sensor placement is difficult to standardize which causes variability between the placements of the sensor in each knee. The

sensors were positioned to try to capture the greatest amount of loading possible on the tibial plateau, underneath the meniscus, between the femoral condyles and the tibia. They were placed as close as they could to the tibial spine, which is the location where the tibia starts curving upwards. The MCL and LCL were cut slightly to allow the sensor to be placed further back posteriorly.

3.1.4 Test Fixture

A custom testing fixture, which was attached to a materials testing machine, was used to secure the knees during testing. The testing fixture consisted of two cylinders that attach over the epoxy compound on the ends of the tibia and femur. The femur of the knee was placed in the base of the testing fixture, and the tibia of the knee was placed in the arms of the testing fixture. The ends of the femur and tibia were fixed to the cylinders, and the femur was not free to move during testing. The testing fixture is shown in Figure 10.

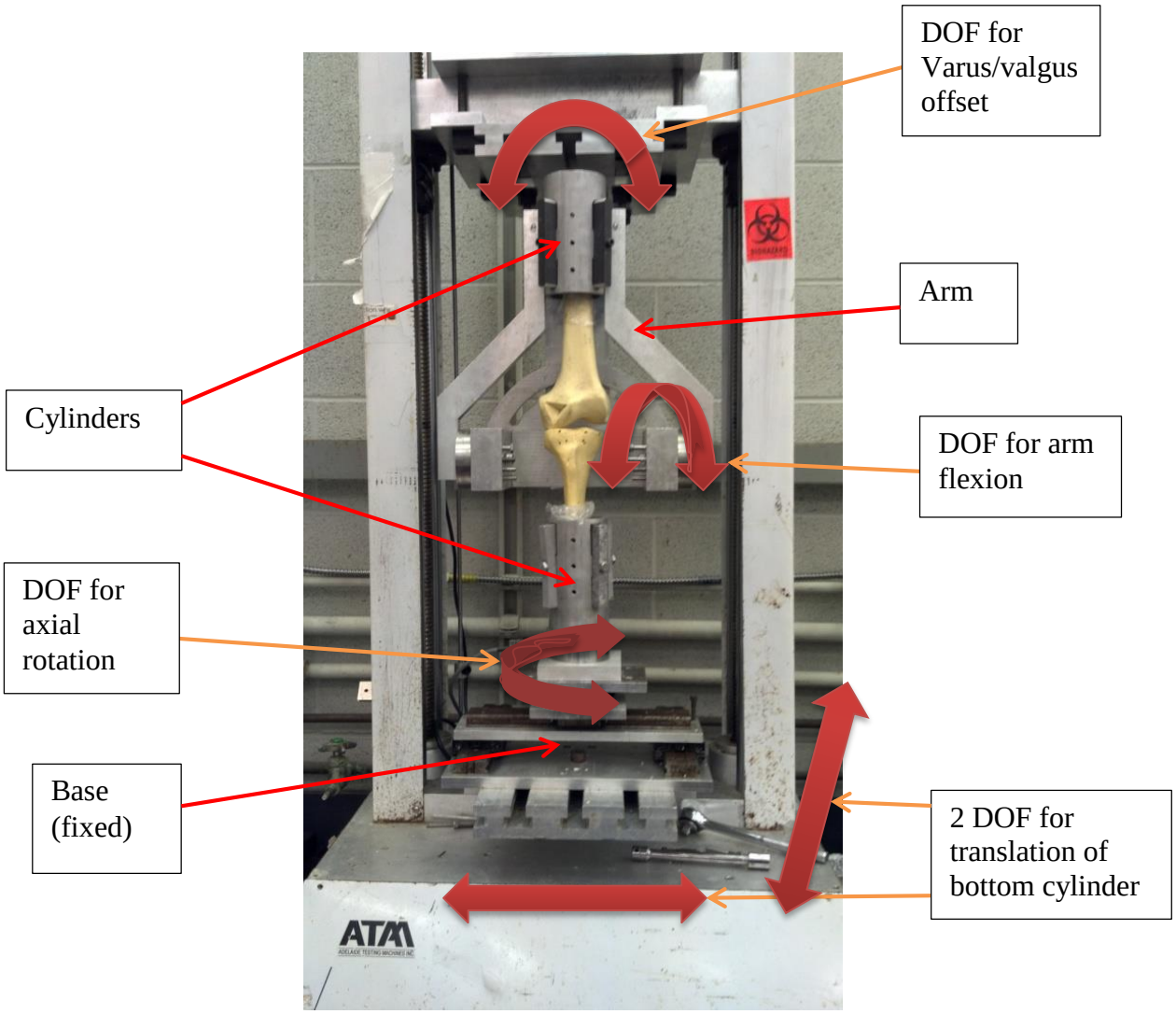

Figure 10. Testing fixture showing degrees of freedom

The arrows indicate the degrees of freedom that are allowed during testing. The arms can be adjusted to accommodate for varus/valgus angulation of the knee, and can be locked into place during testing. The arms can also be flexed, in order to flex the knee, from 0-95 degrees (in 5 degree increments), and can also be locked into place. The base has three degrees of freedom to allow the movement of the tibia in a plane parallel that is parallel to the base of the materials testing machine: translation in both directions of the plane as well as axial rotation of the tibia.

3.1.5 Experimental Procedure

Once the sensor was placed in the knee, the knee was tested as shown by the study design in Figure 11.

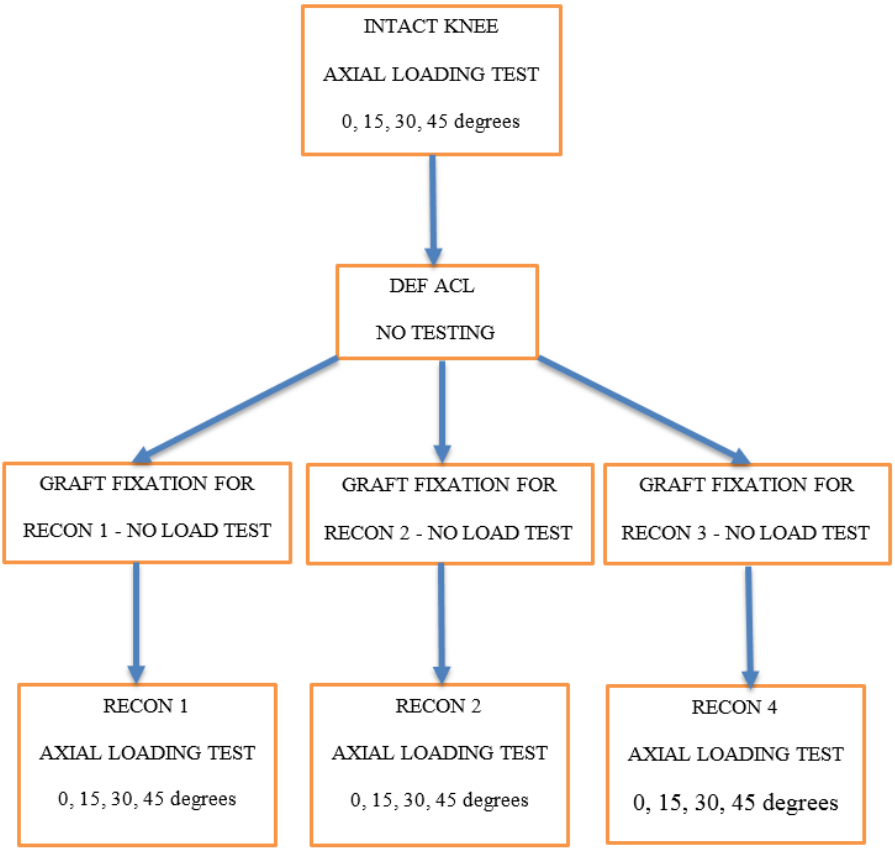

Figure 11. Study Design

The knees were first tested under axial loading at 0, 15, 30, and 45 degrees of flexion with the native ACL intact. For axial loading, 1000 N of loading was applied to the testing jig using a materials testing machine (ATM; Adelaide Testing Machines Inc., Toronto, Ontario, Canada), as shown in Figure 11. The loading was measured with a 1000lb (4448.2N) load cell,

and the calibration of the load cell was checked before testing by placing 12 calibrated 100kg weights on top of the load cell.

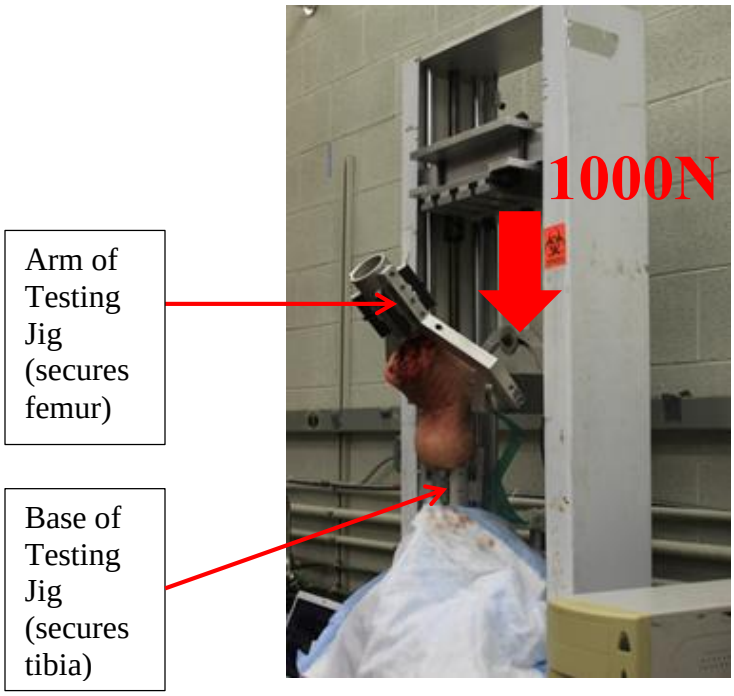

Figure 12. Materials testing machine used for knee compression

Thereafter, the ACL was removed and double-bundle ACL reconstruction was performed in a randomized order for Recon 1, Recon 2 and Recon3. For each reconstruction, pressure readings were collected using the sensor during the fixation of the two ACL bundles, without loading, as shown in Table 1. For each test, the reading was taken at the highest sensitivity (High2) and then repeated at the next sensitivity setting, if needed, until none of the cells on the sensor were saturated (raw output reached or exceed 255).

Table 1. Graft fixation testing protocol

Graft Fixation Testing Protocol	
1	30 degrees with no graft
2	0 degrees with no graft
3	0 degrees with PL graft inserted
4	0 degrees with PL graft fixed
5	30 degrees (PL graft fixed)
6	30 degrees with AM graft inserted (PL graft fixed)
7	30 degrees with AM graft fixed (PL graft fixed)

Once the grafts were fixed, the knee was tested under loading at 0, 15, 30, and 45 degrees of flexion for each state of reconstruction. A pressure reading was taken for each test using the sensor. For each test, the reading was taken at the highest sensitivity (High2) and then repeated at the next sensitivity setting, if needed, until none of the cells of the sensor were saturated (raw output reached or exceed 255) because the pressure of the cells cannot be determined when they are saturated.

3.1.6 Experimental Data

Since there is variability in the placement of each sensor in the knee, there is not a universal anatomical set of coordinates that can be used to describe the pressure that is placed on the

sensor. Thus, a local coordinate system will be established along the edges of each side of the sensor, as shown in Figure 13.

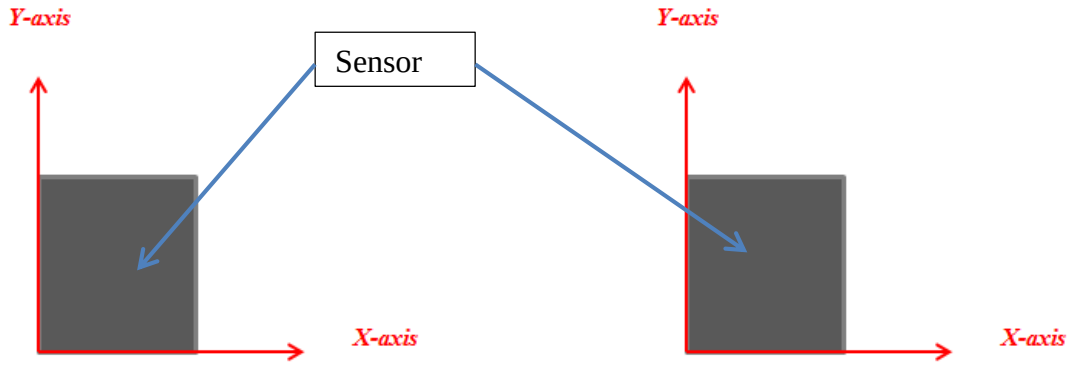

Figure 13. Local coordinate system established along the edges of each side of the sensor

Since human knees are symmetric, Side A of the sensor in a right knee will correspond to the lateral tibio-femoral compartment, whereas Side A of the sensor in a left knee will correspond to the medial tibio-femoral compartment. Similarly, Side B of the sensor in a right knee will correspond to the medial tibio-femoral compartment, whereas Side B of the sensor in a left knee will correspond to the lateral tibio-femoral compartment. Moreover, the axes will be shifted for the left knee so that the axes are in the same position relative to the meniscus for right and left knees, as shown in Figure 14.

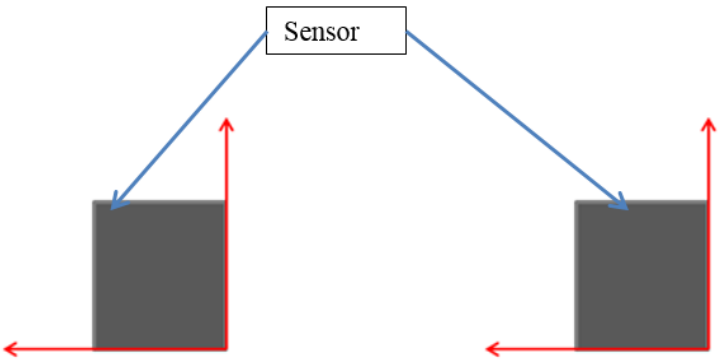

Figure 14. Local coordinate system established shifted for left knees

Therefore, the location of the peak pressure and the location of the center of pressure in each of the two meniscal compartments of the knee cannot be computed because global anatomical coordinates cannot be established to describe these quantities in a standardized way. Thus, only the change in location of peak pressure and the change in the location of the center of pressure can be computed, because the magnitude of the change in location for these two quantities does not depend on the coordinate system that they are computed in. The algorithm used to calculate these two quantities is given in Appendix A.

Not all of the contact between the femoral condyles and tibia is captured by the sensor due to the variability in the size of each knee and the placement of the sensor in each knee. Therefore, the average pressure and area of each of the two meniscal compartments of the knee cannot be computed because there is no way to gauge how much of the total contact between the tibia and each side of the femoral condyles is not being measured. Only the value of the peak pressure in each meniscal compartment of the knee can be computed. The algorithm used to calculate the value of peak pressure is given in Appendix A.

3.1.7 Statistics

Statistical tests were performed using MINITAB software (Minitab Inc., State College, PA, USA). The Kruskil-Wallis test, which is a one-way analysis of variance for testing whether non-parametric samples originate from the same distribution, was used to examine if double-bundle ACL reconstruction had an effect on peak pressure, location of peak pressure, and location of center of pressure in the knee. Pair-wise testing was used to determine where significance occurred if a factor proved significant. Significance was set at $p=0.05$ for all tests.

3.2 SENSOR CALIBRATION

Electronic pressure sensors need to be calibrated, which means that the relation between the raw output of each cell and the pressure applied to each cell needs to be established. For this study, the sensor was placed in the knee joint (on top of the tibial plateau but below the meniscus). The sensor was used to measure static pressure that was taken when axial loading was applied to the knee joint using a materials testing machine (1000N), so drift was not taken into account. Previous studies using pressure sensitive film in the knee joint have found that the peak pressure with the native (intact) ACL ranges from around 4-6MPa [26] with an applied load of 1000N. Therefore, this study attempted to calibrate the sensor from 0MPa to 6MPa, which is the expected pressure range. Three kinds of calibration were investigated for the sensor in this study: bladder, materials testing machine, and polyuretherane rollers.

3.2.1 Calibration Using a Bladder

Using a bladder to apply a pressure on the sensor will provide an approximately uniform pressure distribution over the area of the sensor that is in contact with the bladder. The advantage of using a uniform pressure distribution for calibration is that there is should be minimal variation of pressure applied to the cells across the sensor. For this method of calibration, a bladder was used to apply a pressure to the sensor by placing a bicycle tire's inner tube between two rigid, parallel surfaces, as shown in Figure 15. A clear acrylic sheet was used for the top surface, and steel was used on the bottom surface. Bolts were used to hold the two surfaces in place. The ends of the inner tube were clamped at the edge of the fixture so that air would not escape from the inner tube, as shown in Figure 15.

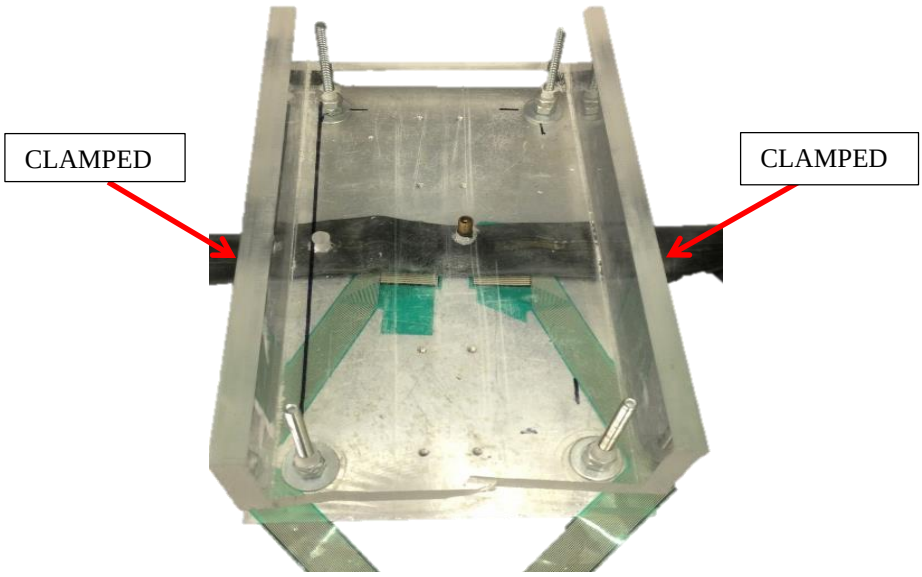

Figure 15. Bladder setup: bicycle tire inner tube placed between two parallel surfaces

The inner tube is made out of butyl, and needs to be constrained by a fixture or casing that is made out of a stiffer material so that the inner tube can be pressurized. If the inner tube is not sufficiently constrained, it will burst when it is pressurized. Although the bicycle inner tube was clamped at the ends of the fixture, the inner tube still expanded outside of the fixture when it was pressurized. The inner tube was able to be inflated to 20psi (0.14MPa) before it started expanding outside of the fixture and burst.

3.2.1.1 Calibration Data

The pressure inside the tire inner tube was measured using the pressure gage on the pump that was used to inflate it. The sensor was placed below the inner tube, and on top of the steel plate of the fixture. Since the sensor is designed to be water proof, air that is caught inside the sensor during the manufacturing process cannot escape when the sensor is loaded. Thus, around 25% of the sensor had to be left uncovered by the inner tube to give the air inside of the sensor room to move around [35]. If the entire sensor was covered by the inner tube, no pressure reading would show up as the air would support the pressure applied to the sensor. At higher loads, this could damage the sensor as the air trapped inside the sensor could be forced out of the sensor. The pressure distribution inside of the inner tube was approximately uniform, as shown in Figure 16.

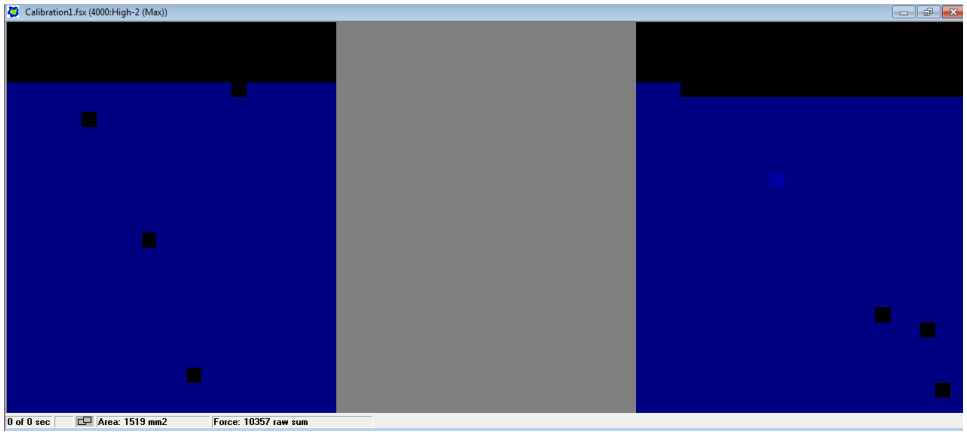

Figure 16. Data recorded by the sensor using the bladder

The tire inner tube was inflated using the pump, and static readings were taken from the sensor in approximately 0.014MPa increments for a range of 0-0.14MPa. This process was used to collect data for the High2, High1, Mid2, Mid1, and Default sensitivity settings. The Low3, Low2 and Low1 sensitivity settings were omitted because they were not able to measure the pressure that the inner tube placed on the sensor. Figure 17 shows the linear trend line of applied pressure versus the raw output of each cell for both sides of the sensor (since the entire sensor was placed in the fixture). The average raw output of all the cells was calculated by summing the total raw output of the sensor and dividing it by the number of cells that were activated (cells which had non-zero output). However, since pressure applied to the sensor is approximately uniform, the difference between the average raw output of all the cells and the actual raw output of each cell is negligible. Thus, for calibration using the bladder, the average raw output of the all the cells is assumed to be equal to raw output of each cell. Complete data for all the sensitivity settings is given in Appendix B. Only one sensor (n=1) was used for testing, and each pressure reading was taken twice and the average of the two readings was reported.

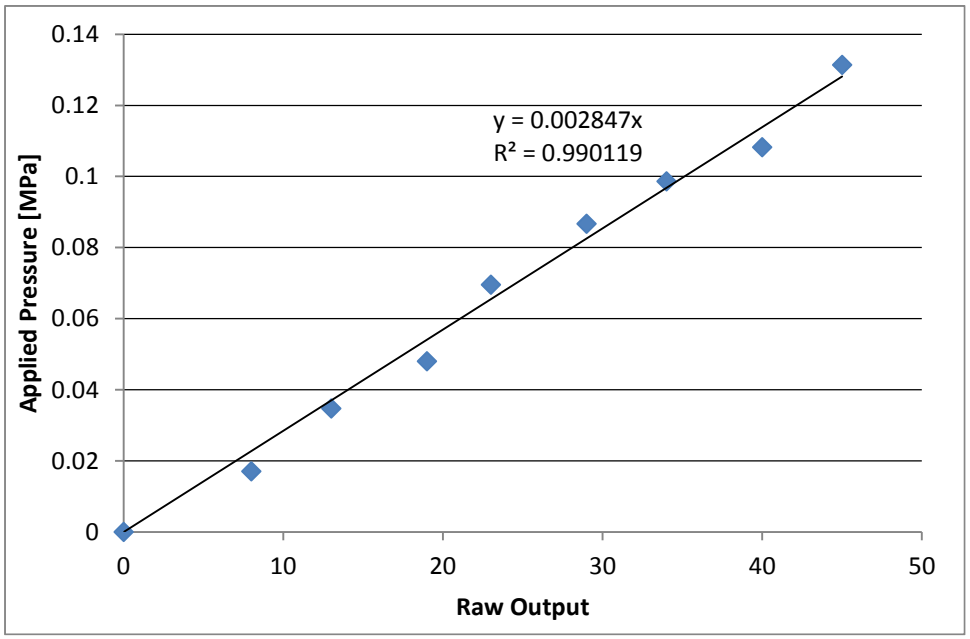

Figure 17. Linear trend line of the High2 sensitivity setting for applied pressure as a function of raw output

Table 2 shows that the trend lines for all sensitivity settings are strongly linear, as all sensitivity settings have a value for the coefficient of determination greater than 0.98. All sensitivity settings were tested at a range of 0-0.14MPa, at increments of 0.014MPa.

Table 2. Slope of the linear trend line of applied pressure vs. average raw output of all sensitivity settings

Sensitivity	Slope	r^2	Calibrated Pressure Range [MPa]
High2	0.002847	0.9901	0 - 0.14
High1	0.004731	0.9921	0 - 0.14
Mid2	0.008423	0.9899	0 - 0.14
Mid1	0.01536	0.9953	0 - 0.14
Default	0.02358	0.9906	0 - 0.14

3.2.1.2 Limitations

The trend line of the plot of the applied pressure as a function of the raw output can be used to calibrate the sensor because it establishes the relation between the raw output of a cell and the pressure applied to it. However, the limitation of using the tire inner tube is that it is only able to reach a pressure of around 0.14MPa. This is much lower than the 4-6MPa contact pressure that was found in the tibial-femoral compartment during 1000N of axial loading in previous studies. Thus, the trend line would need to be extrapolated in order to calibrate the sensor for the expected 4-6MPa contact pressure.

3.2.2 Calibration Using a Materials Testing Machine

A materials testing machine (Instron 5500R Model 4204; Instron Corporation, Canton, MA, USA) with a 50kN load-cell was used to apply a pressure to the sensor. Each sensor was placed between two pieces of 1.6mm-thick 90A polyurethane (PU) rubber sheet; the lower layer covered the entire platen, while the upper layer's surface area was smaller ($621mm^2$ on each side of the sensor) than the area of the sensor ($920.7mm^2$ on each side of the sensor). Since the upper layer's surface area was smaller than the area of the sensor, all the pressure applied by the platens passed through the sensor. The configuration of the sensor loaded with the materials testing machine is shown in Figure 18.

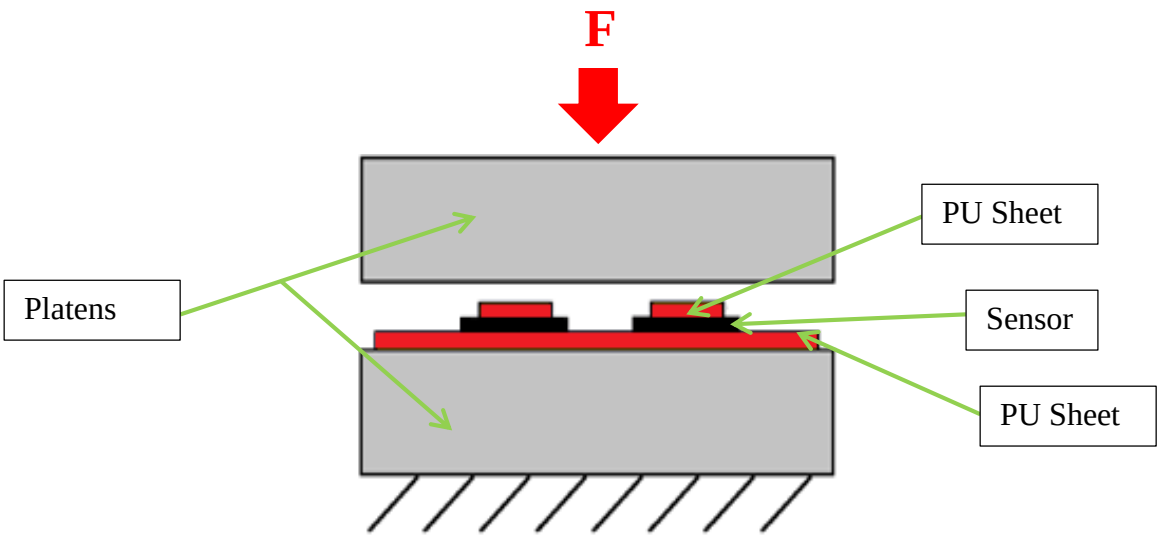

Figure 18. Materials testing machine setup

The average applied pressure to the sensor is equal to the pressure that was applied to the sensor by the crosshead of the materials testing machine, and can be calculated by using the force that the crosshead places on the PU sheets on top of the sensor and the PU sheet's area, which is given by:

$$P_{applied} = \frac{F}{A} \tag{3.1}$$

Figure 19 shows the pressure applied to the sensor by the platens are non-uniform. The greatest pressure is the region of contact roughly in the center of the platens (lighter region), and the pressure decreases as near the edges of the contact (darker region).

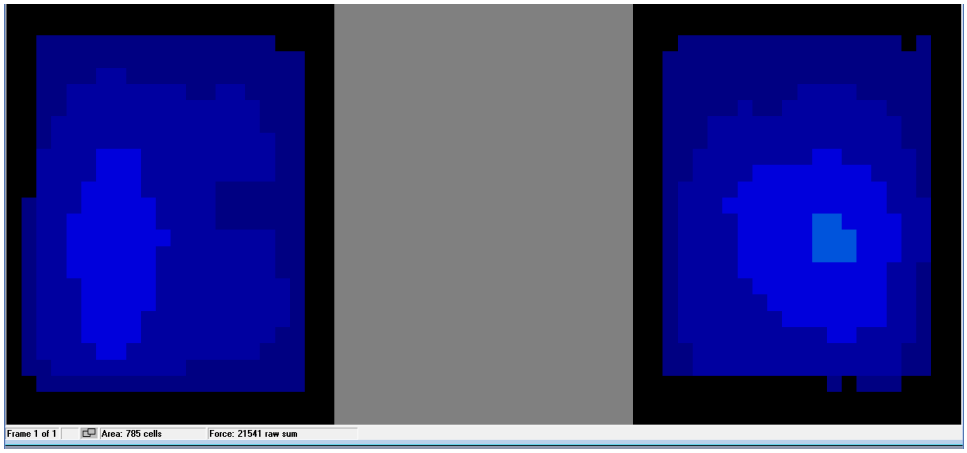

Figure 19. Output of the sensor to the applied pressure from the materials testing machine

Since the pressure applied to the sensor by the platens is non-uniform, as shown in Figure 19, the average raw output of each cell will be used to determine the relationship between the raw output of the sensor and the pressure applied to the sensor. The average raw output of each cell is calculated by dividing the total raw output of the sensor by the number of cells that the PU sheet covers, which is approximately 800 cells (400 on each side of the sensor).

3.2.2.1 Comparison of the Response of Each Side of the Sensor to Applied Pressure

Since the pressure applied to the sensor by the platens is non-uniform, as shown in Figure 19, the average raw output of each sensor was recorded when both sides of the sensor were loaded together, and when each side of the sensor was loaded independently. This will give insight into how the response of the cells varies for these two different loading conditions, and is given in Table 3 for the High2 and High1 sensitivity settings, Table 4 for the Mid2 and Mid1 sensitivity settings, and Table 5 for the Default and Low3 sensitivity settings. Note that "Side A" refers to the left hand sensing region, and "Side B" refers to the right hand sensing region of the sensor. The sensors were loaded until they were saturated or reached a load of 1.21MPa.

Table 3. Comparison of the average raw output of each cell for each side of sensor for the High2 and High1 sensitivity settings for a given applied average pressure to the sensor

Average Applied Pressure [MPa]	Average Raw Output									
	High2					High1				
	Side A	Side B	Whole Sensor	Percent Difference Side A and Whole Sensor	Percent Difference Side B and Whole Sensor	Side A	Side B	Whole Sensor	Percent Difference Side A and Whole Sensor	Percent Difference Side B and Whole Sensor
0.00	0.00	0.00	0.00	0.00	0.00	0.00	0.00	0.00	0.00	0.00
0.04	4.33	4.50	4.40	1.53	3.77	16.54	21.85	19.08	14.28	13.52
0.08	27.00	32.59	29.66	9.40	18.77	33.11	37.46	35.38	6.63	5.72
0.12	47.23	57.74	52.49	10.55	20.03	47.89	49.43	48.68	1.63	1.53
0.16	75.49	75.88	75.69	0.27	0.52	62.08	60.04	61.04	1.70	1.65
0.20	98.03	95.98	97.00	1.06	2.12	75.03	73.14	74.07	1.29	1.26
0.40						89.14	83.25	86.15	3.42	3.41
0.60						99.79	96.03	97.90	1.92	1.92
0.80										

Table 4. Comparison of the average raw output of each cell for each side of the sensor for the Mid2 and Mid1sensitivity settings for a given average applied pressure to the sensor

Average Applied Pressure [MPa]	Average Raw Output									
	Mid2					Mid1				
	Side A	Side B	Whole Sensor	Percent Difference Side A and Whole Sensor	Percent Difference Side B and Whole Sensor	Side A	Side B	Whole Sensor	Percent Difference Side A and Whole Sensor	Percent Difference Side B and Whole Sensor
0.00	0.00	0.00	0.00	0.00	0.00	0.00	0.00	0.00	0.00	0.00
0.04	11.47	16.95	13.95	19.52	19.37	8.76	11.70	10.10	14.25	14.66
0.08	21.54	26.37	23.97	10.65	9.53	16.90	19.15	18.02	6.39	6.09
0.12	31.06	33.28	32.19	3.57	3.31	23.12	23.72	23.42	1.29	1.27
0.16	39.05	39.74	39.40	0.89	0.86	27.75	27.85	27.80	0.17	0.18
0.20	46.21	45.15	45.67	1.16	1.15	28.14	28.86	28.49	1.24	1.28
0.40	77.96	76.34	77.14	1.06	1.04	43.46	48.91	46.14	5.98	5.81
0.60	106.25	102.64	104.40	1.75	1.70	56.06	61.31	58.68	4.58	4.39
0.80	130.48	126.73	128.56	1.48	1.44	69.88	74.18	72.08	3.10	2.87
1.01						82.24	87.66	85.02	3.33	3.05
1.21						91.46	101.70	96.63	5.50	5.11

Table 5. Comparison of the average raw output of each cell for each side of the sensor for the Mid2 and Mid1sensitivity settings for a given average applied pressure to the sensor

Average Applied Pressure [MPa]	Average Raw Output									
	Default					Low3				
	Side A	Side B	Whole Sensor	Percent Difference Side A and Whole Sensor	Percent Difference Side B and Whole Sensor	Side A	Side B	Whole Sensor	Percent Difference Side A and Whole Sensor	Percent Difference Side B and Whole Sensor
0.00	0.00	0.00	0.00	0.00	0.00	0.00	0.00	0.00	0.00	0.00
0.04	6.66	8.54	7.55	12.59	12.32	0.00	0.00	0.00	0.00	0.00
0.08	11.55	13.68	12.58	8.56	8.34	0.00	0.00	0.00	0.00	0.00
0.12	15.15	16.81	15.95	5.17	5.20	7.97	9.12	8.52	6.70	6.81
0.16	18.14	19.18	18.66	2.85	2.76	9.41	10.35	9.87	4.72	4.79
0.20	21.17	22.02	21.61	2.02	1.90	11.05	11.54	11.29	2.19	2.18
0.40	31.61	32.90	32.27	2.09	1.93	16.37	16.67	16.53	0.98	0.87
0.60	37.73	41.44	39.60	4.83	4.53	19.51	21.23	20.41	4.50	3.92
0.80	45.44	49.99	47.76	4.99	4.55	22.11	24.67	23.43	5.78	5.16
1.01	53.44	58.50	56.05	4.77	4.29	25.52	28.52	27.06	5.88	5.25
1.21	59.81	66.00	62.99	5.18	4.66	28.70	31.90	30.35	5.59	4.98

Table 4 shows that the largest percentage difference between Sensor A and the Whole Sensor (for all sensitivity settings) is 19.52%, and is located at an applied pressure of 0.04MPa at the Mid2 sensitivity setting. Table 3 shows that the largest percentage difference between Side B and the Whole sensor (for all sensitivity settings) is 20.03%, and is located at 0.12MPa at the High2 sensitivity setting. However, the percentage difference between Sensor A and the Whole Sensor as well as Sensor B and the Whole sensor tends to decrease as the applied pressure is increased for all sensitivity settings.

3.2.2.2 Sensor Data from the Materials Testing Machine

Figure 20 shows the average applied pressure as a function of the average raw output for the Default sensitivity setting for the averaged output of three sensors (n=3). While the sensor exhibits an initial non-linear trend (from raw output of 0 to around 60), the trend after this initial region appears to be approximately linear. In order to calibrate the sensor, the relationship

between the average raw output and the average applied pressure will need to be established. This can be accomplished by fitting a trend line to the data. Note that while the sensors raw output has a range of 0 – 255, Figure 20 only has a range of around 0 – 100. This is a result of the non-uniform pressure distribution shown in Figure 19, since no more pressure can be applied to the sensor once the first cell has become saturated (reaches a value of 255). Each pressure reading was taken twice and the average of the two readings was reported.

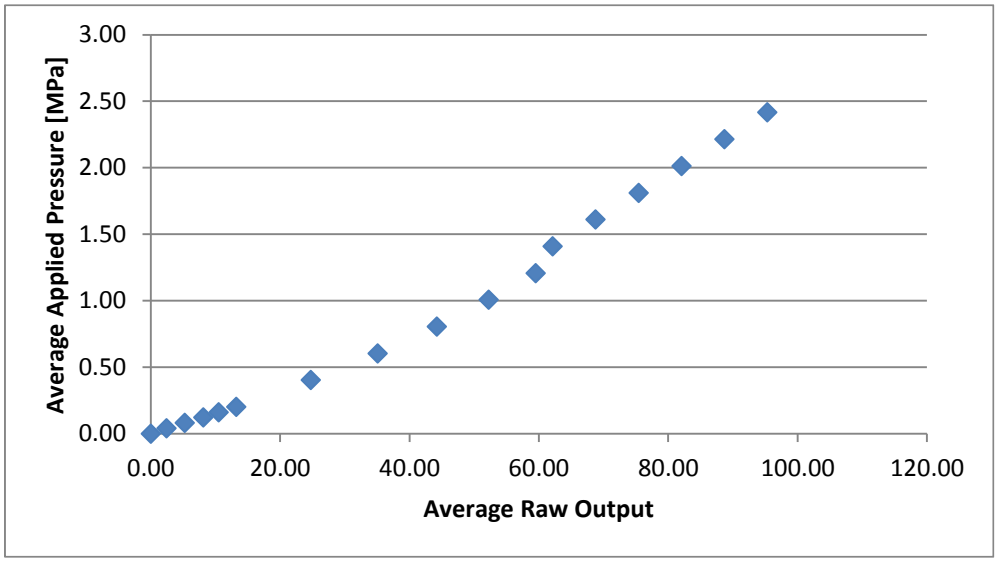

Figure 20. Average applied pressure as a function of average raw output for the Default sensitivity setting

Figure 21 shows the linear trend line of the average applied pressure vs. the average raw output for the Default sensitivity setting. The coefficient of determination is the greatest when the zero point is excluded from the trend line with a non-zero y-intercept (r^2=0.98), and the lowest when the zero point is included in the trend line with a zero y-intercept (r^2=0.97). However, the zero point needs to be included in the trend line with a zero y-intercept to prevent

negative pressure for low raw output, and ensure that a value of zero for raw output corresponds to a value of zero for applied pressure.

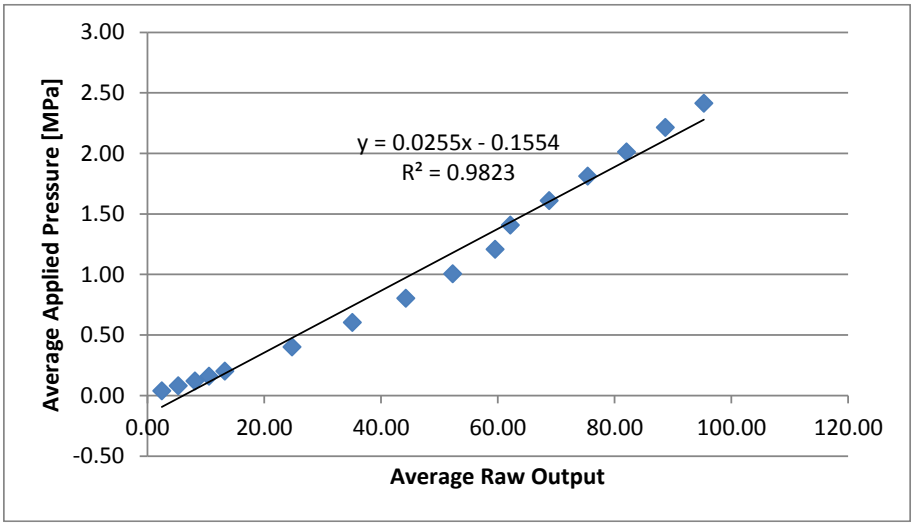

(a) Zero point excluded from trend line, and trend line has non-zero y-intercept

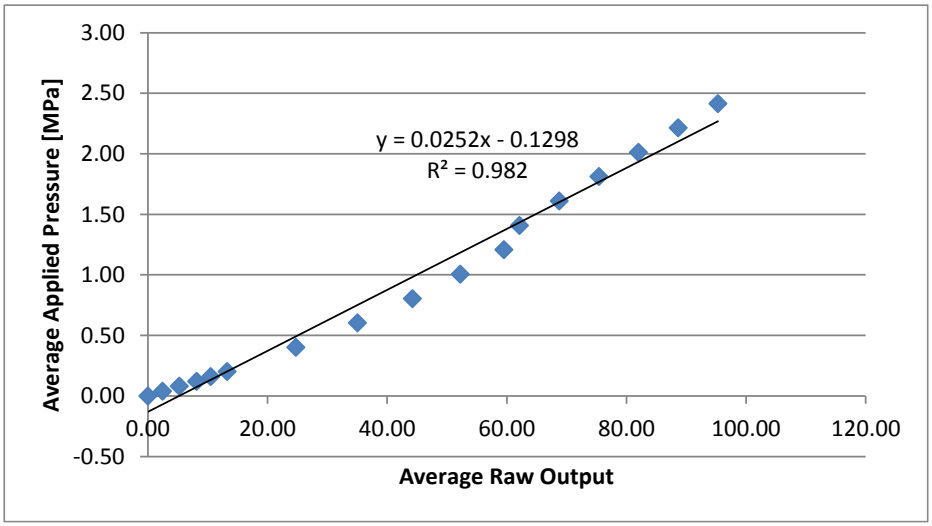

(b) Zero point included in trend line, and trend line has non-zero y-intercept

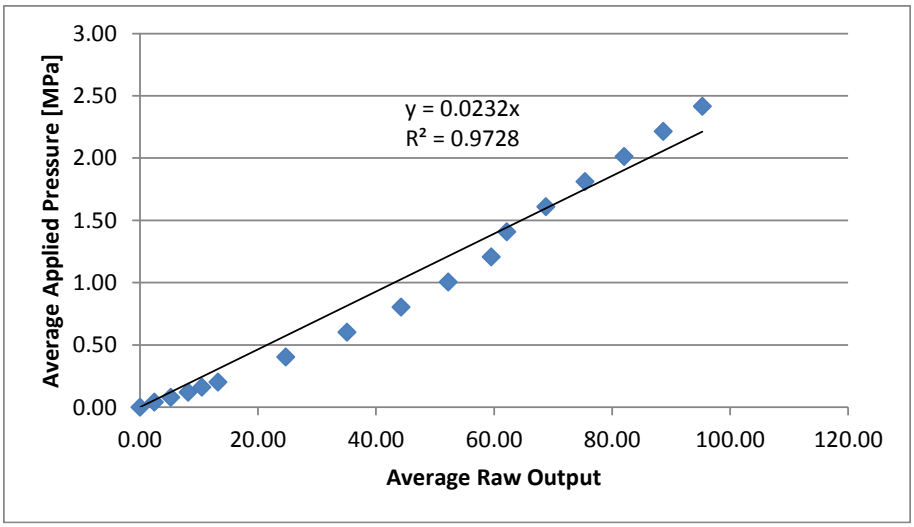

(c) Zero point included from trend line, and trend line has zero y-intercept

Figure 21. Linear trend line of average applied pressure as a function of average raw output for the Default sensitivity setting

Figure 22 shows the power trend line of the average applied pressure vs. the average raw output for the Default sensitivity setting. The coefficient of determination (r^2=0.99) is higher than the linear trend line (when the zero point is included and the trend line has a zero y-intercept).

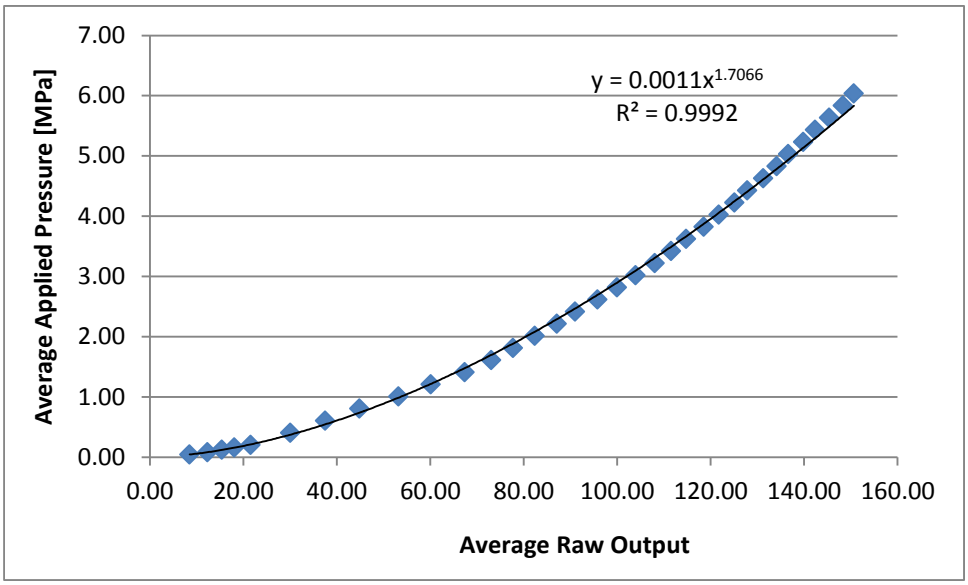

Figure 22. Power trend line of the average applied pressure as a function of the average raw output for the Default sensitivity setting

Figure 23 shows the polynomial trend line of the average applied pressure vs. the average raw output for the Default sensitivity setting. For the quadratic trend line, excluding the zero point and having a non-zero y-intercept has a negligible difference on the value of the coefficient. Thus, the zero point should be included and the trend line should have a zero y-intercept so that a reading of zero for raw output will correspond to a value of zero for applied pressure.

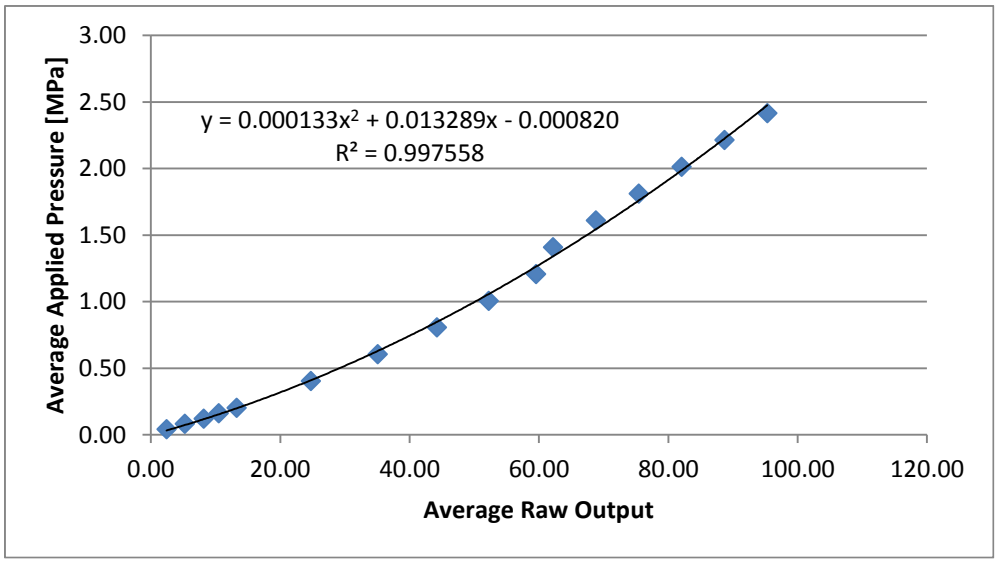

(a) Zero point excluded from trend line, and trend line has non-zero y-intercept

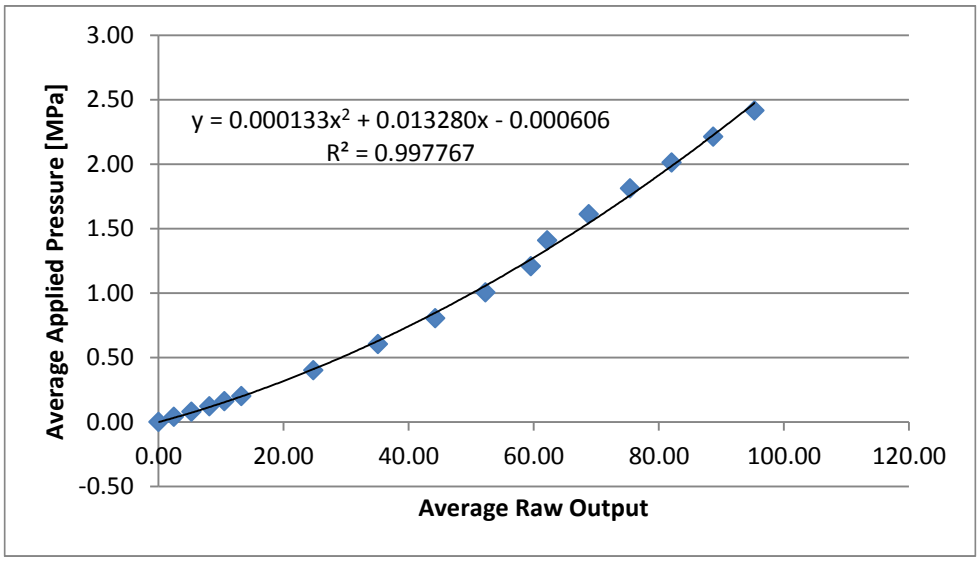

(b) Zero point included in trend line, and trend line has non-zero y-intercept

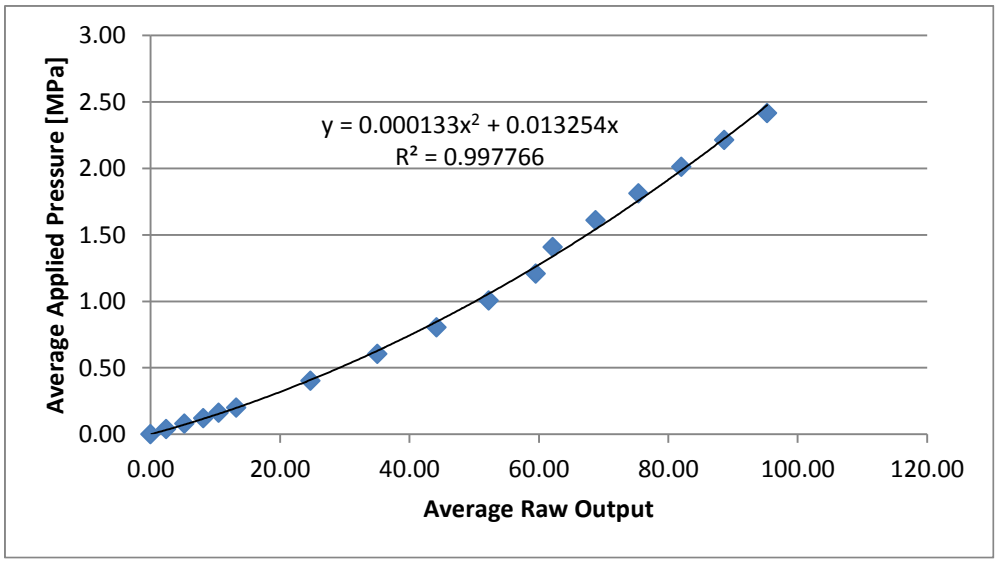

(c) Zero point included from trend line, and trend line has zero y-intercept

Figure 23. Polynomial (quadratic) trend line of the average applied pressure as a function of the average raw output for the Default sensitivity setting

Figure 24 shows the linear, quadratic, power and quadratic trend line of the average raw output as a function of the average applied pressure plotted for a range of 0 – 255 (which is the full range of the raw output of the sensor). Figure 24 shows that while all three trend lines follow a similar path initially, the quadratic trend line diverges from the other two trend lines when the raw output is around a value of 100. This does not match the linear trend for higher values of raw output that was observed in Figure 20. Thus, the power trend line is the best fit for the data, since it is best able to match the initial non-linear trend, as well as the linear trend for higher values of average raw output.

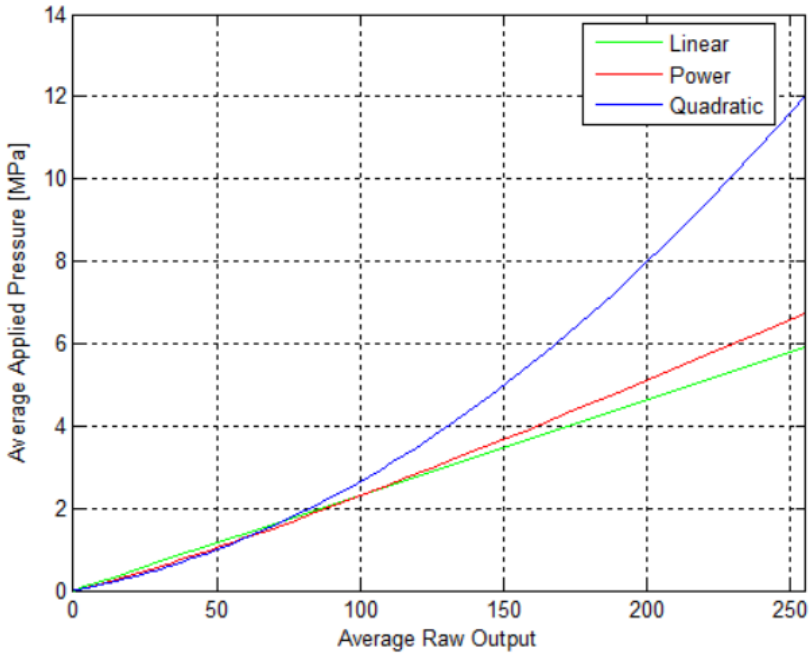

Figure 24. Comparison of linear, power, and quadratic trend lines

The process outlined above was used to collect data for the High2, High1, Mid2, Mid1, Default and Low3 sensitivity settings, and is summarized in Table 6. Data was not collected for the Low2 and Low1 sensitivity settings because a sufficient range of calibration (0MPa – 6MPa) was achieved with the Low3 sensitivity setting, thus, the Low2 and Low3 sensitivity setting will not be used with this application. Complete data for all the sensitivity settings is given in Appendix B. Note that all sensitivity settings were saturated at the end of the calibrated pressure range.

Table 6. Power trend line equation of applied pressure vs. average raw output of all sensitivity settings

Sensitivity Setting	Power Trend Line Equation	r^2	Calibrated Pressure Range [MPa]
High2	$y=0.00121x^{1.06922}$	0.99	0 - 0.12
High1	$y=0.00237x^{1.04793}$	0.99	0 - 0.28
Mid2	$y=0.00391x^{1.08431}$	0.99	0 - 0.60
Mid1	$y=0.00754x^{1.10103}$	0.99	0 - 1.21
Default	$y=0.0116x^{1.1486}$	0.99	0 - 2.42
Low3	$y=0.0366x^{1.1097}$	0.99	0 - 6.24

3.2.2.3 Limitations

The trend line of the plot of the average applied pressure as a function of the average raw output can be used to calibrate the sensor because it establishes the relation between the raw output of a cell and the pressure applied to it. However, the limitation of using the materials testing machine is that the pressure applied to the sensor by the platens is not uniform, as shown in Figure 19. Thus, the calibration will not be based on the entire range of output of the sensor (0 – 255) since no more pressure can be applied to the sensor once the first cell has become saturated (reaches a value of 255).

3.2.3 Calibration Using Polyurethane Rollers

Two polyurethane rollers of the same length and diameter (0.1m length and 0.055m diameter) were used in a fixture to place pressure on the sensor. The device was based on a design built at the University of Iowa [21]. The fixture consists of two rollers that were attached to gears and built into an aluminum frame, as shown in Figure 25. The aluminum frame was mounted to a

connecting rod so that it was able to move relative to the base. A Space Saver pneumatic cylinder (Space Saver: Mead, Chicago, IL, USA) was placed below the frame, so that when the cylinder was pressurized its piston would travel upward, pushing the aluminum frame away from the base. The cylinder can be connected to an air compressor so that it can be pressurized. There is a gap in the aluminum frame between the two rollers so that when the cylinder is pressurized, it would cause the bottom roller to make contact with the top roller. The frame was designed so that the two cylinders are close together, but not in contact, when the cylinder is not pressurized. The pressure inside of the cylinder will exert a pressure on the piston of the cylinder when it pushes the cylinder into contact with the aluminum frame. Thus, the equivalent force which is acting through the center of the frame will push down on the rollers, causing an approximately uniform pressure distribution over the line of contact of the rollers, excluding the edges of the rollers [3].

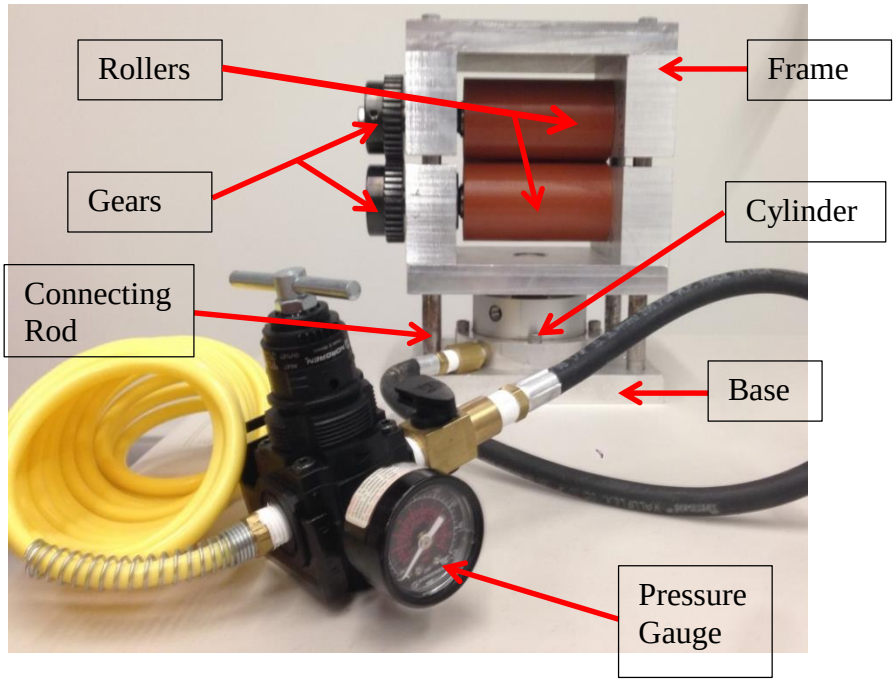

Figure 25. Polyuretherane Roller Fixture

Figure 26 shows the approximately uniform pressure distribution at the line of contact between the two cylinders (at points sufficiently far away from the edge of the cylinders), over the cylinders longitudinal axis.

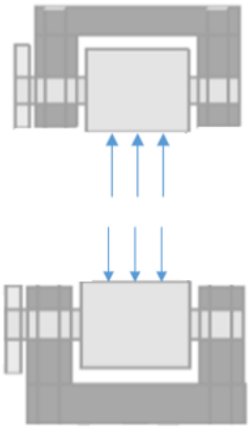

Figure 26. Pressure distribution over line of contact of cylinders

The contact pressure area and the peak contact pressure of the two cylinders can be calculated by using Hertz's contact stress theory. The force that the cylinder's piston would exert on the aluminum frame is proportional to the pressure inside the cylinder, and is given by the manufacturer as 707lb of force for 100psi of pressure inside the cylinder, for a cylinder with a bore of 3 inches. Converting to SI units, and assuming that the force – pressure relation given by the manufacturer can be extrapolated to lower pressures, the force that is exerted by the cylinder on the aluminum frame is given as:

$$F = 4561.2\, P_{cylinder} \tag{3.1}$$

3.2.3.1 Contact between Two Cylinders with Parallel axes

The contact of the fixture can be modeled as contact of two cylinders with parallel axes, so Hertz's contact stress theory, which a theory of elastic contact between bodies, can be used to find the contact area and peak contact pressure of the two cylinders. The assumptions of Hertz's contact stress theory are [12]:

i. Surfaces are continuous and non-conforming
ii. Strains are small
iii. Solids are elastic
iv. Surfaces are frictionless

Assumptions i, ii, iii imply that the contact between the two surfaces is much smaller than the effective radius of curvature of the two surfaces. In the case of this fixture, the two rollers have the same radius, so the effective radius is the same as the rollers radius, which is given as 0.0275m. The half width of the line of contact between the two rollers can be calculated as [12]:

$$b = \sqrt{\frac{2F(1-\nu^2)d}{E\pi l}} \tag{3.2}$$

The resulting contact between the two rollers will be an approximately uniform pressure along the line of contact of the rollers, excluding the edges of the rollers. The maximum pressure of the line of contact between the two rollers can be calculated as [12]:

$$P_{max} = \frac{2F}{\pi b l} \tag{3.3}$$

Using Equations 3.1 – 3.3, the contact width and the maximum pressure of the line of contact between the two rollers can be calculated for various pressures inside of the cylinder. Figure 27 shows the pressure profile for contact between two cylinders.

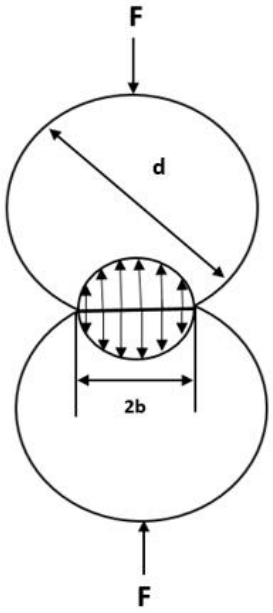

Figure 27. Pressure profile for contact between two cylinders

The pressure gauge on the air compressor was used to determine the air pressure inside of the cylinder. The pressure inside of the cylinder, the force placed on the bottom of the roller, the half width of the line of contact, and the maximum pressure between the rollers are given in Table 7 for 0.14MPa (20psi) to 0.55MPa (80psi) in increments of 0.14MPa.

Table 7. Maximum pressure and contact width of the line of contact between the rollers for a range of pressures inside the cylinder

Pressure inside Cylinder ($P_{cylinder}$) [MPa]	Force (F) [N]	Contact Half Width (b) [m]	Maximum Pressure (P_{max})[MPa]
0.14	628.98	0.0009	4.39
0.28	1257.96	0.0013	6.20
0.41	1886.94	0.0016	7.60
0.55	2515.91	0.0018	8.77

3.2.3.2 Calibration Data

The sensor was rolled through the rollers, one side at a time, with an approximately uniform pressure distribution over the line of contact of the rollers, as shown in Figure 28. The peak pressure over the line of contact was calculated using Equations 3.1 – 3.3. The time-dependent pressure (dynamic pressure) was recorded as the sensor was passed through the rollers. The output of the sensor was exported as an array in an ASCII file, and imported into a programing environment to calculate the maximum output of each cell as the sensor was passed though the rollers. The algorithm for this is given in Appendix A. However, due to the high peak pressures generated between the rollers, as shown in Table 7, only the Default and Low3 sensitivity settings were able to be calibrated using the rollers. One sensor (n=1) was used for testing.

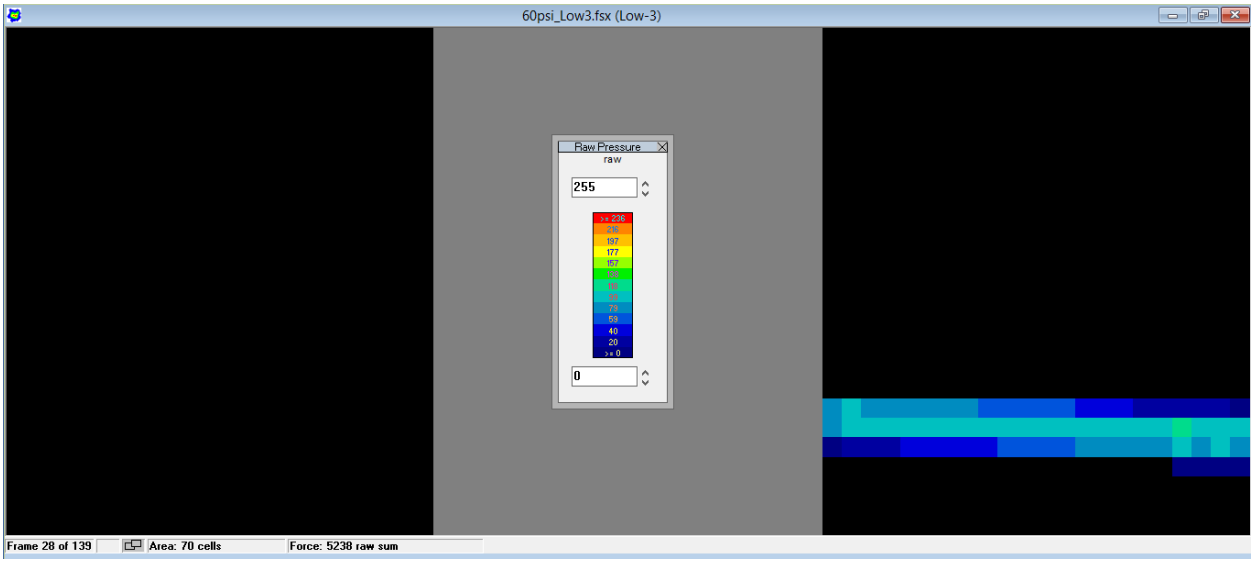

Figure 28. Output of the sensor to the applied pressure from the polyurethane rollers

Each side of the sensor was loaded separately, and the peak value for raw output for each cell of the sensor was determined. Then the average raw output of the sensor was calculated as the total raw output (determined by the sum peak value for raw output for each cell) divided by the number of cells in the sensor. Table 8 shows the average raw output for each side of the sensor, and the sensor as a whole, as a result of the pressure applied by the rollers for the Default sensitivity setting. Table 8 also shows the standard deviation of the average raw output for each side of the sensor, which gives an indication of the spatial variation of the sensor. Note that each pressure reading was taken twice, and the average of the two readings was reported.

Table 8. Average raw output as a result of applied pressure for the Default sensitivity setting

Applied Pressure [MPa]	Side A		Side B		Average Raw Output (Both Sides)
	Average Raw Output	Stand. Dev.	Average Raw Output	Stand. Dev.	
0.00	0.00	0.00	0.00	0.00	0.00
4.39	161.39	6.49	165.52	10.10	163.45
5.11	174.58	7.27	184.96	8.52	182.14
5.84	190.58	7.46	208.65	7.89	198.23
6.20	200.30	7.90	217.48	6.24	208.89

Figure 29 shows the applied pressure as a function of raw output for the Default sensitivity setting. The trend line is strongly linear (r^2=0.99). However, the sensor is not calibrated for the whole range of raw output (0 – 255), since the lowest pressure above 0Mpa that can be applied by the rollers is 4.39MPa (which is generated by 0.14MPa of pressure inside of the cylinder, as shown in Table 7), and no more pressure can be applied to the sensor once the first cell has become saturated (reaches a value of 255), which occurs at a maximum pressure of 6.20MPa between the rollers.

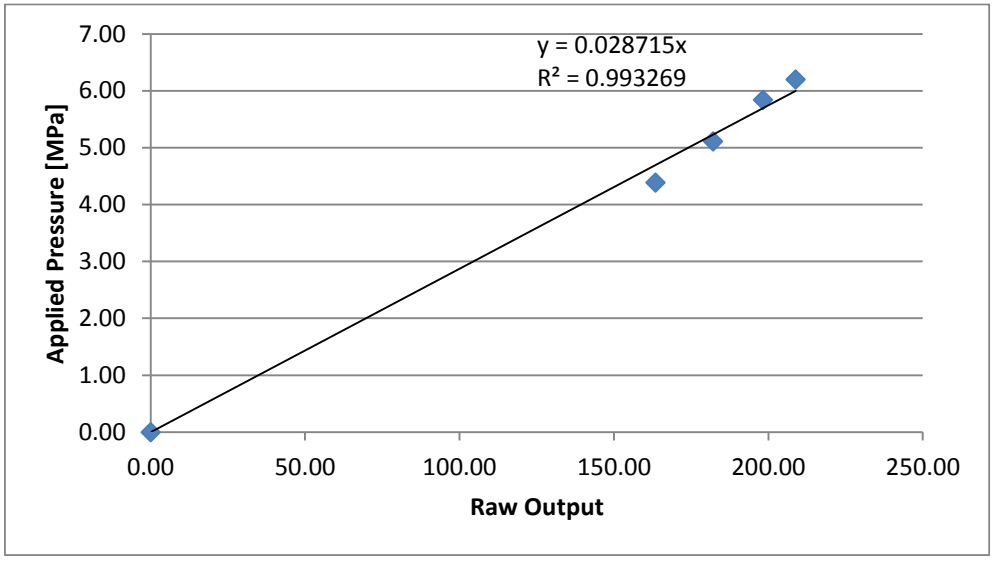

Figure 29. Applied pressure as a function of raw output for the Default sensitivity setting

Table 9 shows the average raw output as a result of the applied pressure for each side of the sensor, and the sensor as a whole (both sides) as a result of the pressure applied by the rollers for the Low3 sensitivity setting.

Table 9. Average raw output as a result of applied pressure for the Low3 sensitivity setting

Applied Pressure [MPa]	Side A		Side B		Average Raw Output (Both Sides)
	Average Raw Output	Stand. Dev.	Average Raw Output	Stand. Dev.	
0.00	0.00	0.00	0.00	0.00	0.00
4.39	74.73	3.12	77.20	1.85	75.97
5.11	85.12	2.81	88.14	2.87	86.23
5.84	96.58	2.58	99.35	3.12	98.52
6.20	101.86	2.17	105.48	3.91	103.67
6.92	109.52	2.41	112.87	4.42	110.89
7.60	118.11	2.97	120.64	5.56	119.38

Figure 30 shows the output as a function of applied pressure for the Low3 sensitivity setting. The trend line is strongly linear (r^2=0.99). However, the sensor is not calibrated for the whole range of raw output (0 – 255), since the lowest pressure that can be applied by the rollers is 4.39MPa (which is generated by 0.14MPa of pressure inside of the cylinder, as shown in Table 7 above), and no more pressure can be applied to the sensor once the first cell has become saturated (reaches a value of 255), which occurs at a maximum pressure of 7.60MPa between the rollers.

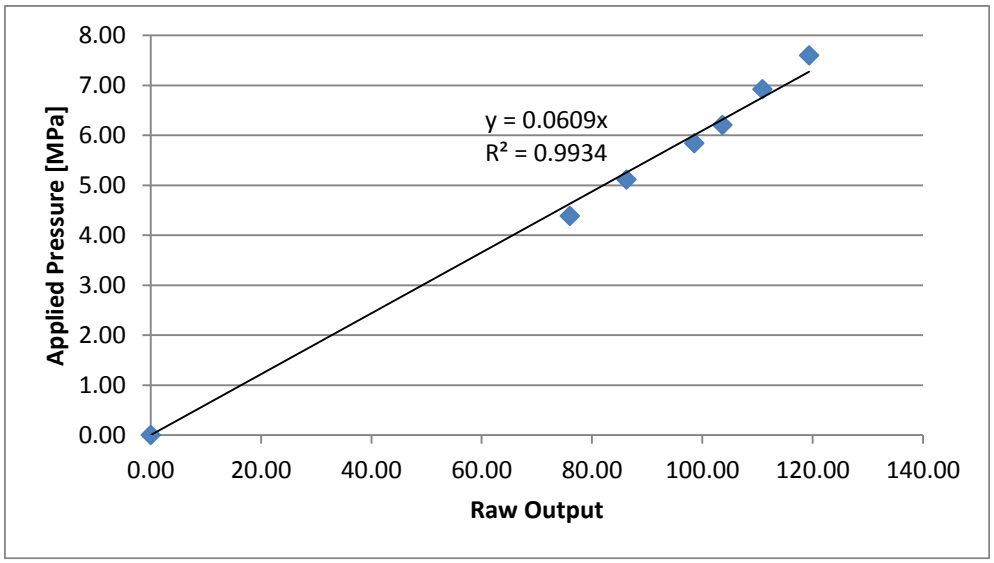

Figure 30. Raw output as a function of applied pressure for the Low3 sensitivity setting

3.2.3.3 Limitations

The trend line of the plot of the applied pressure as a function of the raw output can be used to calibrate the sensor because it establishes the relation between the raw output of a cell and the pressure applied to it. However, a limitation of using the rollers is that the peak pressure applied to the sensor by the rollers does not allow for the calibration of all the sensitivity settings (since the lowest pressure that can be applied by the rollers is 4.39MPa, as shown in Table 7). Also, the calibration will not be based on the entire range of output of the sensor (0 – 255), since no more pressure can be applied to the sensor once the first cell has become saturated (reaches a value of 255), which occurred at 6.20MPa for the Default sensitivity setting and 7.60MPa for the Low3 sensitivity setting.

3.2.4 Calibration Summary

Figure 31 shows a comparison of calibrated output of the three calibration methods as a function of raw output (0-255) for the Default sensitivity setting (a similar trend can be observed for all the sensitivity settings). Note that one sensor was used to collect data for the bladder, three sensors were used to collect data for the materials testing machine, and one sensor was used to collect data for the rollers. A new sensor was used for each calibration. Thus, variability between the calibrated outputs can be attributed to both using different sensors as well as the method of calibration used. Data for all sensitivity settings is given in Appendix B.

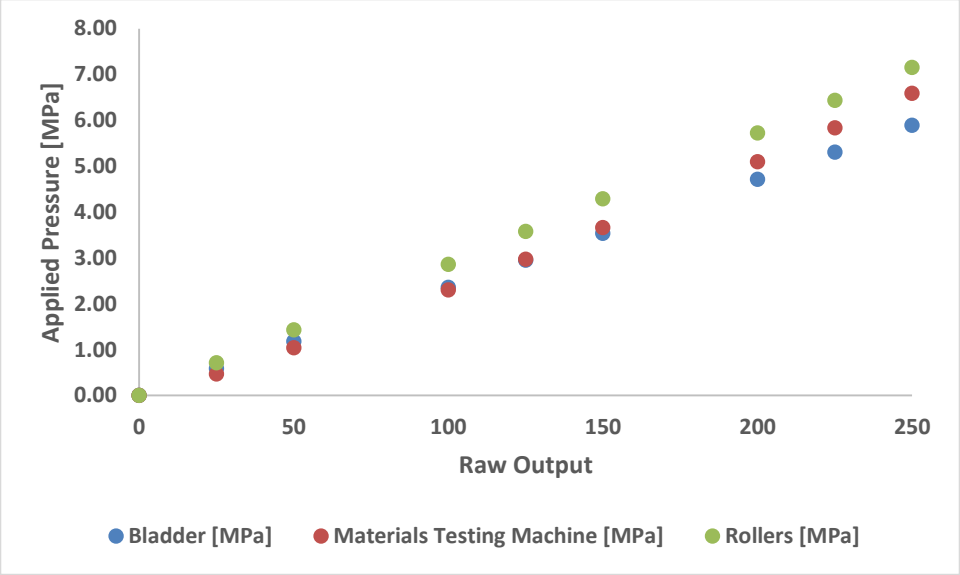

Figure 31. Comparison of calibrated output [MPa] of the three calibration methods as a function of raw output for the Default sensitivity setting

Figure 31 above shows that initially (raw output less 50), all three methods of calibration produce roughly the same applied pressure. However, as raw output is increased, the value for applied pressure given by the bladder's calibration is the highest, and the value for applied

pressure given by the rollers calibration is the lowest. While the bladder and roller method of calibration were both based on an approximately uniform pressure distribution, the bladder method was only able to calibrate the sensor for a range of 0-0.14MPa (High2, High1, Mid2, Mid1, and Default sensitivity settings) and the roller method was only able to calibrate the sensor starting at a pressure (aside from 0MPa) of 4.39MPa (Default and Low3 sensitivity settings). The materials testing machine's calibration data will be used in this study because it includes data for all six sensitivity settings, as well as the longest calibration range for each sensitivity setting (High2, High1, Mid2, Mid1, Default, and Low3).

4.0 EXPERIMENTAL RESULTS

4.1 AXIAL LOADING

For axial loading, 1000N of loading was applied to the testing fixture using a materials testing machine. The knees were first tested under axial loading at 0, 15, 30, and 45 degrees of flexion with the native ACL intact. Thereafter, the ACL was removed and double-bundle ACL reconstruction was performed. Three different graft fixation tensions were used: AM/PL: 30N/10N (referred to as "Recon 1"), AM/PL: 10N/30N (referred to as "Recon 2"), and AM/PL: 40N/40N (referred to as "Recon 3." After each reconstruction, the knees were again tested under axial loading at 0, 15, 30, and 45 degrees of flexion. Pressure readings were taken for each loading test.

4.1.1 Sample Sensor Output

Figure 32 - Figure 35 show the output (pressure distribution in MPa) of the sensor for 0, 15, 30, and 45 degrees in the intact state for a left knee. As the knee is flexed, the pressure distribution tends to shift posteriorly. The entire pressure distribution is not captured by the sensor, which is a limitation of the sensor because the peak contact pressure and location of peak contact pressure between the tibia and the femur will be assumed to be captured by the sensor. Also, the location of center of pressure will be affected by not capturing the entire pressure distribution.

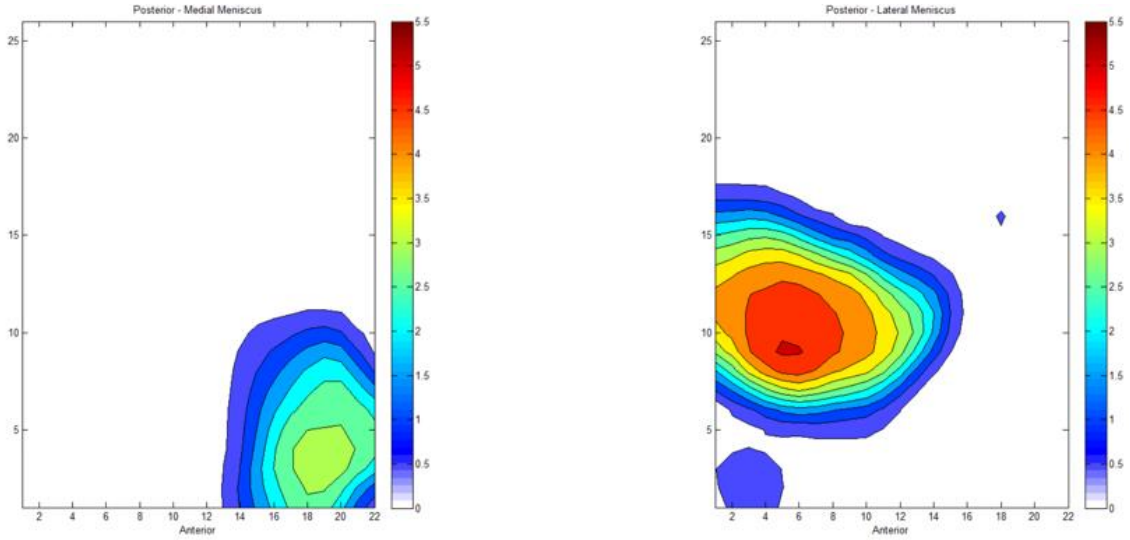

Figure 32. Pressure distribution [MPa] of the sensor at 0 degrees of flexion

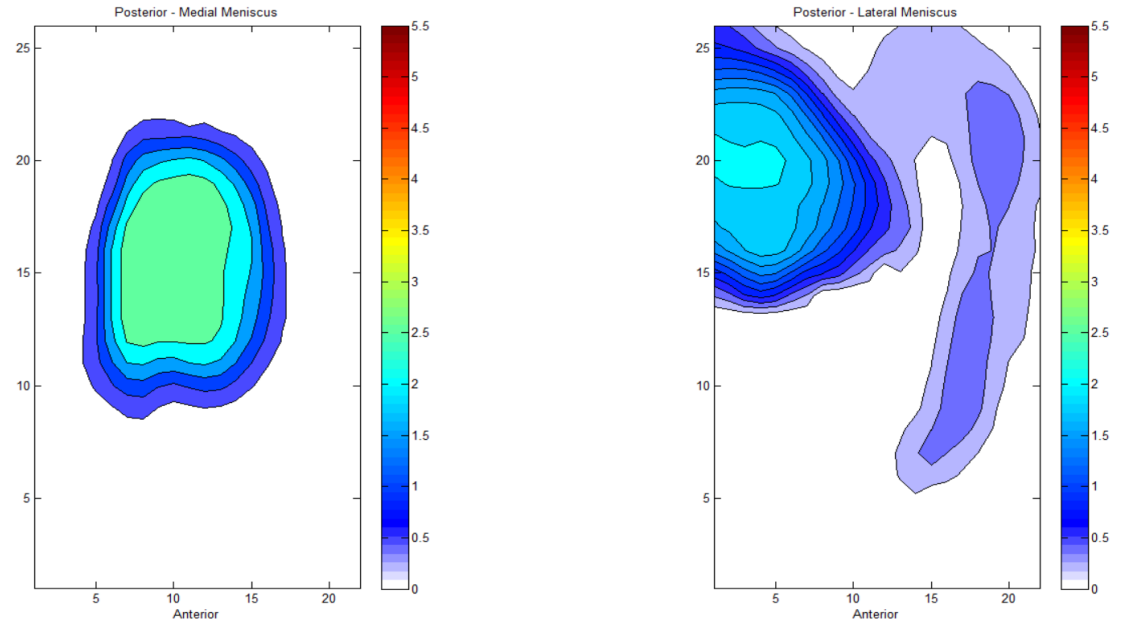

Figure 33. Pressure distribution [MPa] of the sensor at 15 degrees of flexion

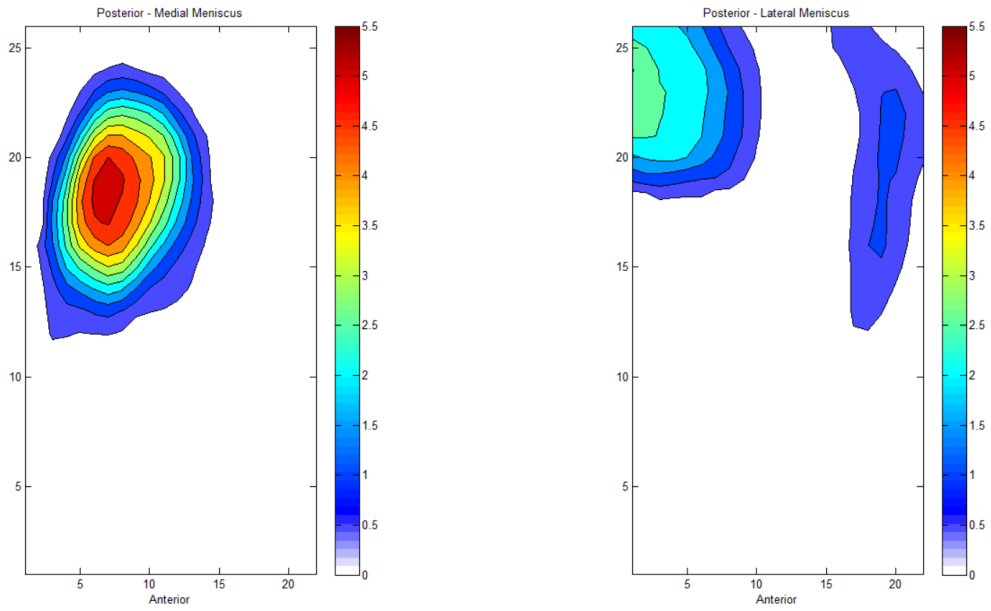

Figure 34. Pressure distribution [MPa] of the sensor at 30 degrees of flexion

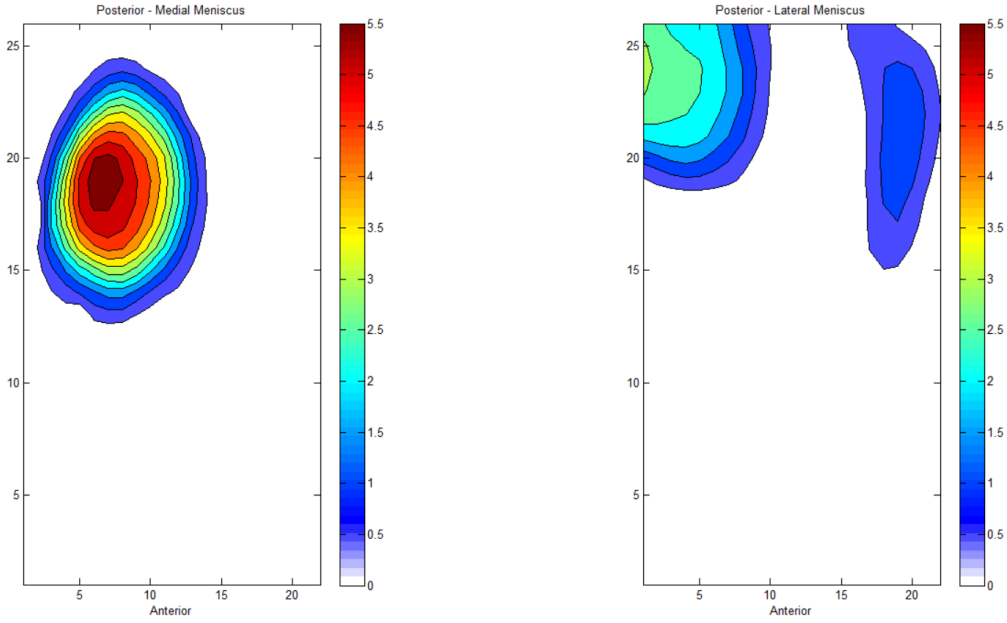

Figure 35. Pressure distribution [MPa] of the sensor at 45 degrees of flexion

4.1.2 Peak Pressure

The average peak pressure and standard deviation for all 12 samples is shown in Figure 36 for 0 degrees of flexion, Figure 37 for 15 degrees of flexion, Figure 38 for 30 degrees of flexion, and Figure 39 for 45 degrees of flexion. Complete data for each specimen is listed in Appendix C. No statistical significance was found between the intact state and any of the reconstructions for either the lateral or medial tibio-femoral compartments at any of the flexion angles.

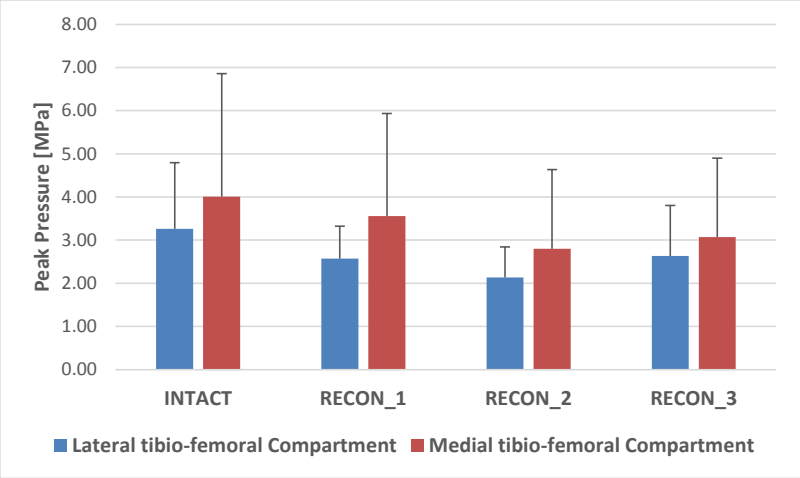

Figure 36. Average peak pressure and standard deviation at 0 degrees of flexion in the lateral and medial tibio-femoral compartments

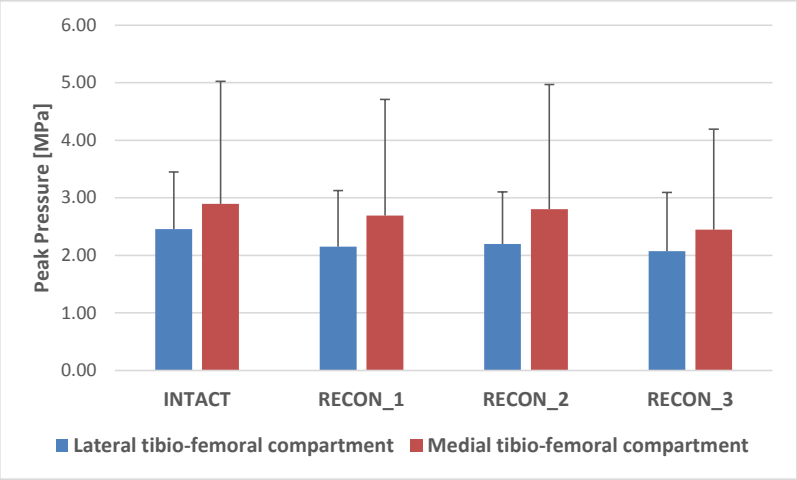

Figure 37. Average peak pressure and standard deviation at 15 degrees of flexion in the lateral and medial tibio-femoral compartments

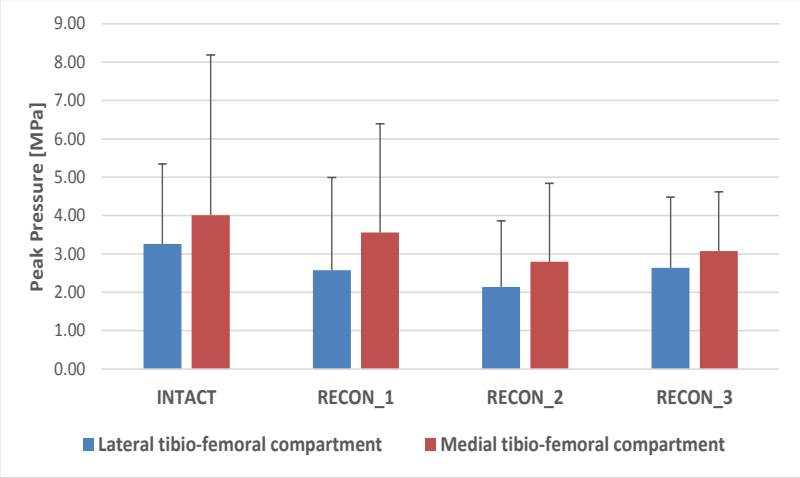

Figure 38. Average peak pressure and standard deviation at 30 degrees of flexion in the lateral and medial tibio-femoral compartments

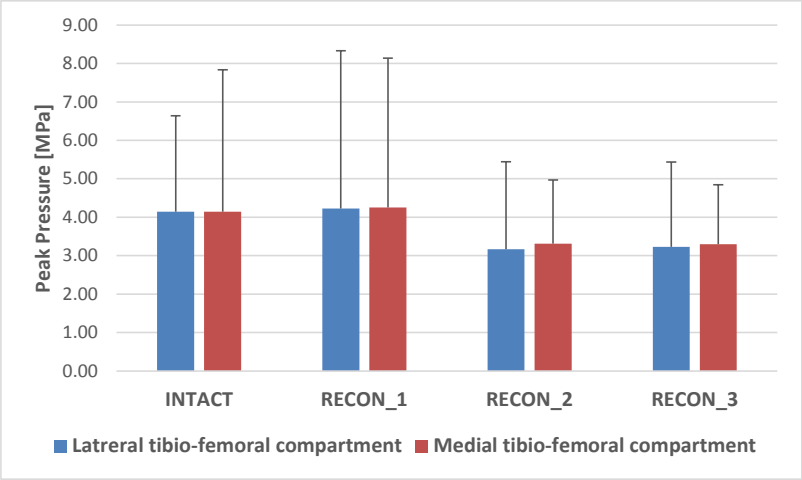

Figure 39. Average peak pressure and standard deviation at 45 degrees of flexion in the lateral and medial tibio-femoral compartments

The average lateral tibio-femoral compartment peak pressure is slightly higher than the average medial tibo-femoral compartment peak pressure (around 10 – 20 percent difference) for 0, 15 and 30 degrees of flexion. The average peak pressure in both compartments is about the same for 45 degrees of flexion. Since the standard deviations of the peak pressure in both the medial and lateral tibio-femoral compartments at 0, 15, 30, and 45 degrees of flexion are large with respect to their averages, a clear trend of how the location of peak pressure changes cannot be established.

4.1.3 Change in Location of Peak Pressure

The average change in location of peak pressure and standard deviation between each reconstruction and the Intact state for all 12 samples is shown in Figure 40 and Figure 41 for 0 degrees of flexion, Figure 42 and Figure 43 for 15 degrees of flexion, Figure 44 and Figure 45 for 30 degrees of flexion, Figure 39 for 45 degrees of flexion. Complete data for each specimen is listed in Appendix C. No statistical significance was found between the changes in location of

peak pressure between any of the reconstructions for either the lateral or medial tibio-femoral compartments at any of the flexion angles.

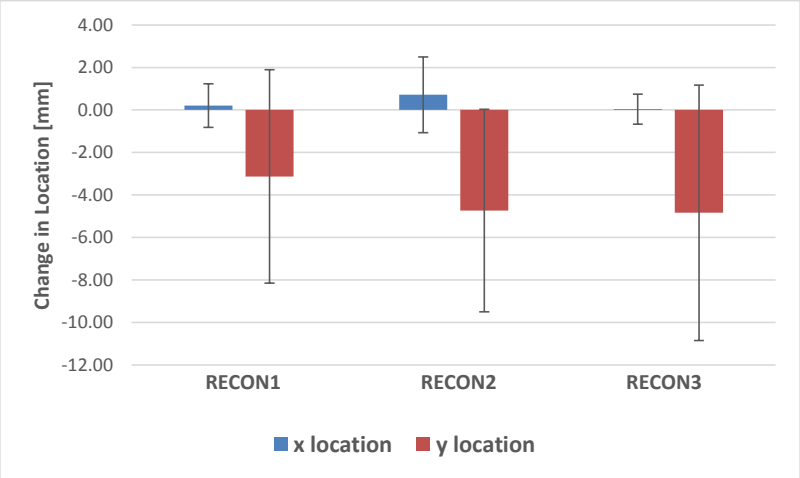

Figure 40. Average change in location of peak pressure and standard deviation at 0 degrees of flexion in the lateral tibio-femoral compartment

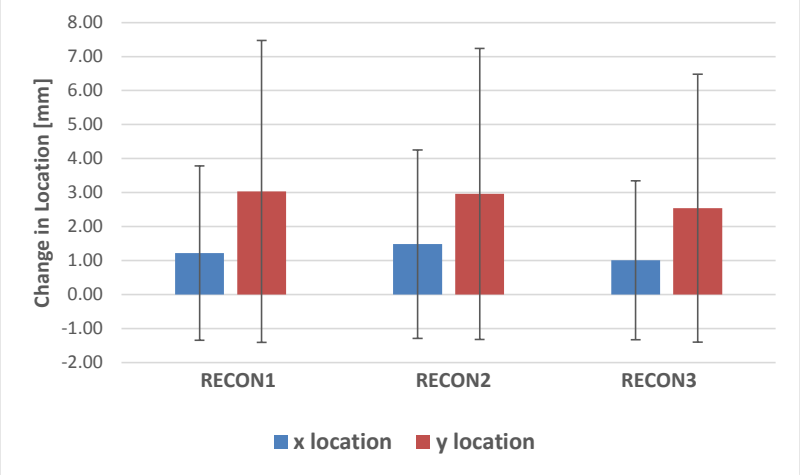

Figure 41. Average change in location of peak pressure and standard deviation at 0 degrees of flexion in the medial tibio-femoral compartment

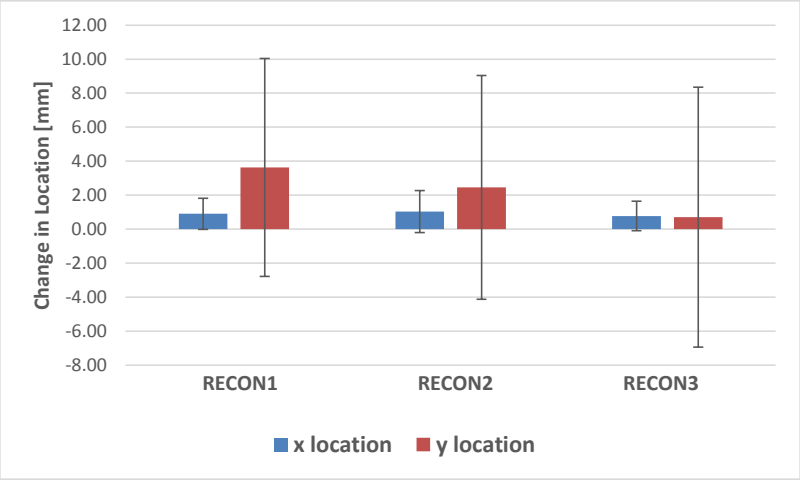

Figure 42. Average change in location of peak pressure and standard deviation at 15 degrees of flexion in the lateral tibio-femoral compartment

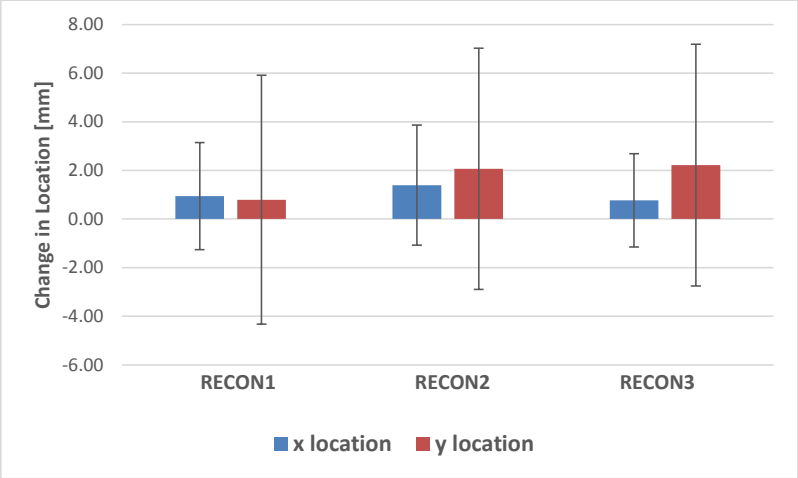

Figure 43. Average change in location of peak pressure and standard deviation at 15 degrees of flexion in the medial tibio-femoral compartment

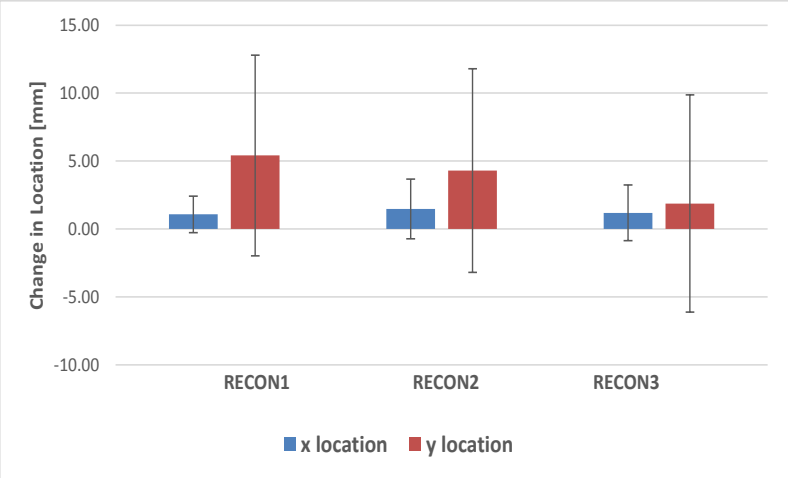

Figure 44. Average change in location of peak pressure and standard deviation at 30 degrees of flexion in the lateral tibio-femoral compartment

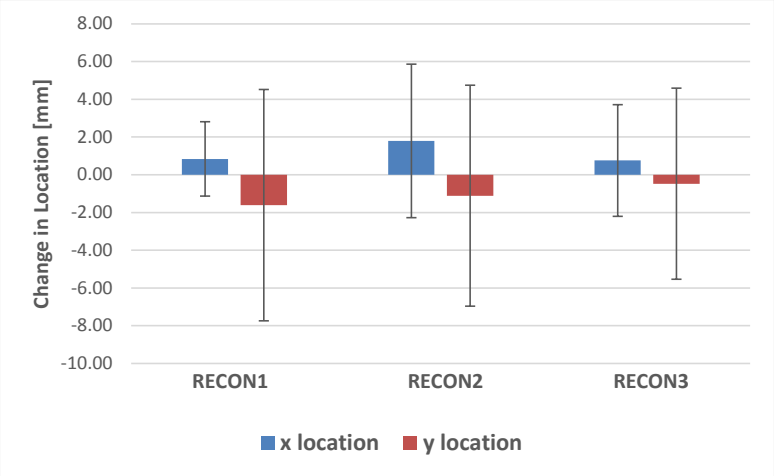

Figure 45. Average change in location of peak pressure and standard deviation at 30 degrees of flexion in the medial tibio-femoral compartment

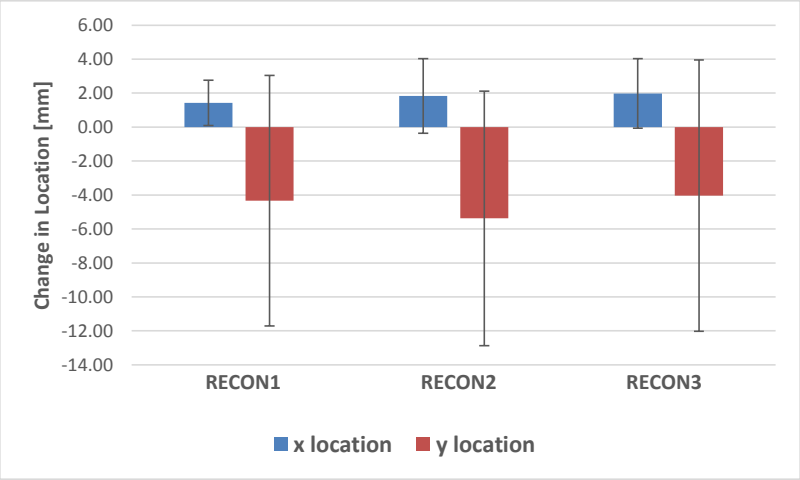

Figure 46. Average change in location of peak pressure and standard deviation at 45 degrees of flexion in the lateral tibio-femoral compartment

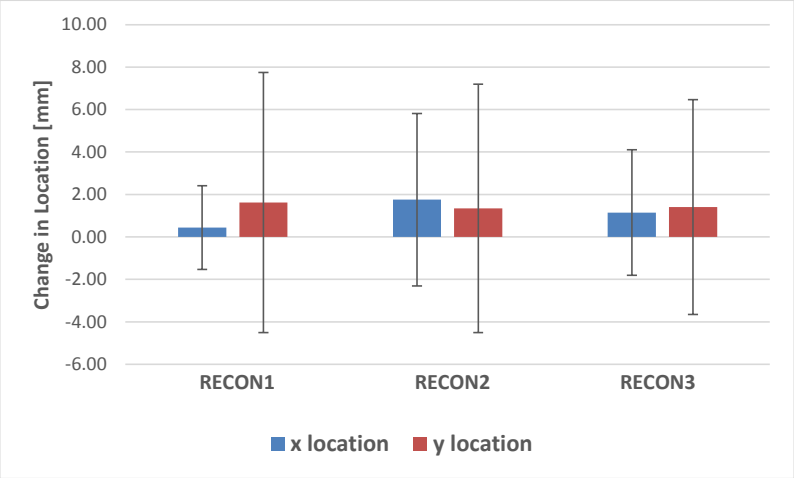

Figure 47. Average change in location of peak pressure and standard deviation at 45 degrees of flexion in the medial tibio-femoral compartment

Since the standard deviations of the change in location of peak pressure in both the medial and lateral tibio-femoral compartments at 0, 15, 30, and 45 degrees of flexion are large with respect to their averages, a clear trend of how the location of peak pressure changes cannot be established.

4.1.4 Change in Location of Center of Pressure

The average change in location of center of pressure between each reconstruction and the Intact state for all 12 samples is shown in Figure 48 and Figure 49 for 0 degrees of flexion, Figure 50 and Figure 51 for 15 degrees of flexion, Figure 52 and Figure 53 for 30 degrees of flexion, Figure 54 and Figure 55 for 45 degrees of flexion. Complete data for each specimen is listed in Appendix C. No statistical significance was found between the changes in location of peak pressure between any of the reconstructions for either the lateral or medial tibio-femoral compartments at any of the flexion angles.

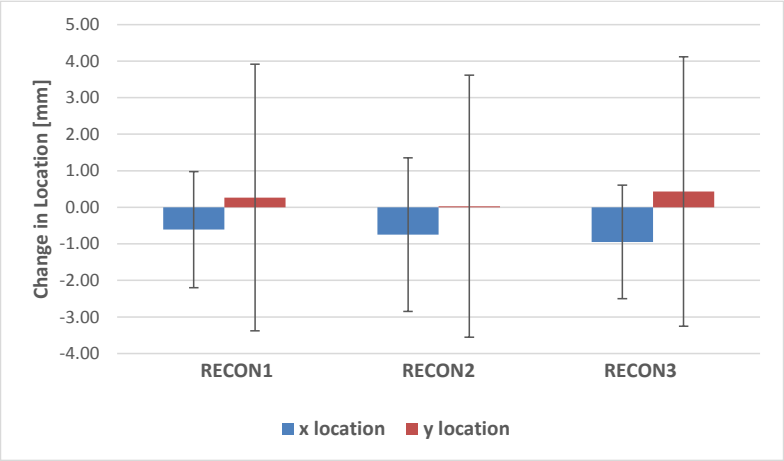

Figure 48. Average change in location of center of pressure and standard deviation at 0 degrees of flexion in the lateral tibio-femoral compartment

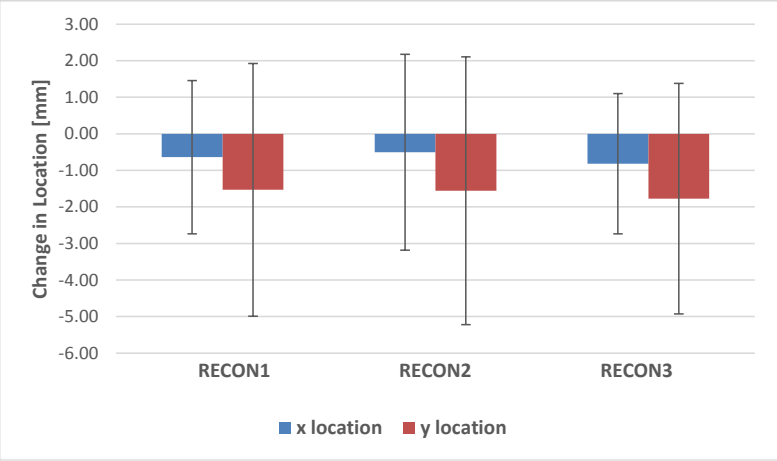

Figure 49. Average change in location of center of pressure and standard deviation at 0 degrees of flexion in the medial tibio-femoral compartment

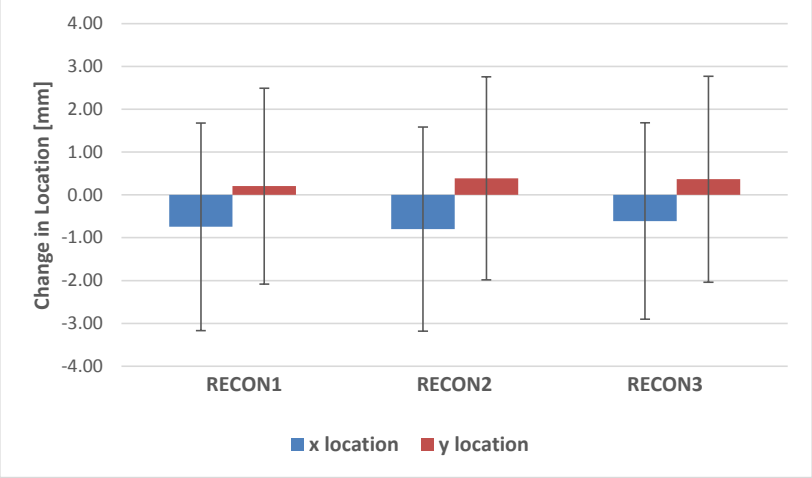

Figure 50. Average change in location of center of pressure and standard deviation at 15 degrees of flexion in the lateral tibio-femoral compartment

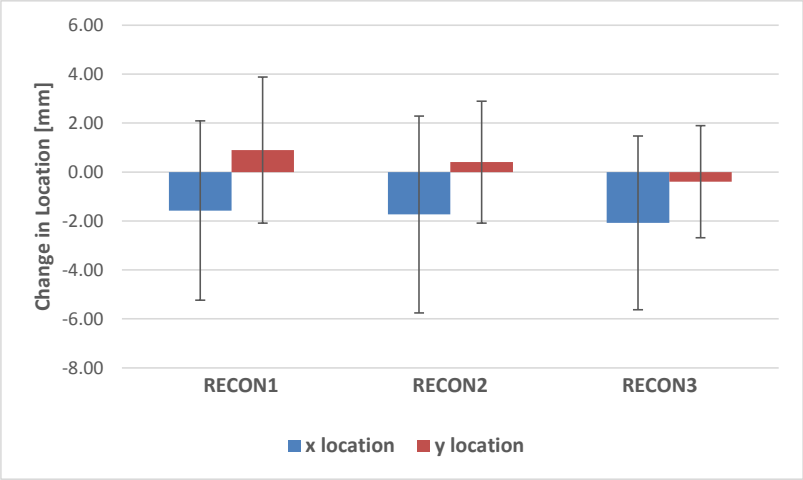

Figure 51. Average change in location of center of pressure and standard deviation at 15 degrees of flexion in the medial tibio-femoral compartment

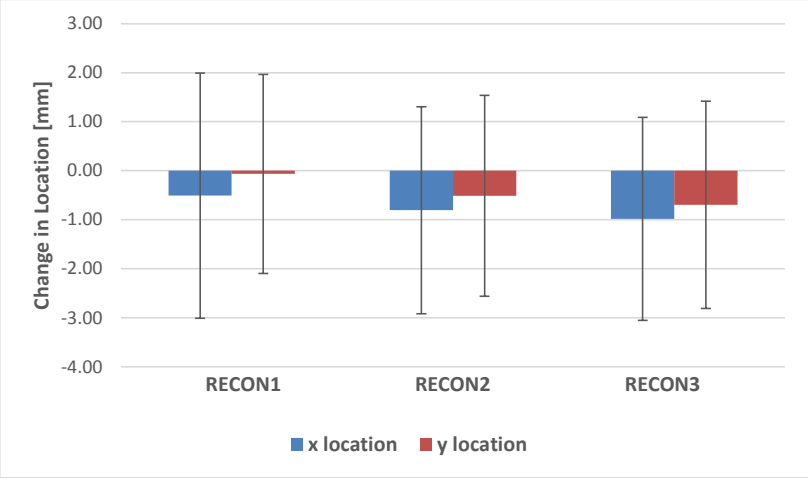

Figure 52. Average change in location of center of pressure and standard deviation at 30 degrees of flexion in the lateral tibio-femoral compartment

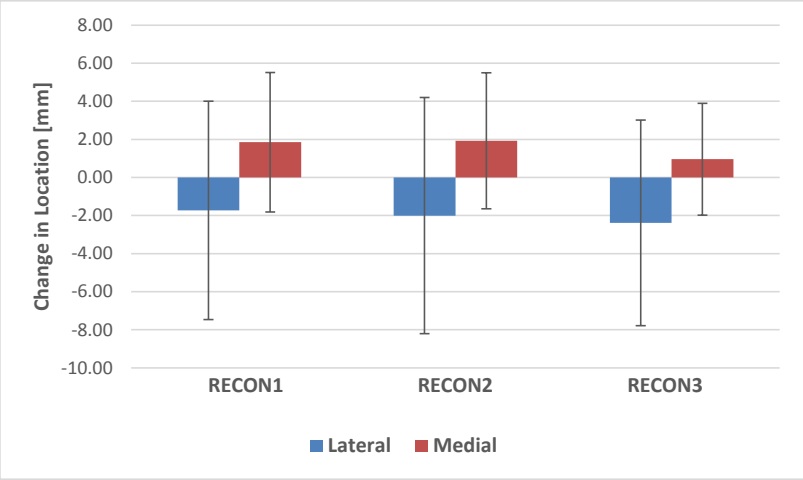

Figure 53. Average change in location of center of pressure and standard deviation at 30 degrees of flexion in the medial tibio-femoral compartment

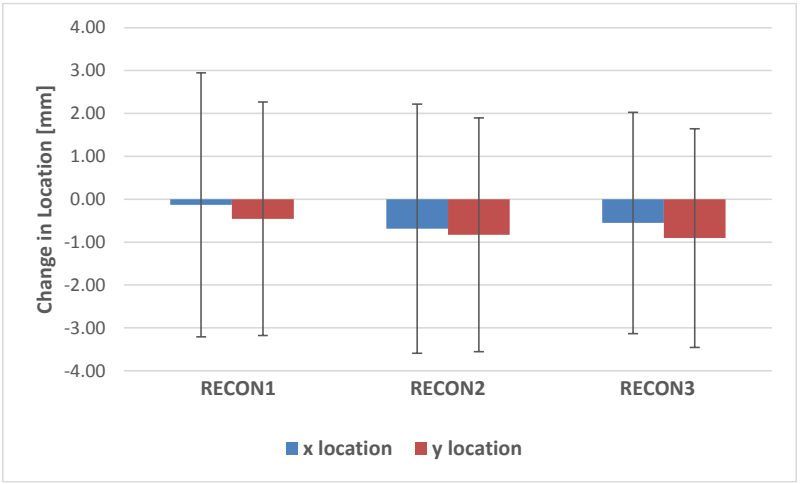

Figure 54. Average change in location of center of pressure and standard deviation at 45 degrees of flexion in the lateral tibio-femoral compartment

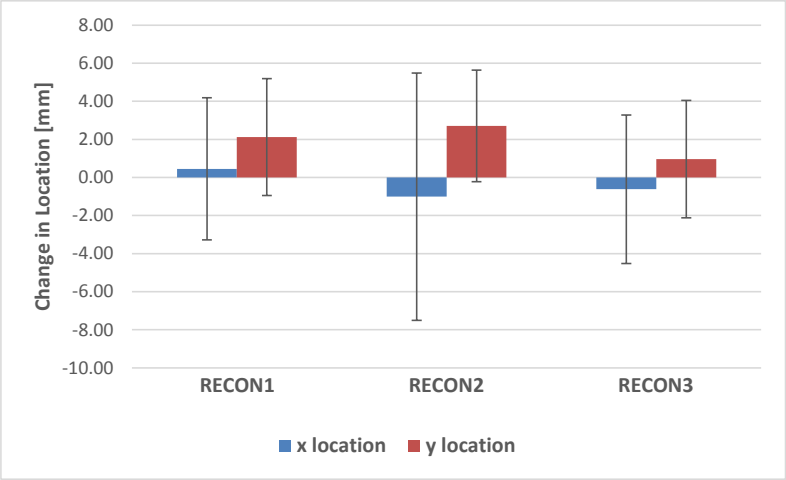

Figure 55. Average change in location of center of pressure and standard deviation at 45 degrees of flexion in the medial tibio-femoral compartment

Since the standard deviations of the change in location of center of pressure in both the medial and lateral tibio-femoral compartments at 0, 15, 30, and 45 degrees of flexion are large with respect to their averages, a clear trend of how the location of peak pressure changes cannot be established.

4.2 GRAFT FIXATION WITHOUT AXIAL LOADING

For graft fixation, no axial loading was placed on the knee. For each reconstruction, the PL bundle was fixed first with the knee at 0 degrees (full extension), and then AM bundle was fixed at 30 degrees. The order that the three ACL reconstructions were performed in the knee was randomized for each specimen. For each reconstruction, pressure readings were collected using the sensor during the fixation of the two ACL bundles as shown in Table 1 above.

4.2.1 Sensor Output

Figure 56 - Figure 62 shows show the output (pressure distribution in MPa) of the sensor during graft fixation (Recon1) for a left knee. The entire pressure distribution is not captured by the sensor, which is a limitation of the sensor because the peak contact pressure and location of peak contact pressure between the tibia and the femur will be assumed to be captured by the sensor. Also, the location of center of pressure will be affected by not capturing the entire pressure distribution.

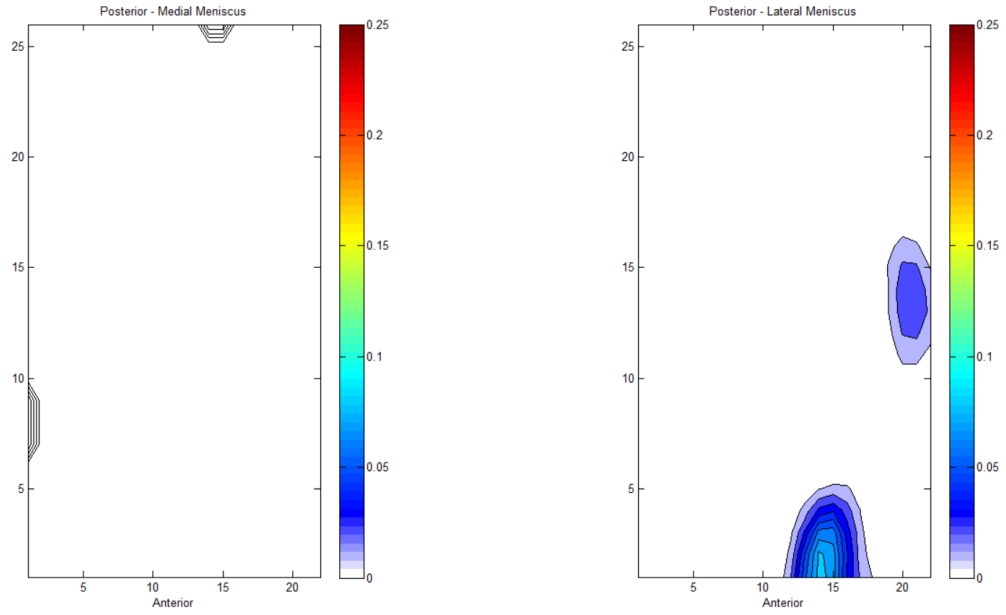

Figure 56. Pressure distribution of [MPa] of 30 degrees with no graft

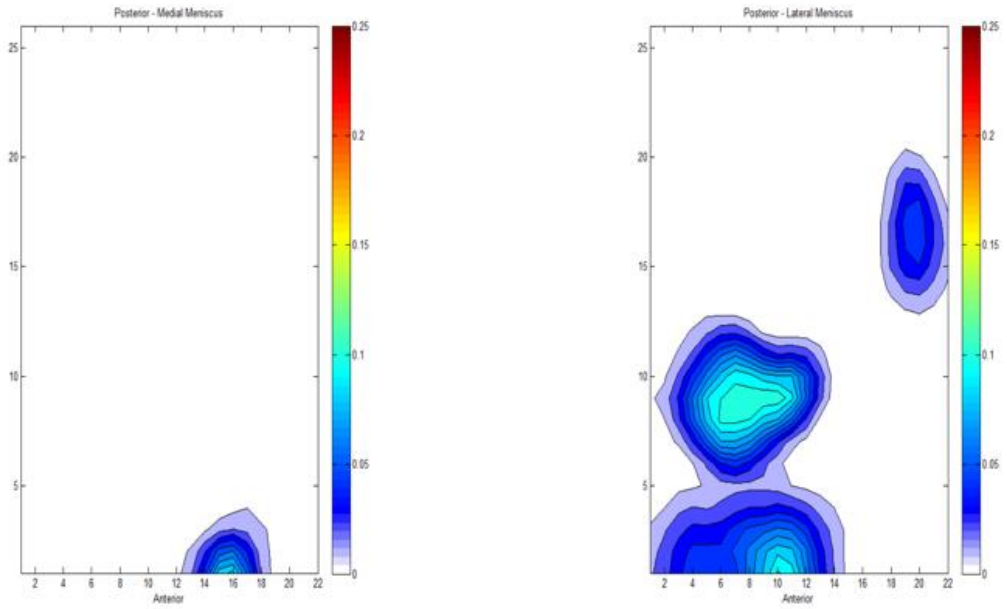

Figure 57. Pressure distribution [MPa] of 0 degrees with no graft

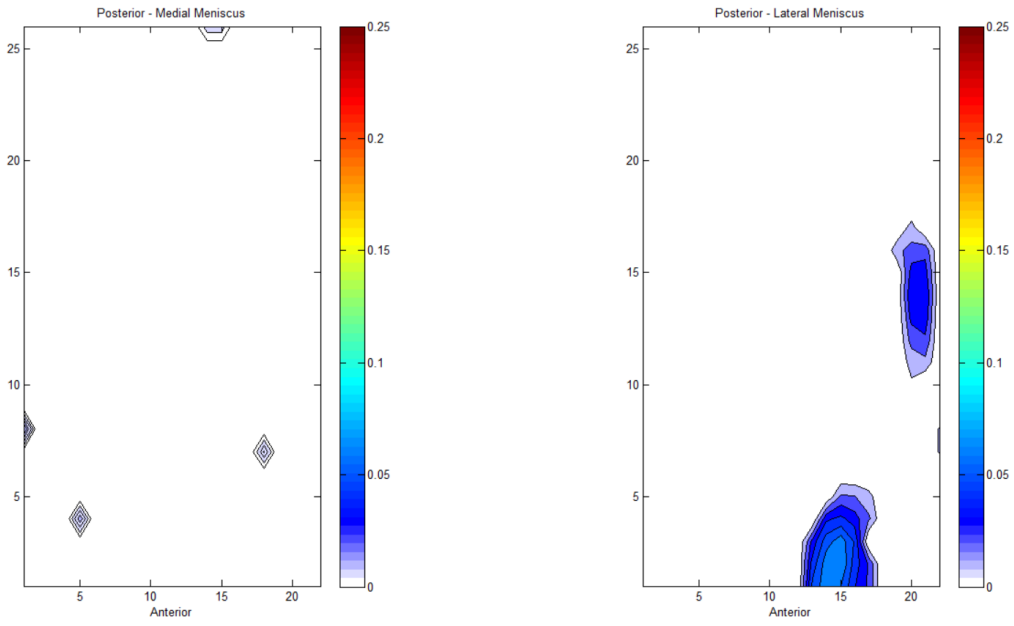

Figure 58. Pressure distribution [MPa] of 0 degrees with PL graft inserted

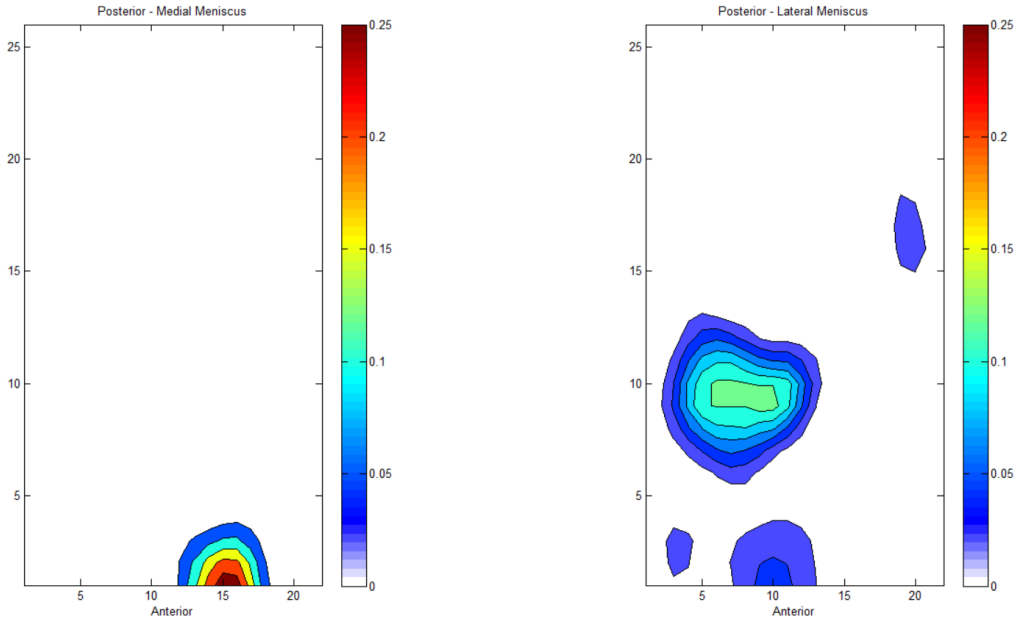

Figure 59. Pressure distribution [MPa] of 0 degrees with PL graft fixed

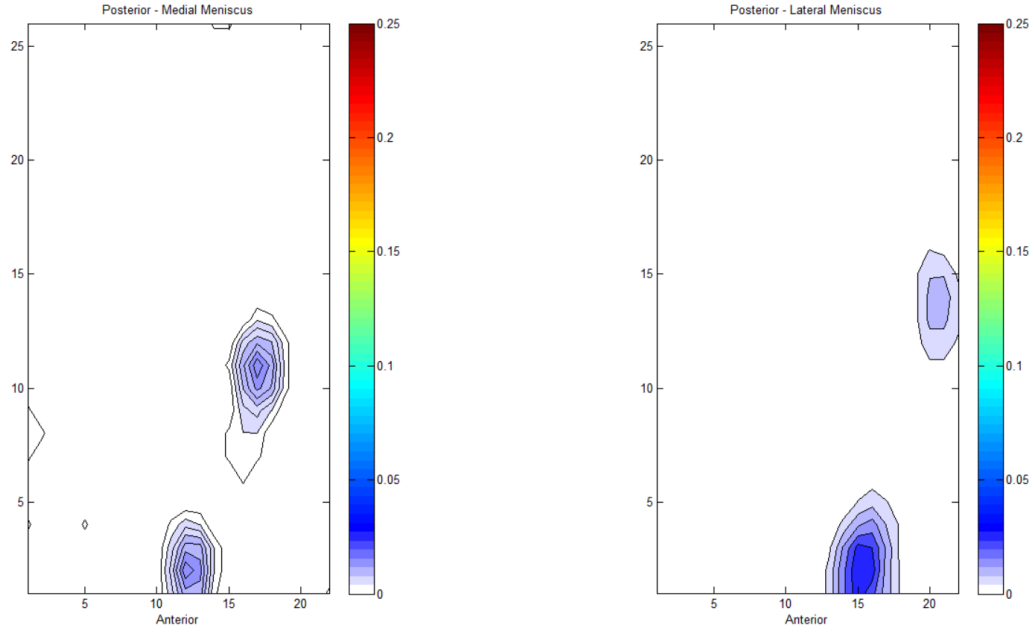

Figure 60. Pressure distribution [MPa] of 30 degrees (PL graft fixed)

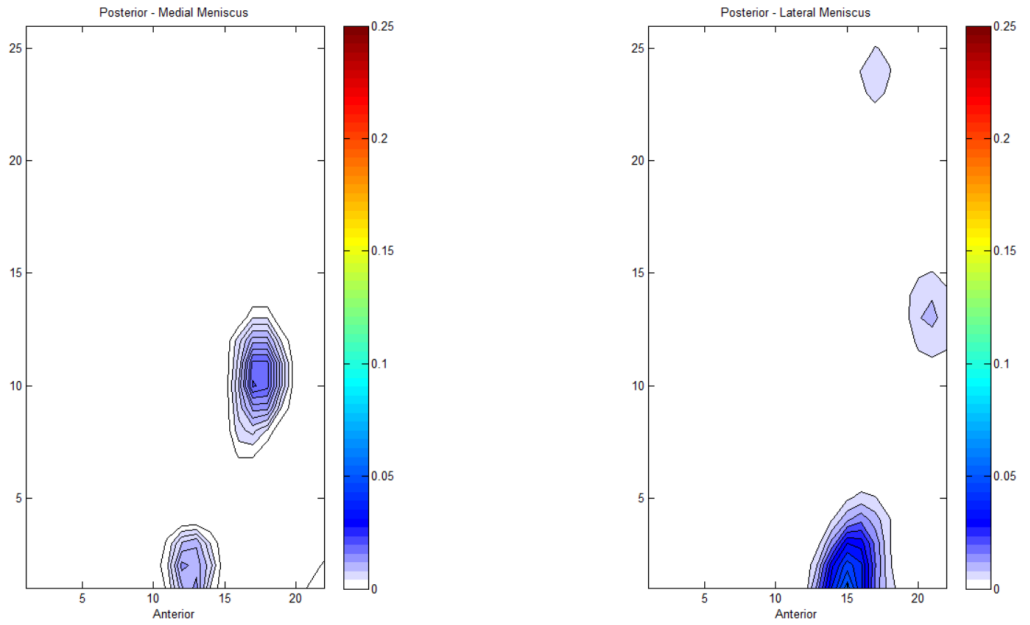

Figure 61. Pressure distribution [MPa] of 30 degrees with AM graft inserted (PL graft fixed)

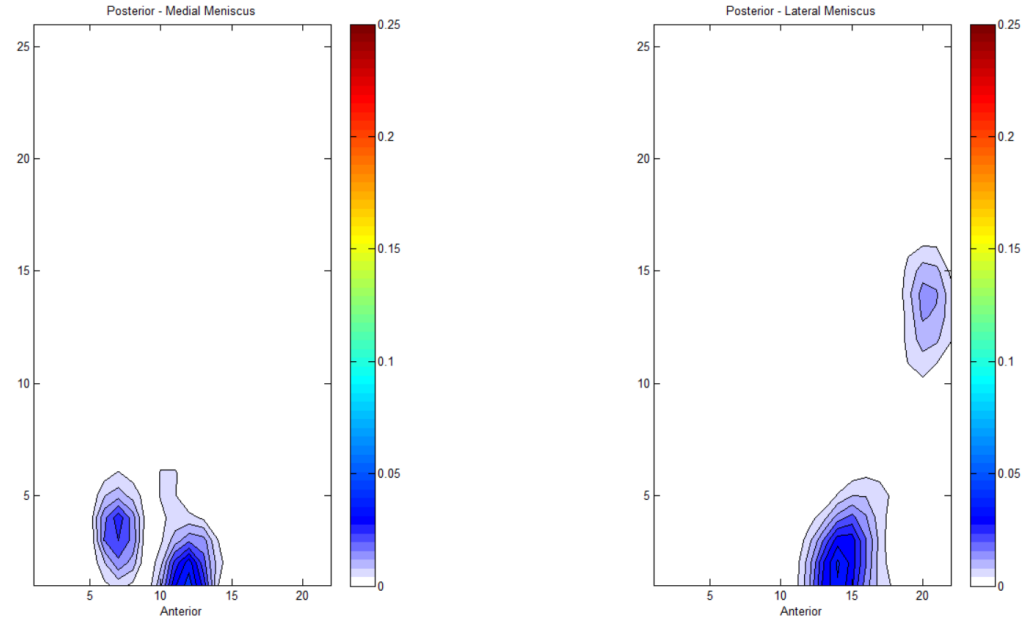

Figure 62. Pressure distribution [MPa] of 30 degrees with AM graft fixed (PL graft fixed)

4.2.2 Peak Pressure

The average peak pressure and standard deviation for each reconstruction for all 12 samples during graft fixation is shown in Figure 63 - Figure 69. Complete data for each specimen is listed in Appendix C. No statistical significance was found between any of the peak pressures of the three reconstructions for either the lateral or medial tibio-femoral compartments at any of the stages during graft fixation.

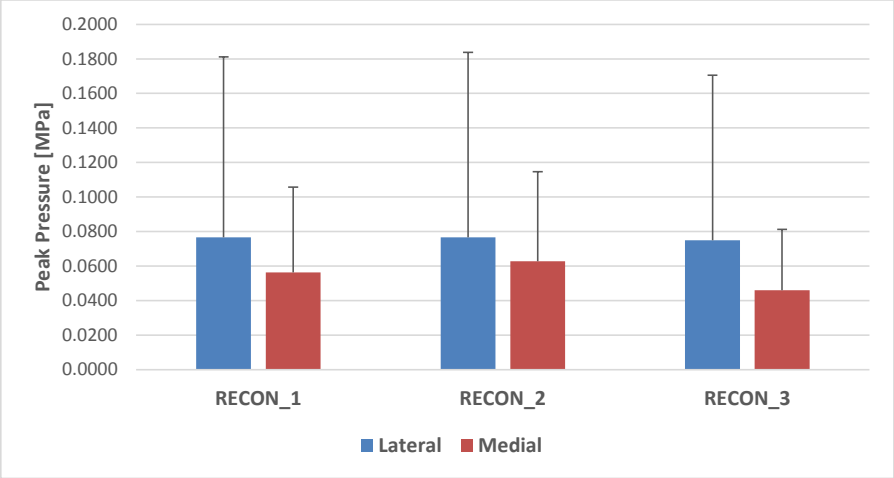

Figure 63. Average peak pressure and standard deviation at 30 degrees of flexion with no graft

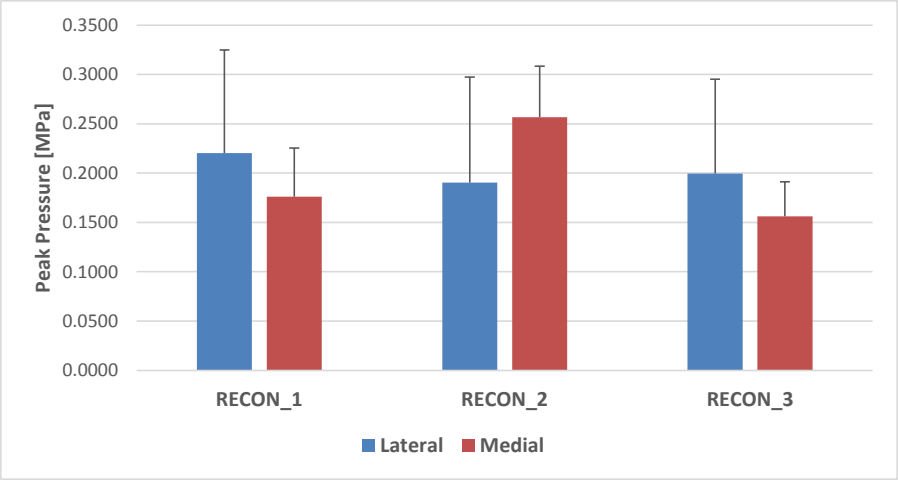

Figure 64. Average peak pressure and standard deviation at 0 degrees of flexion with no graft

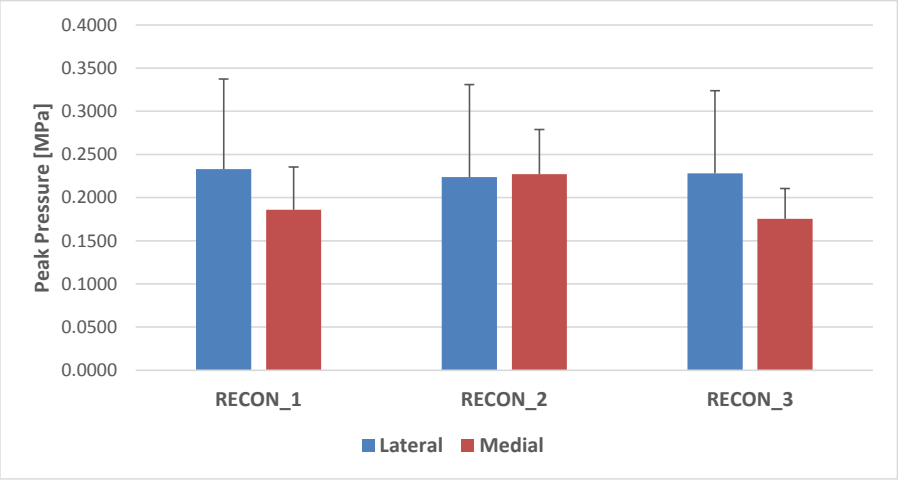

Figure 65. Average peak pressure and standard deviation at 0 degrees of flexion with PL graft inserted

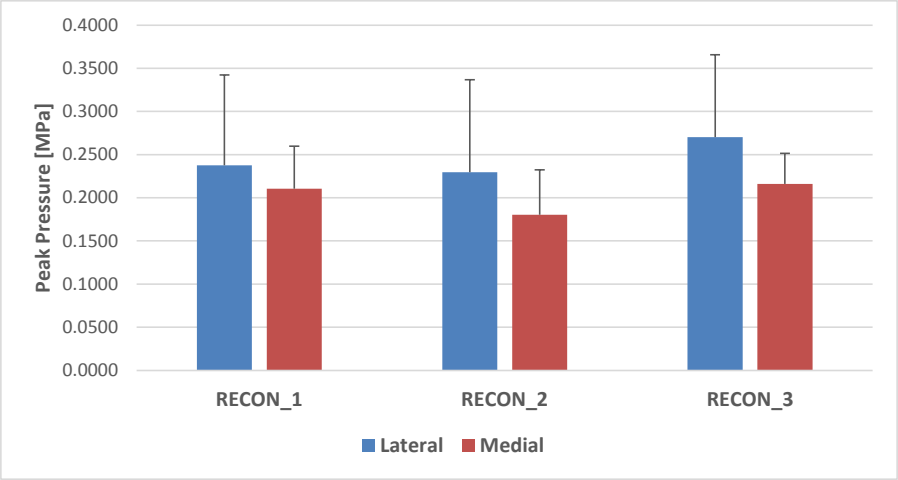

Figure 66. Average peak pressure and standard deviation at 0 degrees of flexion with PL graft fixed

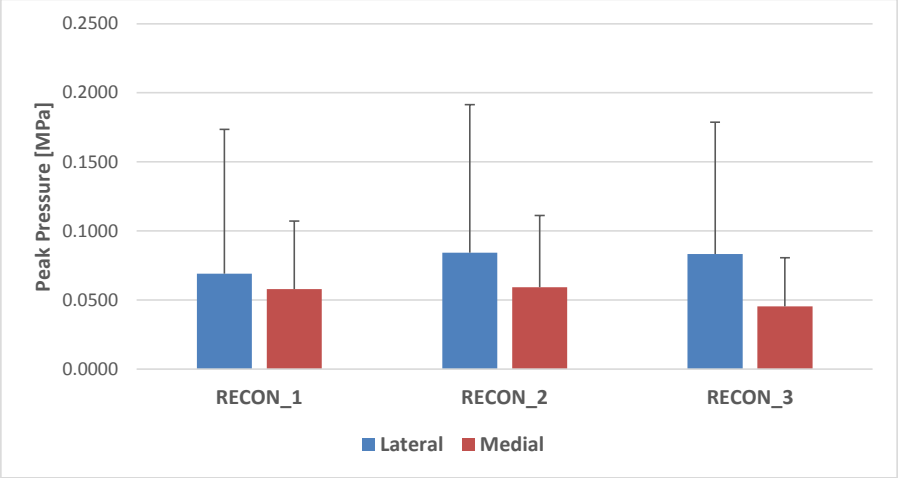

Figure 67. Average peak pressure and standard deviation at 30 degrees of flexion with PL graft fixed

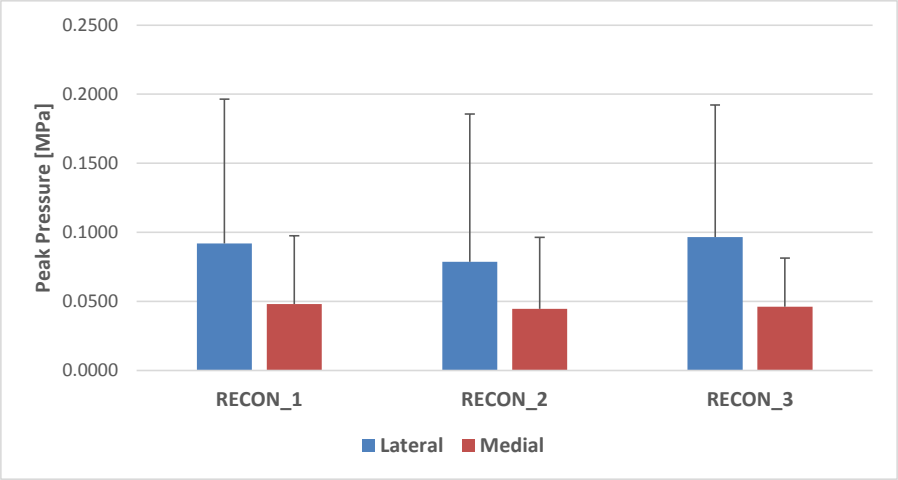

Figure 68. Average peak pressure and standard deviation at 30 degrees of flexion with AM graft inserted and PL graft fixed

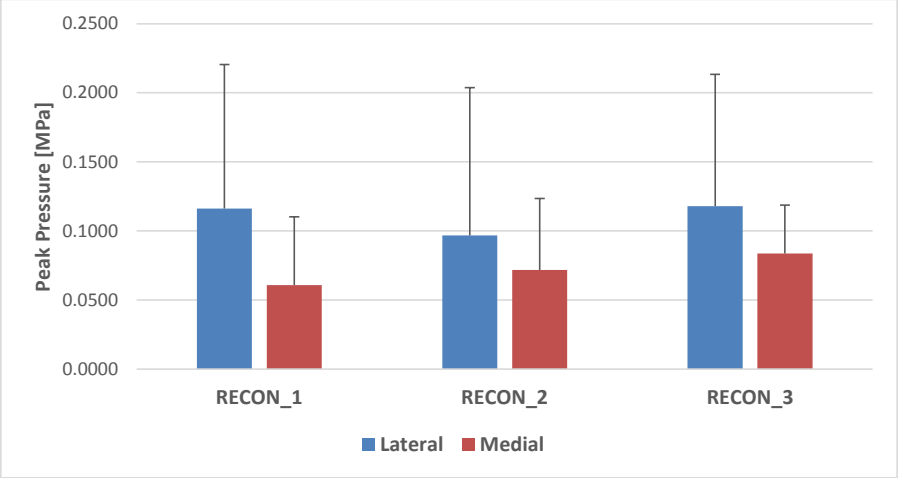

Figure 69. Average peak pressure and standard deviation at 30 degrees of flexion with AM graft fixed and PL graft fixed

Since the standard deviations of the stages of graft fixation are large with respect to their averages, a clear trend of how the change in peak pressure changes during the fixation of the ACL grafts cannot be established.

4.2.3 Change in Location of Peak Pressure

The average change in location of peak pressure (graft fixation protocol given in Table 1 above) and standard deviation for all 12 samples during graft fixation for each reconstruction is shown in Figure 70 - Figure 79. Complete data for each specimen is listed in Appendix C. No statistical significance was found between the changes in location of peak pressure of the deficient knee (no AM or PL graft) and after the PL/AM grafts were inserted or fixed for any of three reconstructions for either the lateral or medial tibio-femoral compartments.

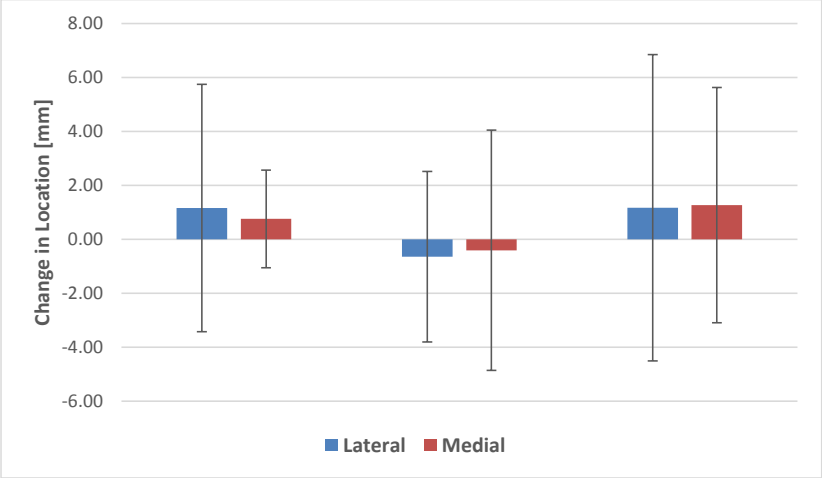

Figure 70. Average change in location of peak pressure and standard deviation between PL graft inserted and no PL/AM graft at 0 degrees of flexion in the lateral tibio-femoral compartment

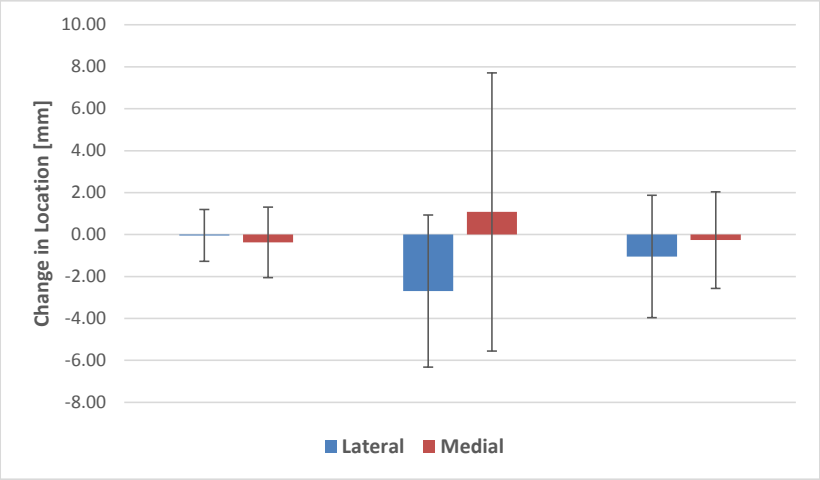

Figure 71. Average change in location of peak pressure and standard deviation between PL graft inserted and no PL/AM graft at 0 degrees of flexion in the medial tibio-femoral compartment

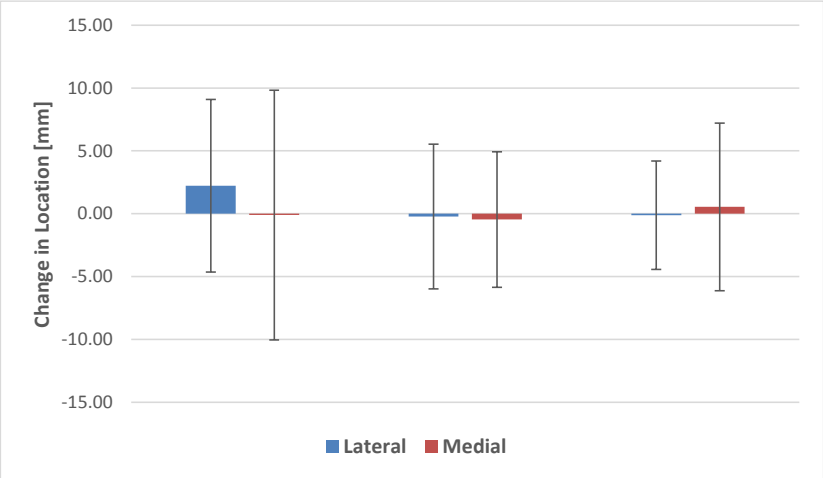

Figure 72. Average change in location of peak pressure and standard deviation between PL graft fixed and no PL/AM graft at 0 degrees of flexion in the lateral tibio-femoral compartment

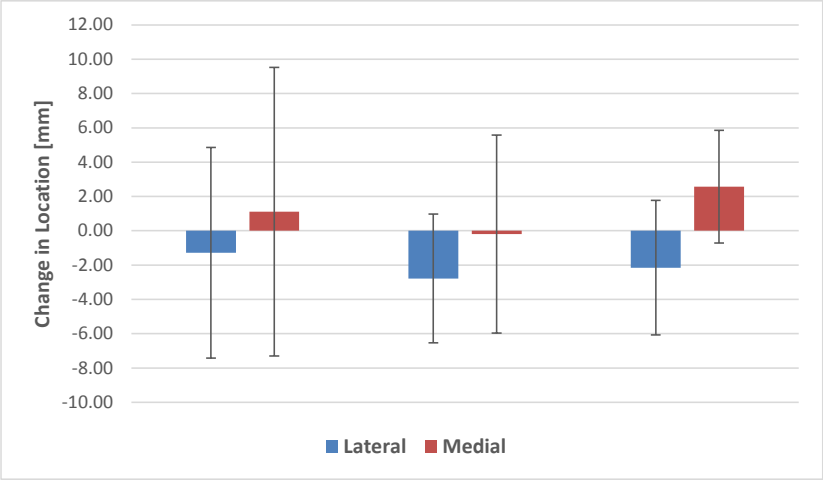

Figure 73. Average change in location of peak pressure and standard deviation between PL graft fixed and no PL/AM graft at 0 degrees of flexion in the medial tibio-femoral compartment

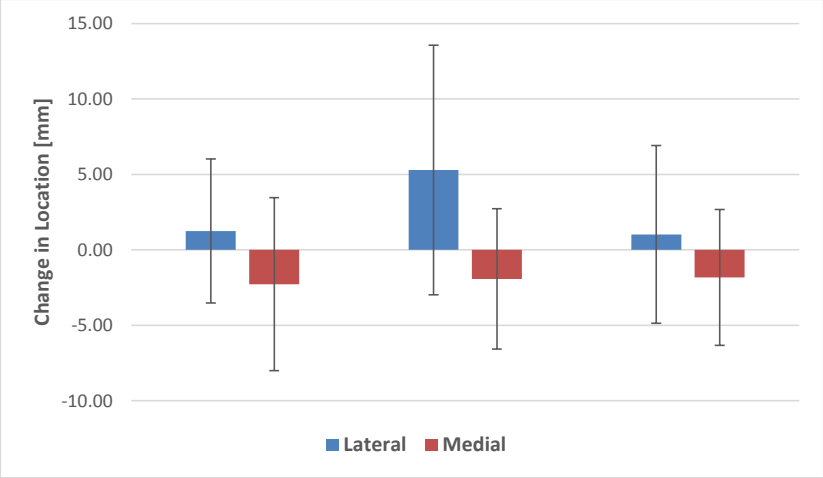

Figure 74. Average change in location of peak pressure and standard deviation between PL graft fixed and no PL/AM graft at 30 degrees of flexion for the lateral tibio-femoral compartment

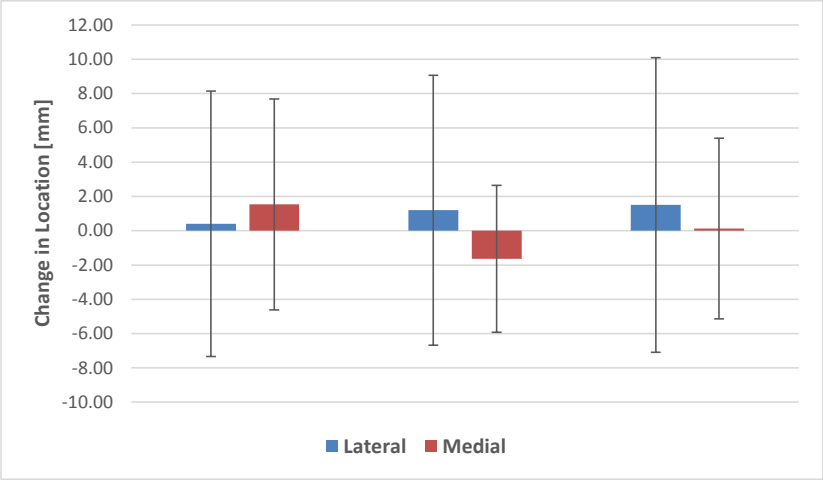

Figure 75. Average change in location of peak pressure and standard deviation between PL graft fixed and no PL/AM graft at 30 degrees of flexion for the medial tibio-femoral compartment

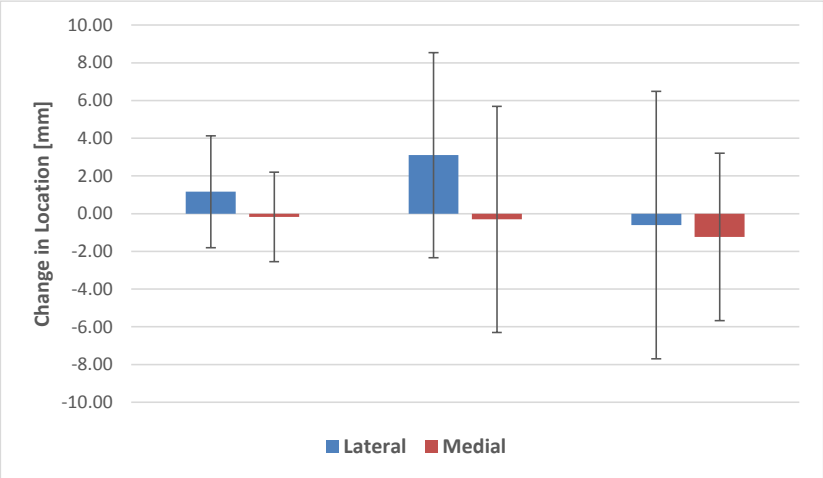

Figure 76. Average change in location of peak pressure and standard deviation between AM graft inserted (PL graft fixed) and no PL/AM graft at 30 degrees of flexion in the lateral tibio-femoral compartment

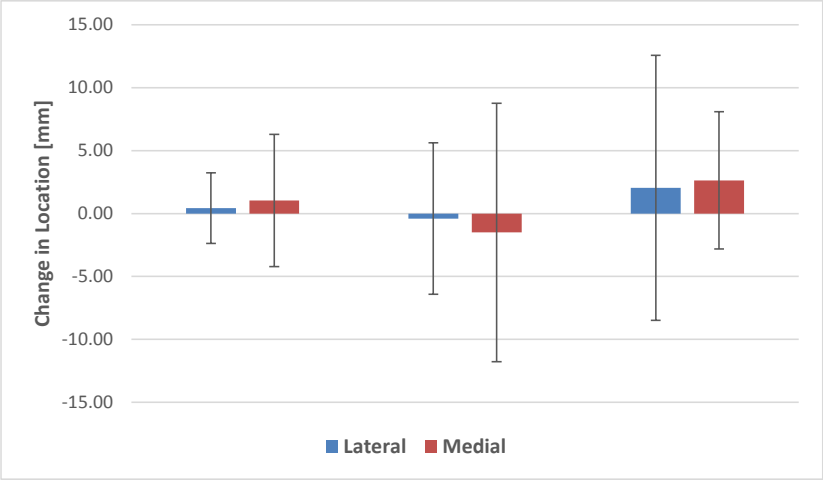

Figure 77. Average change in location of peak pressure and standard deviation between AM graft inserted (PL graft fixed) and no PL/AM graft at 30 degrees of flexion in the medial tibio-femoral compartment

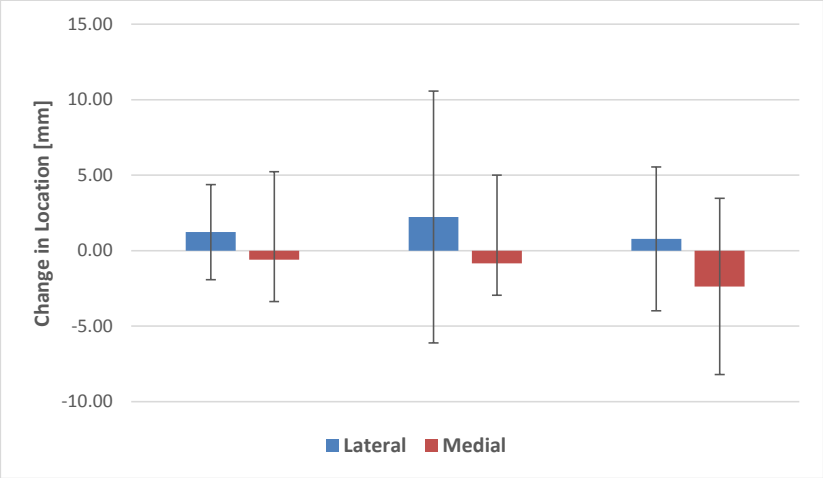

Figure 78. Average change in location of peak pressure and standard deviation between AM graft fixed (PL graft fixed) and no PL/AM graft at 30 degrees of flexion in the lateral tibio-femoral compartment

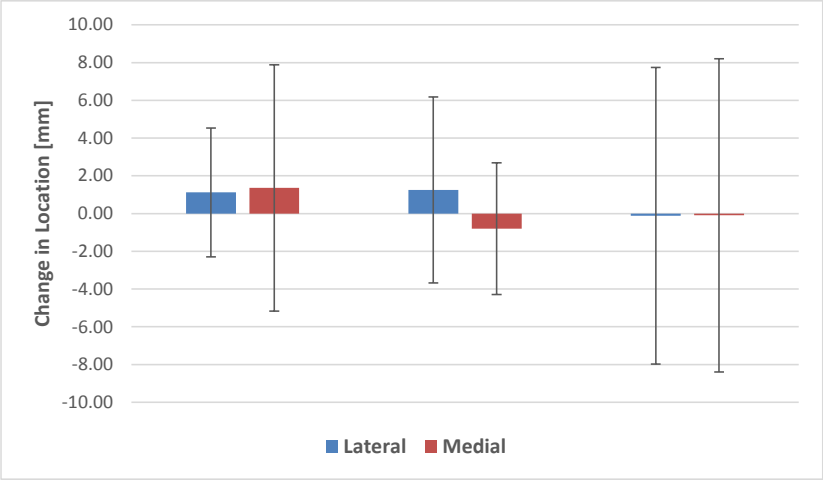

Figure 79. Average change in location of peak pressure and standard deviation between AM graft fixed (PL graft fixed) and no PL/AM graft at 30 degrees of flexion in the medial tibio-femoral compartment

Since the standard deviations of the stages of graft fixation are large with respect to their averages, a clear trend of how the change in location of peak pressure changes during the fixation of the ACL grafts cannot be established.

4.2.4 Change in Location of Center of Pressure

The average change in location of center of pressure and standard deviation for all 12 samples during graft fixation is shown in Figure 80 - Figure 89. Complete data for each specimen is listed in Appendix C. No statistical significance was found between the changes in location of center of pressure of the deficient knee (no AM or PL graft) and after the PL/AM grafts were inserted or fixed for any of three reconstructions for either the lateral or medial tibio-femoral compartments.

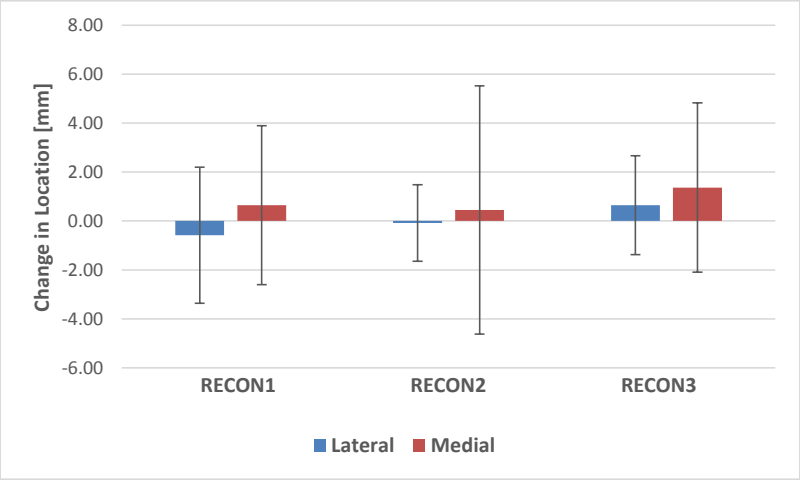

Figure 80. Average change in location of center of pressure and standard deviation between PL graft inserted and no PL/AM graft at 0 degrees of flexion in the lateral tibio-femoral compartment

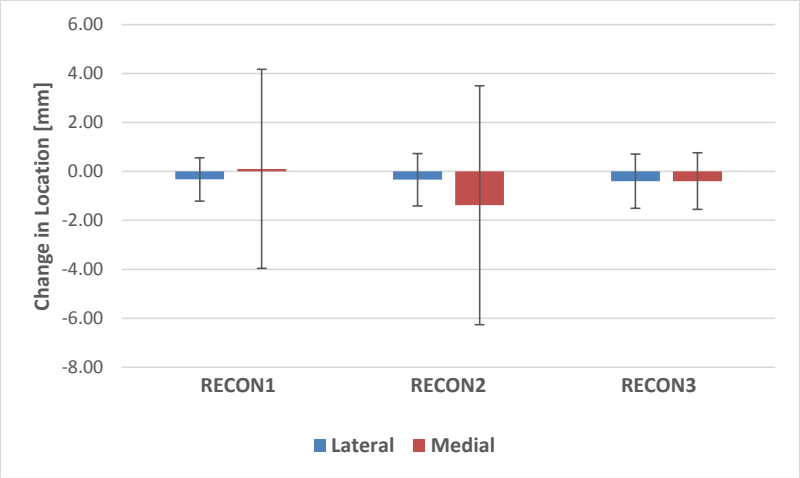

Figure 81. Average change in location of center of pressure and standard deviation between PL graft inserted and no PL/AM graft at 0 degrees of flexion in the medial tibio-femoral compartment

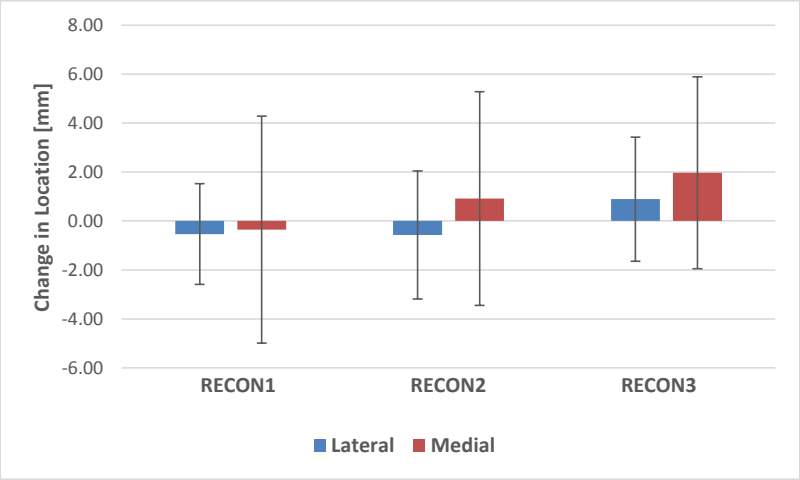

Figure 82. Average change in location of center of pressure and standard deviation between PL graft fixed and no PL/AM graft at 15 degrees of flexion in the lateral tibio-femoral compartment

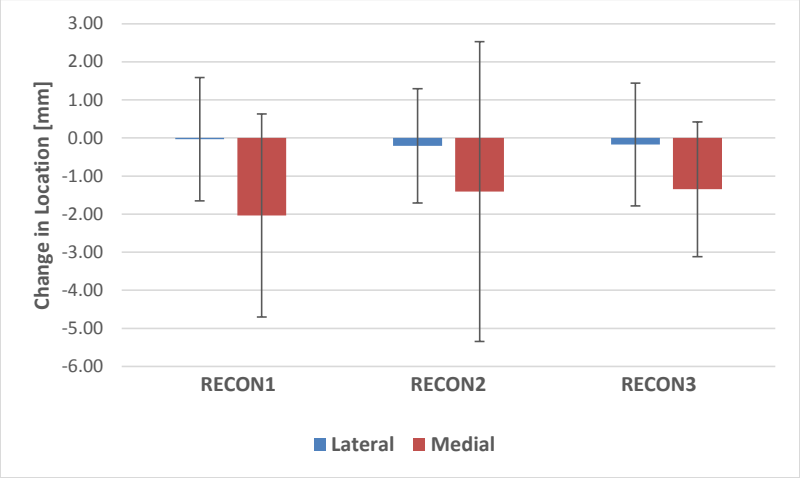

Figure 83. Average change in location of center of pressure and standard deviation between PL graft fixed and no PL/AM graft at 15 degrees of flexion in the lateral tibio-femoral compartment

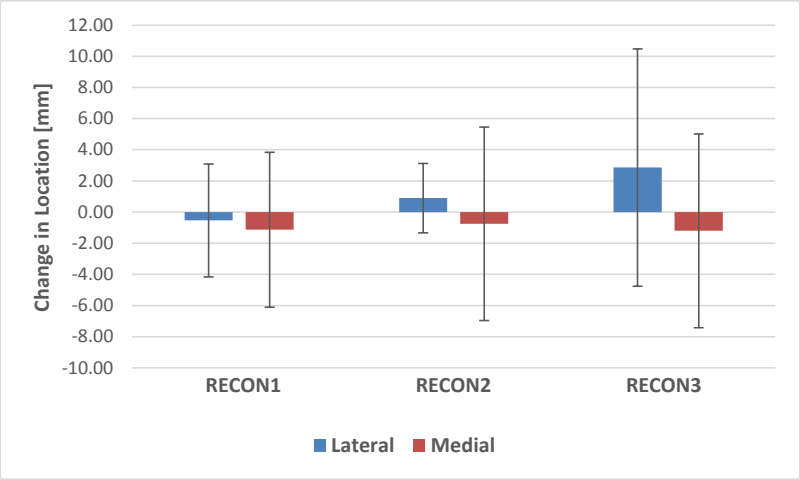

Figure 84. Average change in location of center of pressure and standard deviation between PL graft fixed and no PL/AM graft at 30 degrees of flexion in the lateral tibio-femoral compartment

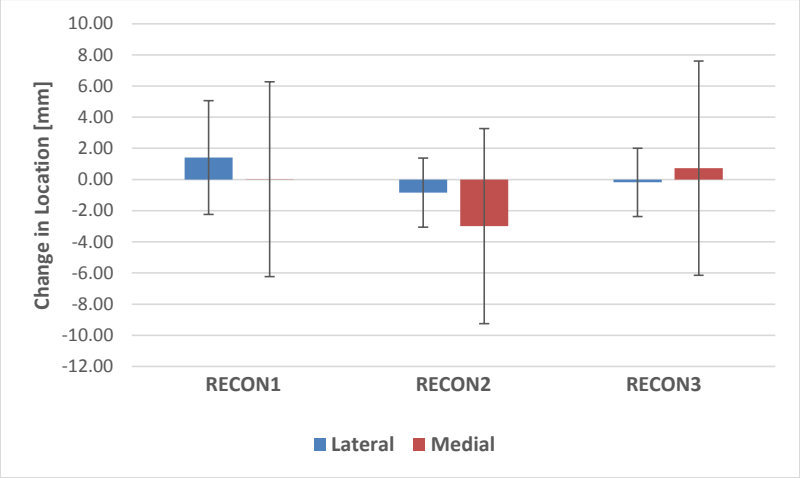

Figure 85. Average change in location of center of pressure and standard deviation between PL graft fixed and no PL/AM graft at 30 degrees of flexion in the medial tibio-femoral compartment

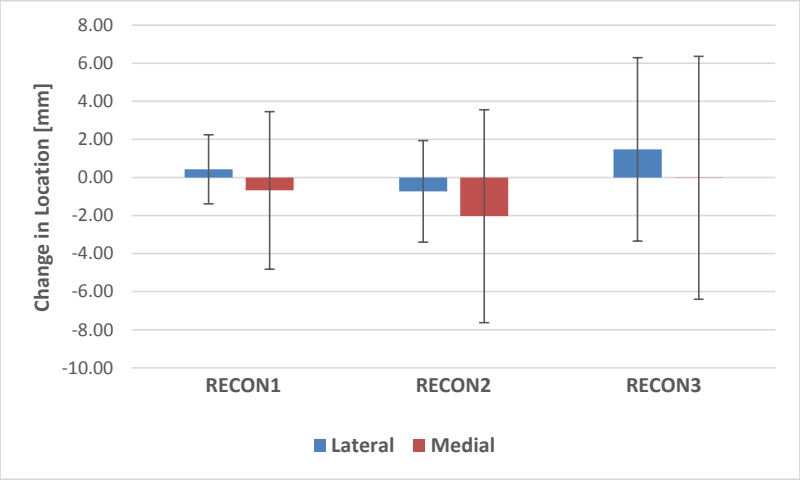

Figure 86. Average change in location of center of pressure and standard deviation between AM graft inserted (PL graft fixed) and no PL/AM graft at 30 degrees of flexion in the lateral tibio-femoral compartment

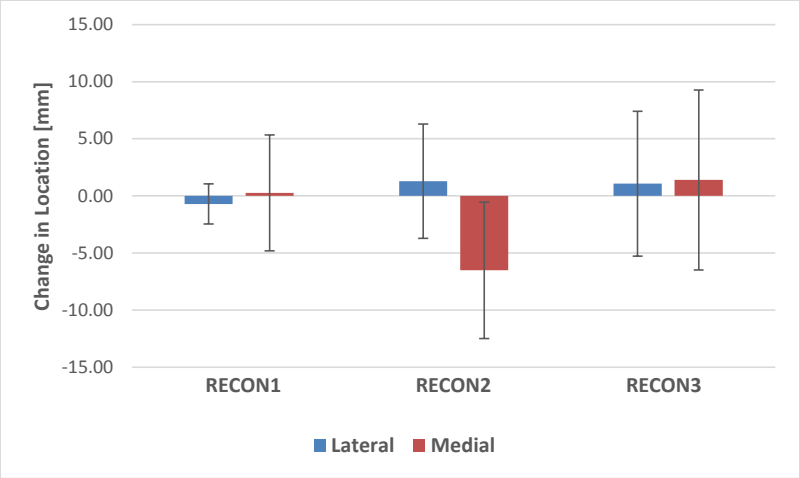

Figure 87. Average change in location of center of pressure and standard deviation between AM graft inserted (PL graft fixed) and no PL/AM graft at 30 degrees of flexion in the medial tibio-femoral compartment

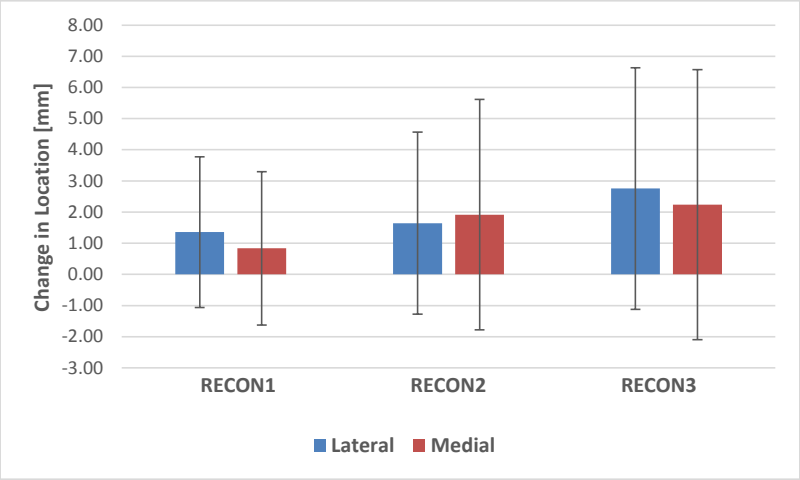

Figure 88. Average change in location of center of pressure and standard deviation between AM graft fixed (PL graft fixed) and no PL/AM graft at 30 degrees of flexion in the lateral tibio-femoral compartment

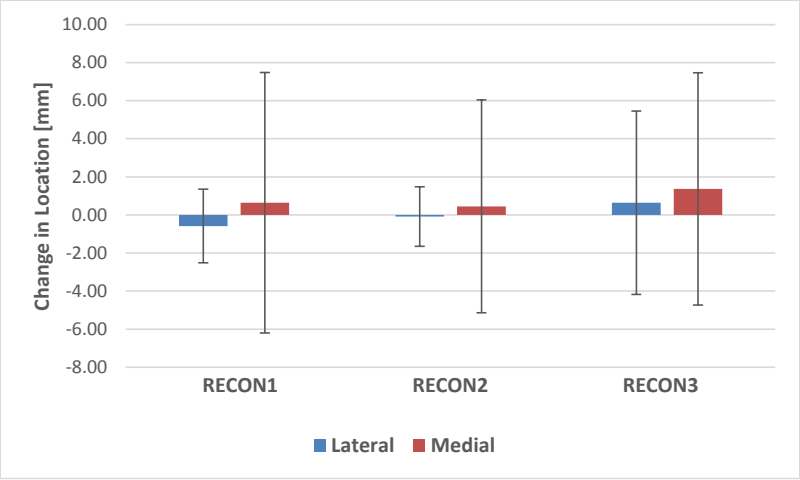

Figure 89. Average change in location of center of pressure and standard deviation between AM graft fixed (PL graft fixed) and no PL/AM graft at 30 degrees of flexion in the medial tibio-femoral compartment

Since the standard deviations of the stages of graft fixation are large with respect to their averages, a clear trend of how the change in location of center of pressure changes during the fixation of the ACL grafts cannot be established.

4.3 DISCUSSION

This study showed that double-bundle ACL reconstruction did not significantly change the peak contact pressure of the intact knee. Twelve knees were included in this study. In this study, 1000 N of axial loading was applied to the knees with the knees placed in a testing fixture, and pressure measurements were taken with the Tekscan K-4000 electronic pressure sensor (K-Scan; Tekscan, Inc., Boston, MA, USA). The skin and flesh was left intact during testing, and the effect of anatomic double-bundle ACL reconstruction on peak static tibio-femoral contact pressure, location of peak pressure, and location of center of pressure at 0, 15, 30, and 45 degrees of knee flexion was examined. The results of this study are shown in Table 10.

Table 10. Mean peak pressure [MPa] and standard deviation of the data reported by this study

	LATERAL		MEDIAL	
ANGLE	MEAN	STD DEV	MEAN	STD DEV
0	2.518	2.335	4.89	0.904
15	2.814	1.838	2.87	1.152
30	3.65	1.69	2.838	1.383
45	4.442	1.602	2.734	1.883

Comparing this study to other studies, Morimoto et al. used Fuji Film (Fuji Photo Film Co. Ltd., Tokyo, Japan), which is pressure sensitive film, to measure the tibio-femoral joint

contact pressure and area after single-bundle and double-bundle anatomic ACL reconstruction [26]. Their data included the static peak pressure of ACL intact knees for both the medial and lateral tibio-femoral compartment for nineteen specimens, tested at 0, 15, 30, and 45 degrees of flexion with 1000 N of axial loading. The knees were placed in a testing fixture during loading, and the skin and flesh were left intact during testing. The results of their study is shown in Table 11.

Table 11. Mean peak pressure [MPa] and standard deviation of the data reported by Morimoto et. al

	LATERAL		MEDIAL	
ANGLE	MEAN	STD. DEV.	MEAN	STD. DEV.
0	5.64	1.19	4.87	1.21
15	4.87	1.08	4.78	0.75
30	5.08	1.15	4.37	0.94
45	5.01	1.55	4.64	1.25

For the lateral tibio-femoral compartment, the largest difference between the results of mean peak pressure in this study and the results of mean peak pressure that Morimoto et. al reported was at 0 degrees of flexion, were there was a 76 percent difference; the difference between the two studies decreased for every successive angle, until there was a 12 percent difference at 45 degrees of flexion. For the medial tibio-femoral compartment, the smallest difference between the results in this study and the results that Morimoto et. al reported was at 0 degrees of flexion, were there was a zero percent difference; the difference between the two studies increased for every successive angle, until there was a 51 percent difference at 45 degrees of flexion. The standard deviations of the mean peak pressure for both the medial and lateral

tibio-femoral compartments at all four flexion angles were higher in the results of this study than in the results reported by Morimoto et. al.

Allarire et al. used Fuji film (Fuji Photo Film Co. Ltd., Tokyo, Japan) to measure tibio-femoral joint contact pressure after a tear of the posterior root of the medial meniscus [1]. Their data included the static peak pressure of ACL intact knees for the medial tibio-femoral compartment for nine specimens, tested at 0, 30, 60, and 90 degrees of flexion with 1000 N of axial loading. The knees were placed in a testing fixture during testing, and the skin and flesh were left intact during testing. The results of their study are shown in Table 12.

Table 12. Mean peak pressure [MPa] and standard deviation of the data reported by Allaire et. al

	MEDIAL	
ANGLE	MEAN	STD DEV
0	5.3	0.3
30	4.7	0.2

For the medial tibio-femoral compartment, the largest difference the between the results of mean peak pressure in this study and the results of mean peak pressure that Allaire et. al reported was at 0 degrees of flexion, were there was an eight percent difference; the difference between the two studies increased at 30 degrees of flexion, were there was a 49 percent difference. The standard deviations of the mean peak pressure for the medial tibio-femoral compartments at both 0 and 30 degrees of flexion were higher in the results of this study than in the results reported by Allaire et. al.

Paci et. al used the Tekscan model K-6900 sensor (K-Scan; Tekscan, Inc., Boston, MA, USA) to measure tibio-femoral joint contact pressure with release of the type I anterior

intermeniscal ligament [28]. Their data included the static peak pressure of ACL intact knees for the medial tibio-femoral compartment for five specimens, tested at with 1000 N of axial loading. The knees were placed in a testing fixture during loading. In contrast to the testing fixture used in this study, which measured the static pressure at 0, 15, 30, and 45 degrees of flexion, the testing fixture that Paci et. al used measured the pressure continuously with 1000 N of axial loading while the knee was flexed from 0 to 60 degrees. The skin was left intact during testing. The results of their study are shown in Table 13.

Table 13. Mean peak pressure [MPa] of the data reported by Paci et. al

	MEDIAL
ANGLE	MEAN
0	2.4
15	2.6
30	3.3
45	4.8

For the medial tibio-femoral compartment, the largest difference between the results of mean peak pressure in this study and the results of mean peak pressure that Paci et. al reported was at 0 degrees of flexion, were there was an 68 percent difference; the smallest difference between the two studies was at 15 degrees of flexion, were there was a 9 percent difference.

Seitz et. al used the Tekscan model K-4000 sensor (K-Scan; Tekscan, Inc., Boston, MA, USA) to measure tibio-femoral joint contact pressure with a partial menisectomy at the medial posterior horn [31]. Their data included the static peak pressure of ACL intact knees for both the medial and lateral tibio-femoral compartment for ten specimens, tested at 0 and 30 degrees of flexion with 1000 N of axial loading. The knees were placed in a testing fixture during loading,

and the skin, fat, muscles, and tendons were removed prior to testing. The results of their study are shown in Table 14.

Table 14. Mean peak pressure [MPa] and standard deviation of the data reported by Seitz et. al

	LATERAL		MEDIAL	
ANGLE	MEAN	STD DEV	MEAN	STD DEV
0	3	1.3	2.7	1.3
30	2.8	0.8	3.2	1.2

For the lateral tibio-femoral compartment, the largest difference between the results of mean peak pressure in this study and the results of mean peak pressure that Seitz et. al reported was at 0 degrees of flexion, were there was a 17 percent difference; the difference between the two studies decreased at 30 degrees, were there was a 0 percent. For the medial tibio-femoral compartment, the largest difference between the results in this study and the results that Seitz et. al reported was at 0 degrees of flexion, were there was a 57 percent difference; the difference between the two studies decreased at 30 degrees, were there was a 10 percent difference. The standard deviations of the mean peak pressure for the lateral tibio-femoral compartment at 0 and 30 degrees of flexion were higher in the results of this study than in the results reported by Seitz et. al. However, the standard deviations of the mean peak pressure for the medial tibio-femoral compartment at 0 and 30 degrees of flexion were about the same in the results of this study as reported by Seitz et. al.

C.K. Fitzpatrick et. al created a finite element model of the contact between the tibia and femur in the knee joint, as well as the contact between the patellar and the femur, which was based on the kinematics of the human cadaveric knee [13]. The scope of the study included determining the differences in using a finite element model with articular cartilage modeled as

fully deformable versus articular cartilage modeled as a rigid body in order to calculate the contact pressure between the tibia and the femur when loaded with 1000 N of axial loading. Their data included the mean peak pressure in the knee (not listed individually for the lateral and medial compartments) from 0 to 120 degrees of knee flexion for three knees. The results of their study are shown in Table 15.

Table 15. Mean peak pressure [MPa] of the data reported by C.K. Fitzpatrick et. al

ANGLE	DEFORM MEAN	RIGID MEAN
0	4.5	5.2
15	4.9	5.8
30	4.9	4.9
45	4.7	5.0

The differences between the mean peak pressures for modeling articular cartilage as both fully deformable and as a rigid body reported by C.K. Fitzpatrick et. al and the mean peak pressures (of both the lateral and medial tibio-femoral compartments combined) reported in this study was the lowest at 0 degrees of flexion, where there was a six percent difference with the fully deformable mean peak pressure, and an eight percent difference with the rigid body mean peak pressure; the differences were the highest at 30 degrees of flexion, where there was a 52 percent difference with the fully deformable mean peak pressure, and a 67 percent difference with the rigid body mean peak pressure.

5.0 CONCLUSIONS

This study showed that double-bundle ACL reconstruction did not significantly change the peak contact pressure, location of peak pressure, and location of center of pressure of the intact knee. Differences in the mean peak pressures measured in this study and those found in previous studies in ACL intact knees across different flexion angles can be attributed the difference in the sensors used, in cases where pressure sensitive film was used, as well as experimental differences between studies, such as the testing fixture and sensor placement in the knee. In this study, the large standard deviations of the means of the peak pressure, the means of change in location of peak pressure, and the means of change in location of center of pressure can be attributed to ACL reconstruction and sensor placement. Since both were done arthroscopically, leaving the knee capsule intact, there was no way to determine if the condyles were in alignment after the specimen was placed in the testing fixture. Also, the placement of the sensor in the knee, which is also done arthroscopically, may not allow the entire pressure distribution of the contact between the femur and the tibia to be captured, which would affect the output of the sensor. Future testing will address the issues of condylar alignment, as well as make use of smaller sensors, such as the Tekscan K-4011 (K-Scan; Tekscan, Inc., Boston, MA, USA), which will be less invasive in the knee. However, this sensor is about half the size of the sensor used in this study so it will be able to cover less area within the knee.

APPENDIX A

COMPUTATIONAL ALGORITHMS

The algorithms that were used to perform computations in this study are listed below. All code was written in Matlab (Matlab; MathWorks, Natick, MA, USA).

A.1 LOCATION OF PEAK PRESSURE

```
%%Code written by Brandon Marshall on 7/14/2013, and last modified on
%%6/29/2014.  This code is for a LEFT knee.

clear
clc

%input file name
file=input('Enter name of file to read: ','s');

%create file as .xlsx
file1=strcat(file,'.xlsx');

%create filename for results
filename_results=strcat(file,'_results.xlsx');

for v=0:15:45

%create a string out of the
v1=num2str(v);
```

```
%input the sensitivity
sens=menu('Select the
sensitivity','High2','High1','Mid2','Mid1','Default','Low3','Low2','Low1');

if sens == 1
x=0.0000093;
c=0.0007414;
elseif sens == 2
x=0.000024;
c=0.00079;
elseif sens == 3
x=0.000037;
c=0.002524;
elseif sens == 4
x=0.000070;
c=0.006302;
elseif sens == 5
x=0.00021;
c=0.00681;
elseif sens == 6
x=0.0015;
c=0.0024;

end

%Import loaded pressure matrix from excel and apply calibration;
num_B_0=xlsread(file1,v1,'A31:V56')*x-c;
num_A_0=xlsread(file1,v1,'AQ31:BL56')*x-c;

%flip the values of the matrix around

for i=1:26
    n=22;
    for j=1:22

        F_B_0(i,j)=num_B_0(i,n);
        n=n-1;

    end
end

for a=1:26
    b=22;
    for c=1:22

        F_A_0(a,c)=num_A_0(a,b);
        b=b-1;

    end
end

%put all of the values from pressure matrix A into an array
A_0=num_A_0(:);
```

```
%put all of the values from pressure matrix B into an array
B_0=num_B_0(:);

%remove all zero terms from pressure array A

j=1;
for i=1:572

    if A_0(i) > 0

        A_1_0(j)=A_0(i);
        j=j+1;;

    end
end

[r_1,r_2]=size(A_1_0);

%remove all zero terms from pressure array B
g=1;
for f=1:572

    if B_0(f) > 0

        B_1_0(g)=B_0(f);
        g=g+1;

    end
end

[s_1,s_2]=size(B_1_0);

%find the average pressure from final array A
average_A_0=((sum(A_1_0))/(r_2)/1);

%find the average pressure from final array B
average_B_0=((sum(B_1_0))/(s_2));

%find the peak pressure from final array A
peak_A_0=(max(A_1_0));

%find the peak pressur from final array A
r=1;
for i=1:26
    n=22;
    for j=1:22

        if F_A_0(i,j) == peak_A_0

        x_loc_A(r)=j;
        y_loc_A(r)=i;
        r=r+1;
```

```
        end

    end
end

%find the peak pressure from final array B
peak_B_0=(max(B_1_0));

%fine the locaiton of peak from final array B
q=1;
for i=1:26
    n=22;
    for j=1:22

        if F_B_0(i,j) == peak_B_0
                x_loc_B(q)=j;
                y_loc_B(q)=i;
                q=q+1;

        end

    end
end


%Find the total contact area from final array A
total_area_A_0=r_2*0.00000160961535846;

%Find the total contact area from final array B
total_area_B_0=s_2*0.00000160961535846;

%create filename
number=num2str(v);
filename=strcat(file,number);

%build matrix to save in excel
excel(1,1)={'total area (Sensor A)'};
excel(2,1)={num2str(total_area_A_0)};
excel(1,2)={'total area (Sensor B)'};
excel(2,2)={num2str(total_area_B_0)};
excel(1,3)={'average pressure (Sensor A)'};
excel(2,3)={num2str(average_A_0)};
excel(1,4)={'average pressure (Sensor B)'};
excel(2,4)={num2str(average_B_0)};
excel(1,5)={'peak pressure (Sensor A)'};
excel(2,5)={num2str(peak_A_0)};
excel(1,6)={'peak pressure (Sensor B)'};
excel(2,6)={num2str(peak_B_0)};

[w1,w2]=size(x_loc_A);
w3=2*w2+6;
t=0;
for i=7:2:w3
t=t+1;
```

```
excel(1,i)={'x_loc_A'};
excel(2,i)={num2str(x_loc_A(t))};
j=i+1;
excel(1,j)={'y_loc_A'};
excel(2,j)={num2str(y_loc_A(t))};
end

[q1,q2]=size(y_loc_B);
q3=w3+1;
q4=w3+2*q2;
m=0;
for i=q3:2:q4
m=m+1;
excel(1,i)={'x_loc_B'};
excel(2,i)={num2str(x_loc_B(m))};
u=i+1;
excel(1,u)={'y_loc_B'};
excel(2,u)={num2str(y_loc_B(m))};
end
%Write data to excel file
xlswrite(filename_results,excel,v1)

%Plot
subplot(121),contourf(F_A_0)
xlabel('Anterior')
title('Posterior - Medial Meniscus')
subplot(122),contourf(F_B_0)
xlabel('Anterior')
title('Posterior - Lateral Meniscus')
saveas(gcf, filename, 'fig')

clear excel
clear v1
clear x
clear c
clear num_A_0
clear num_B_0
clear r1
clear r2
clear total_area_A_0
clear total_area_B_0
clear s1
clear s2
clear x_loc_A
clear y_loc_A
clear x_loc_B
clear y_loc_B
clear F_B_0
clear F_A_0
clear A_1_0
clear B_1_0

end
```

A.2 LOCATION OF CENTER OF PRESSURE

```
%% Code written by Brandon Marshall on 6/23/2013.  Last modified on
6/26/2014.

clear
clc

%input file name
file=input('Enter name of file to read: ','s');

%Import loaded matrix from excel
num_B=xlsread(file,'.xlsx','7','A27:V52');
num_A=xlsread(file,'.xlsx','7','AQ27:BL52');

%put all of the values from pressure matrix A into an array
A=num_A(:);

%put all of the values from pressure matrix B into an array
B=num_B(:);

%find the sum of A
sum_A=sum(A);

%find the sum of B
sum_B=sum(B);


%flip the values of the matrix around for Matrix side B

for i=1:26
    n=22;
    for j=1:22

        F_B(i,j)=num_B(i,n);
        n=n-1;

    end
end

%flip the values of the matrix around for Matrix side A

for a=1:26
    b=22;
    for c=1:22

        F_A(a,c)=num_A(a,b);
        b=b-1;

    end
end
```

```
%multiply each cell by its distance from the origion (x-coordinate) for
matrix A

for e=1:26

    for f=1:22
    A_x_1(e,f)=f*1.26818*F_A(e,f);

    end

end

A_x_2=A_x_1(:);
A_x=sum(A_x_2)/sum(A)


%multiply each cell by its distance from the origion (y-coordinate) for
matrix A

for u=1:26

    for s=1:22
    A_y_1(u,s)=u*1.2692*F_A(u,s);

    end

end

A_y_2=A_y_1(:);
A_y=sum(A_y_2)/sum(A)

%multiply each cell by its distance from the origion (x-coordinate) for
matrix B

for g=1:26

    for h=1:22
    B_x_1(g,h)=h*1.26818*F_B(g,h);

    end

end

B_x_2=B_x_1(:);

%Output x-coordinate location of center of pressure
B_x=sum(B_x_2)/sum(B)

%multiply each cell by its distance from the origion (y-coordinate) for
matrix B
```

```
for i=1:26

    for j=1:22
    B_y_1(i,j)=i*1.2692*F_B(i,j);

    end

end

B_y_2=B_y_1(:);

%Output y-coordinate locaiton of center of pressure
B_y=sum(B_y_2)/sum(B)
```

A.3 PEAK PRESSURE ON ROLLER

```
%WRITTEN BY BRANDON MARSHALL, 10/27/2013
%THIS CODE WILL READ CONTINOUS OUTPUT FROM THE TEKSCAN K-4011 SENSOR
%AND RETURN THE PEAK VALUE (RAW OUTPUT) THAT PASSES THROUGH EACH SENSEL
%FOR AN AMOUNT OF TIME DEFINED BY THE USER

clear
clc

%Import all data from spread sheet into matlab
N=xlsread('20psi_LeftSide.xlsx','Sheet2','A1:BL3331');

X_matrix=zeros(26,22);

for j=1:26

    for i=1:22

        for p=j+1:2:2799

            for q=i+42:64

                if N(p,q) > X_matrix(j,i)

             X_matrix(j,i)=N(p,q);

                end

            end
        end
```

```
    end
end

%flip the values of the matrix around

for a=1:26
    n=22;
    for b=1:22

        X(a,b)=X_matrix(a,n);
        n=n-1;

    end
end

xlswrite('data',X)
```

APPENDIX B

CALIBRATION DATA

B.1 BLADDER

The complete data captured by the sensor during calibration using the bladder is listed below for the High2, High1, Mid2, Mid1, and Low3 sensitivity settings.

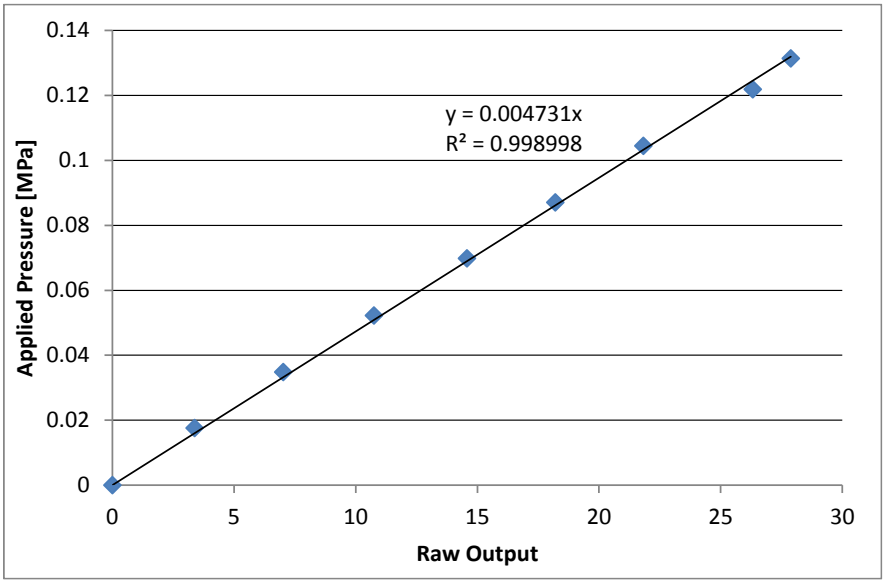

Figure 90. Linear trend line of the High1 sensitivity setting for applied pressure [MPa] as a function of average raw output

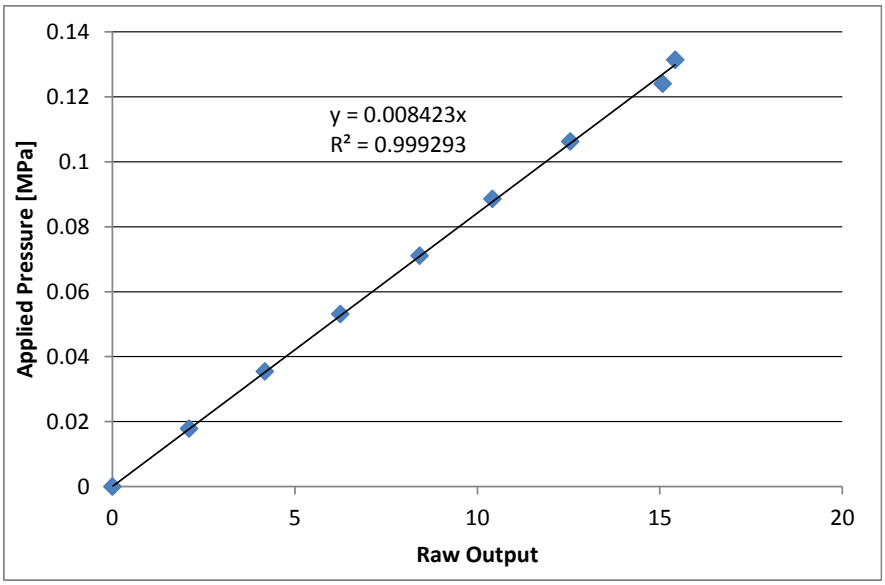

Figure 91. Linear trend line of the Mid2 sensitivity setting for applied pressure [MPa] as a function of average raw output

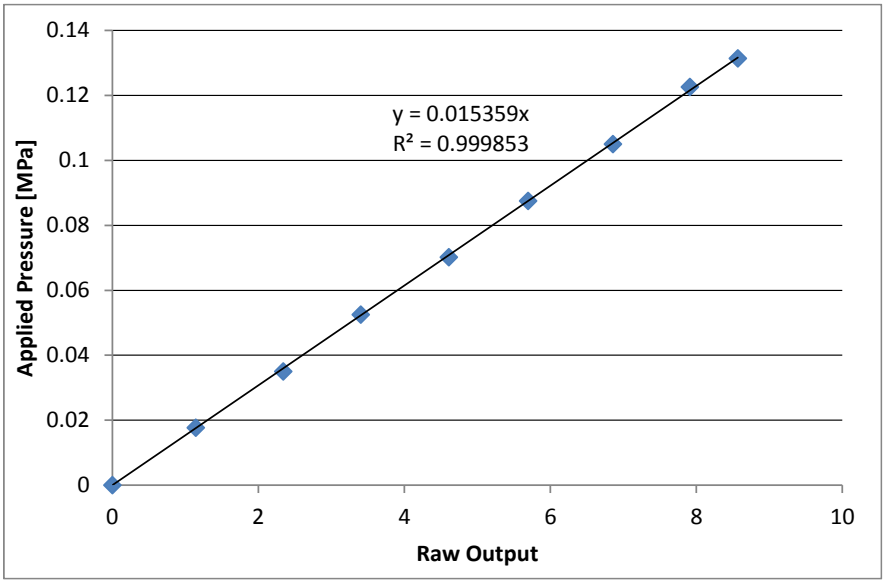

Figure 92. Linear trend line of the Mid1 sensitivity setting for applied pressure [MPa] as a function of average raw output

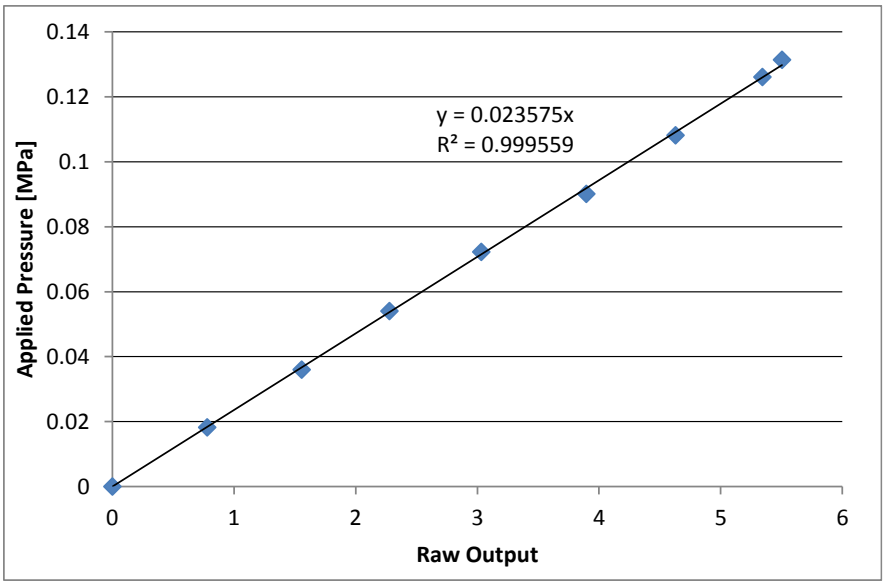

Figure 93. Linear trend line of the Low3 sensitivity setting for applied pressure [MPa] as a function of average raw output

B.2 MATERIALS TESTING MACHINE

The complete data captured by the sensor during calibration on the materials testing machine is listed below for the High2, High1, Mid2, Mid1, and Low3 sensitivity settings.

Table 16. Sensor raw output in response to the average applied pressure [MPa] for 3 sensors at the High2 sensitivity setting

Average Applied Pressure (MPa)	Sensor 1	Sensor 2	Sensor 3	Average Raw Output	RMS Error
	Average Raw Output	Average Raw Output	Average Raw Output		
0.00	0.00	0.00	0.00	0.00	0.00
0.04	25.92	26.09	27.62	26.54	1.33
0.08	50.96	50.68	50.82	50.82	0.20
0.12	76.11	73.19	73.15	74.15	2.40

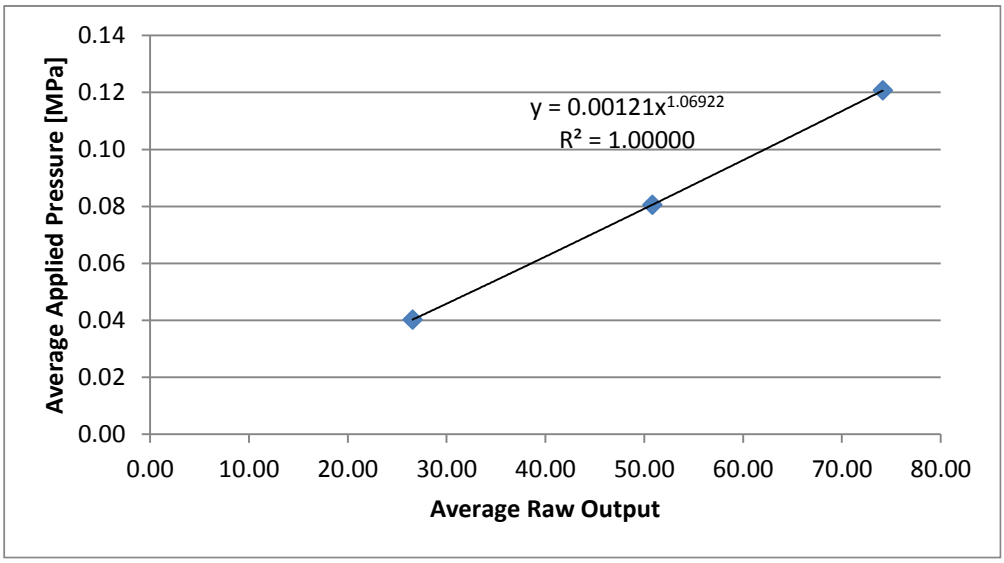

Figure 94. Power trend line for average applied pressure [MPa] vs. raw output (the average of 3 sensors) at the High2 sensitivity setting

Table 17. Sensor raw output in response to the average applied pressure [MPa] for 3 sensors at the High1 sensitivity setting

Average Applied Pressure (MPa)	Sensor 1	Sensor 2	Sensor 3	Average Raw Output	RMS Error
	Average Raw Output	Average Raw Output	Average Raw Output		
0.00	0.00	0.00	0.00	0.00	0.00
0.04	14.70	14.33	15.44	14.82	0.80
0.08	29.50	28.45	29.05	29.00	0.74
0.12	44.07	41.83	42.67	42.86	1.60
0.16	58.38	54.41	55.11	55.97	3.00
0.20	72.34	68.28	67.13	69.25	3.87
0.24	86.10	79.31	78.80	81.40	5.76
0.28	99.08	91.94	93.62	94.88	5.28

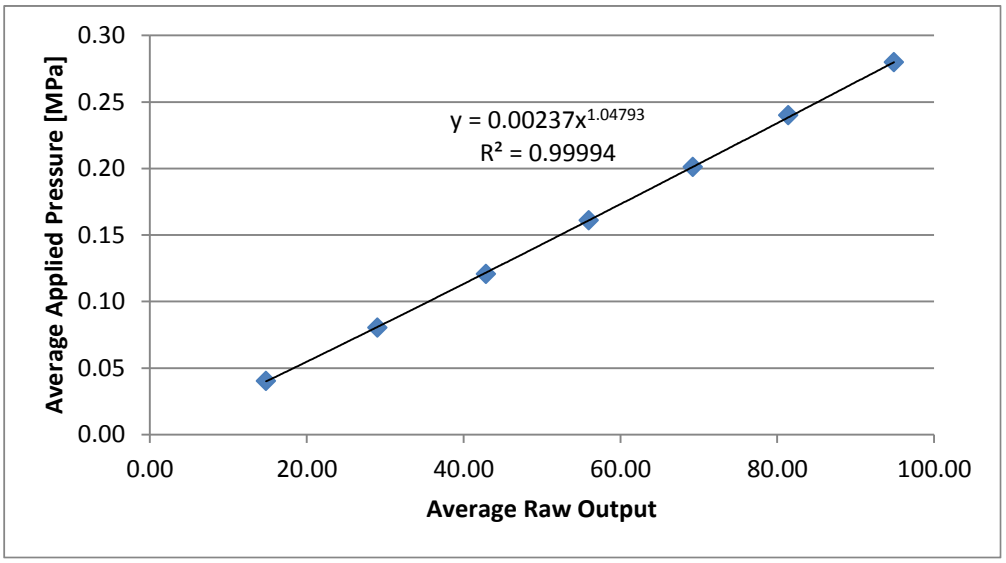

Figure 95. Power trend line for average applied pressure [MPa] vs. raw output (the average of 3 sensors) at the High1 sensitivity setting

Table 18. Sensor raw output in response to the average applied pressure [MPa] for 3 sensors at the Mid2 sensitivity setting

Average Applied Pressure (MPa)	Sensor 1	Sensor 2	Sensor 3	Average Raw Output	RMS Error
	Average Raw Output	Average Raw Output	Average Raw Output		
0.00	0.00	0.00	0.00	0.00	0.00
0.04	8.28	7.51	8.94	8.24	1.01
0.08	16.45	16.27	16.49	16.40	0.16
0.12	24.76	23.50	23.98	24.08	0.90
0.16	32.88	31.23	31.26	31.79	1.33
0.20	40.51	37.64	38.16	38.77	2.16
0.40	75.92	71.02	68.66	71.87	5.24
0.60	103.58	98.84	95.33	99.25	5.86

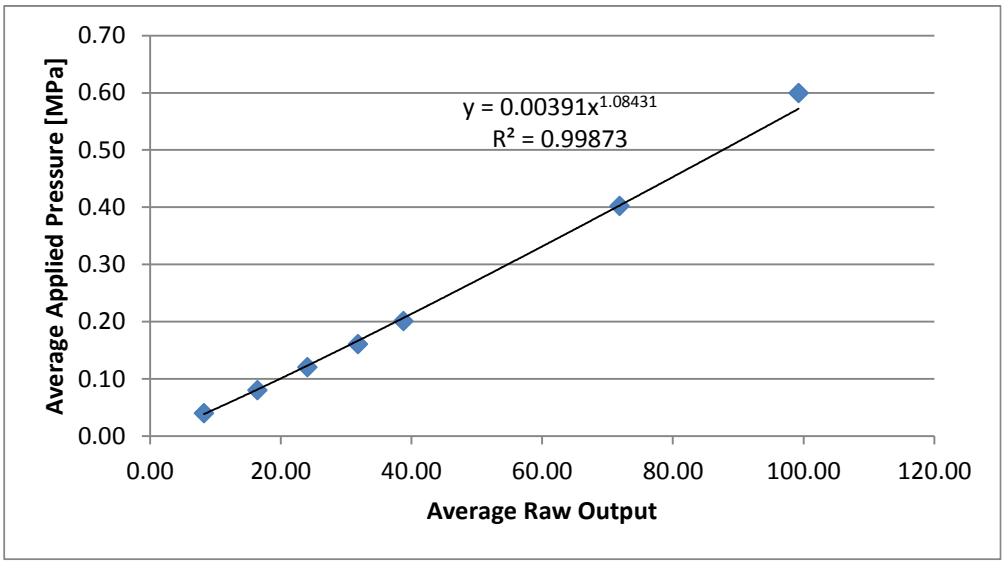

Figure 96. Power trend line for average applied pressure [MPa] vs. raw output (the average of 3 sensors) at the Mid2 sensitivity setting

Table 19. Sensor raw output in response to the average applied pressure [MPa] for 3 sensors at the Mid1 sensitivity setting

Average Applied Pressure (MPa)	Sensor 1	Sensor 2	Sensor 3	Average Raw Output	RMS Error
	Average Raw Output	Average Raw Output	Average Raw Output		
0.00	0.00	0.00	0.00	0.00	0.00
0.04	4.18	3.67	4.54	4.13	0.62
0.08	8.92	8.63	8.73	8.76	0.21
0.12	13.36	12.30	12.98	12.88	0.76
0.16	17.55	16.93	16.83	17.11	0.55
0.20	20.04	20.81	20.50	20.45	0.55
0.40	41.48	38.83	37.37	39.23	2.95
0.60	58.40	54.78	51.77	54.99	4.70
0.80	73.61	68.42	65.17	69.07	6.02
1.01	87.52	80.37	76.67	81.52	7.80
1.21	100.13	91.76	87.91	93.27	8.84

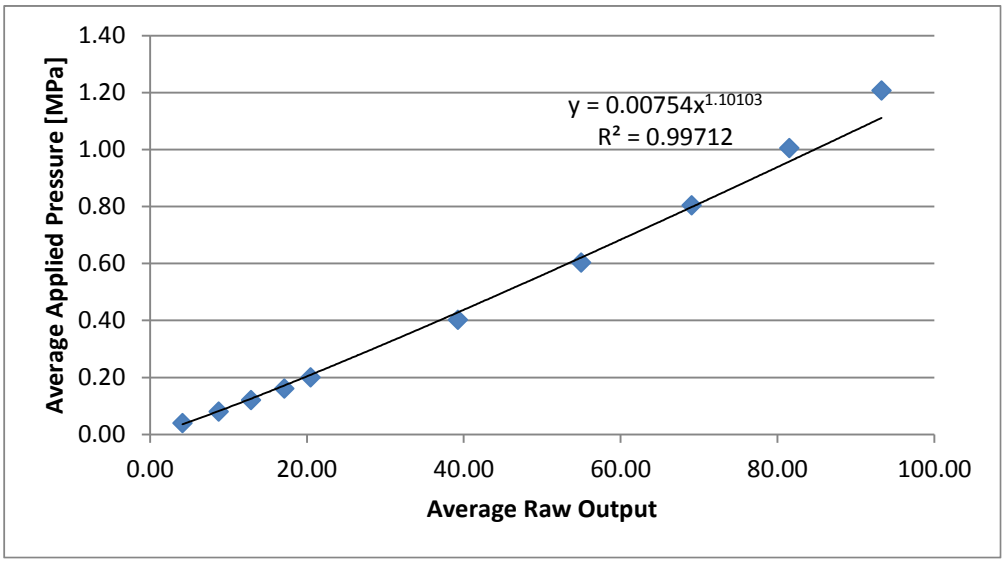

Figure 97. Power trend line for average applied pressure [MPa] vs. raw output (the average of 3 sensors) at the Mid1 sensitivity setting

Table 20. Sensor raw output in response to the average applied pressure [MPa] for 3 sensors at the Default sensitivity setting

Average Applied Pressure (MPa)	Sensor 1	Sensor 2	Sensor 3	Average Raw Output	RMS Error
	Average Raw Output	Average Raw Output	Average Raw Output		
0.00	0.00	0.00	0.00	0.00	0.00
0.04	2.35	2.35	2.57	2.42	0.18
0.08	5.46	4.90	5.31	5.22	0.41
0.12	8.20	8.12	8.07	8.13	0.09
0.16	10.81	10.24	10.44	10.50	0.41
0.20	13.59	13.29	12.81	13.23	0.56
0.40	26.16	24.39	23.61	24.72	1.85
0.60	37.06	34.87	33.21	35.05	2.73
0.80	47.48	43.44	41.73	44.22	4.17
1.01	56.05	51.17	49.49	52.24	4.82
1.21	63.87	58.63	56.05	59.52	5.63
1.41	66.95	60.53	58.93	62.14	6.01
1.61	74.20	66.89	65.22	68.77	6.75
1.81	81.44	73.26	71.51	75.40	7.50
2.01	88.69	79.62	77.80	82.04	8.25
2.21	95.93	85.99	84.09	88.67	9.00
2.42	103.18	92.35	90.38	95.31	9.74

Table 21. Sensor raw output in response to the average applied pressure [MPa] for 3 sensors at the Low3 sensitivity setting

Average Applied Pressure (MPa)	Sensor 1	Sensor 2	Sensor 3	Average Raw Output	RMS Error
	Average Raw Output	Average Raw Output	Average Raw Output		
0.00	0.00	0.00	0.00	0.00	0.00
0.04	0.46	0.68	0.82	0.65	0.26
0.08	2.00	1.86	2.24	2.03	0.27
0.12	3.33	3.12	3.12	3.19	0.17
0.16	4.64	4.28	4.37	4.43	0.27
0.20	5.85	5.42	5.44	5.57	0.34
0.40	11.64	10.71	10.33	10.89	0.95
0.60	16.67	15.42	14.70	15.60	1.41
0.80	21.61	19.83	18.79	20.07	2.01
1.01	25.99	23.59	22.48	24.02	2.54
1.21	26.46	24.15	22.93	24.51	2.54
1.41	29.71	27.09	25.68	27.49	2.89
1.61	32.95	30.04	28.44	30.48	3.24
1.81	36.20	32.98	31.20	33.46	3.59
2.01	39.44	35.92	33.95	36.44	3.93
2.21	42.69	38.87	36.71	39.42	4.28
2.42	45.93	41.81	39.46	42.40	4.63
2.62	49.17	44.75	42.22	45.38	4.98
2.82	52.42	47.70	44.98	48.36	5.33
3.02	55.66	50.64	47.73	51.35	5.67
3.22	58.91	53.58	50.49	54.33	6.02
3.42	62.15	56.53	53.25	57.31	6.37
3.62	65.40	59.47	56.00	60.29	6.72
3.82	68.64	62.41	58.76	63.27	7.07
4.03	71.89	65.36	61.52	66.25	7.41
4.23	75.13	68.30	64.27	69.23	7.76
4.43	78.37	71.24	67.03	72.22	8.11
4.63	81.62	74.19	69.79	75.20	8.46
4.83	84.86	77.13	72.54	78.18	8.81
5.03	88.11	80.07	75.30	81.16	9.15
5.23	91.35	83.02	78.06	84.14	9.50
5.43	94.60	85.96	80.81	87.12	9.85
5.64	97.84	88.90	83.57	90.10	10.20
5.84	101.08	91.85	86.33	93.09	10.55
6.04	104.33	94.79	89.08	96.07	10.89
6.24	107.57	97.73	91.84	99.05	11.24

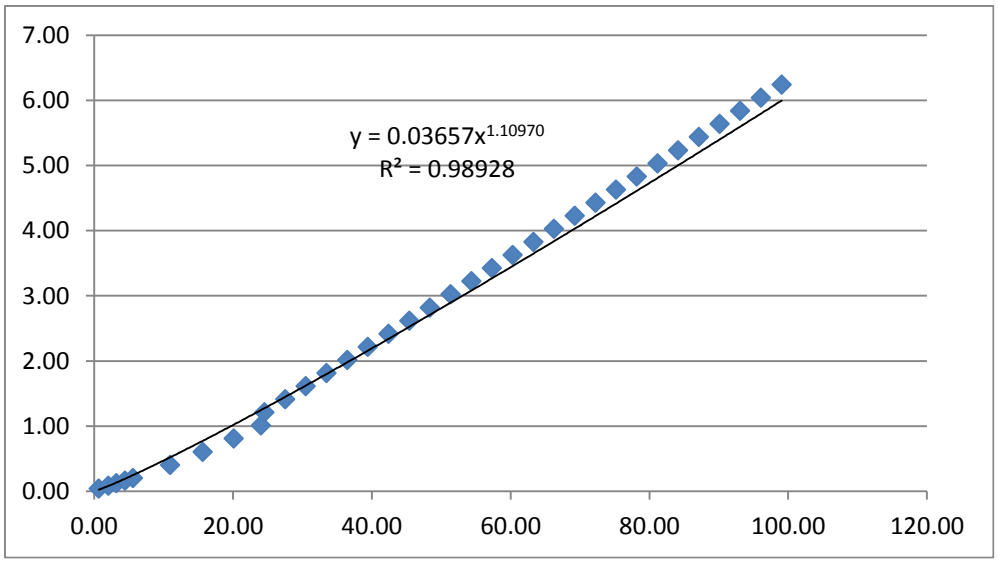

Figure 98. Power trend line for average applied pressure [MPa] vs. raw output (the average of 3 sensors) at the Low3 sensitivity setting

APPENDIX C

EXPERIMENTAL DATA

C.1 AXIAL LOADING

The location of center pressure is given below for 0, 15, 30, and 45 degrees of flexion.

Table 22. Location of center of pressure [mm] for 0 degrees of flexion

Sample Number	Knee	State	Lateral		Medial	
			x [mm]	y [mm]	x [mm]	y [mm]
5	L	INTACT	20.08	12.74	6.34	5.88
		RECON1	20.27	12.82	8.07	6.70
		RECON2	19.85	13.64	7.89	6.46
		RECON3	18.81	12.20	9.92	6.81
6	L	INTACT	19.25	4.54	16.18	9.92
		RECON1	19.28	5.27	16.04	9.98
		RECON2	20.32	4.52	13.56	7.09
		RECON3	20.12	4.94	15.35	9.36
7	L	INTACT	21.31	8.99	19.73	8.13
		RECON1	20.99	8.23	19.34	5.36
		RECON2	20.01	9.02	17.68	5.18
		RECON3	20.83	7.98	18.45	5.53
8	L	INTACT	23.55	7.45	20.78	15.41
		RECON1	21.26	4.48	23.39	6.18
		RECON2	21.81	3.61	23.05	7.67
		RECON3	21.53	3.95	23.65	7.04
9	L	INTACT	16.78	14.91	7.53	10.99
		RECON1	16.95	12.74	9.94	10.75
		RECON2	17.30	13.07	10.22	11.21
		RECON3	16.78	13.27	9.49	9.27
10	L	INTACT	19.90	14.18	11.60	14.98
		RECON1	20.01	13.61	11.53	10.91
		RECON2	19.94	13.80	11.67	13.82
		RECON3	19.53	13.23	11.79	11.32
11	R	INTACT	21.44	7.46	7.92	6.09
		RECON1	20.86	6.37	7.79	5.59
		RECON2	21.81	7.13	7.66	5.73
		RECON3	21.59	6.16	7.63	5.26
12	R	INTACT	17.80	7.95	7.22	16.37
		RECON1	16.28	6.61	6.73	14.45
		RECON2	15.98	7.18	6.25	12.34
		RECON3	16.45	7.26	6.96	15.43
13	R	INTACT	14.55	10.51	15.07	9.99
		RECON1	16.57	8.97	15.19	11.10
		RECON2	17.20	8.52	15.81	11.93
		RECON3	14.37	9.05	16.08	9.98
14	R	INTACT	19.92	13.34	8.07	8.27
		RECON1	20.90	11.67	9.31	11.07
		RECON2	20.18	11.15	10.22	10.21
		RECON3	20.55	11.64	9.44	10.21
15	R	INTACT	20.05	5.73	13.72	16.70
		RECON1	17.51	4.12	19.73	10.83
		RECON2	15.71	3.23	19.34	8.86
		RECON3	17.12	3.79	19.79	9.92
16	R	INTACT	17.91	9.13	13.42	10.86
		RECON1	18.25	8.86	13.38	9.09
		RECON2	17.38	10.49	14.23	11.23
		RECON3	17.36	8.11	13.84	8.93

Table 23. Location of center of pressure [mm] for 15 degrees of flexion

Sample Number	Knee	State	Lateral		Medial	
			x [mm]	y [mm]	x [mm]	y [mm]
5	L	INTACT	18.61	22.92	16.28	18.70
		RECON1	20.10	22.05	15.78	17.06
		RECON2	18.84	22.60	16.60	18.57
		RECON3	18.46	20.27	16.35	16.18
6	L	INTACT	17.44	9.76	16.71	13.17
		RECON1	15.80	12.45	18.12	19.62
		RECON2	19.10	7.73	17.91	16.41
		RECON3	17.57	9.78	17.19	15.27
7	L	INTACT	18.75	13.40	19.59	8.98
		RECON1	18.20	12.15	19.65	9.47
		RECON2	17.88	16.28	17.16	6.86
		RECON3	18.02	12.76	19.11	8.55
8	L	INTACT	25.18	15.04	18.68	19.06
		RECON1	21.19	10.03	17.60	14.73
		RECON2	21.54	10.61	18.60	16.20
		RECON3	21.61	9.07	18.55	15.44
9	L	INTACT	16.31	13.48	10.28	15.58
		RECON1	16.76	13.70	10.88	15.93
		RECON2	16.65	13.11	11.22	13.47
		RECON3	16.86	13.44	10.85	14.68
10	L	INTACT	17.93	18.43	12.88	18.78
		RECON1	16.86	18.40	12.72	20.43
		RECON2	16.18	18.66	12.50	20.56
		RECON3	17.21	16.86	13.02	18.74
11	R	INTACT	19.86	11.97	10.43	12.17
		RECON1	19.25	11.19	10.57	14.88
		RECON2	20.67	10.44	12.25	11.83
		RECON3	20.96	9.65	12.26	12.20
12	R	INTACT	16.13	16.52	11.56	17.79
		RECON1	17.11	14.23	11.13	18.78
		RECON2	16.76	14.92	11.22	18.34
		RECON3	16.54	14.53	11.07	18.50
13	R	INTACT	11.80	13.03	15.65	14.14
		RECON1	13.12	10.80	15.30	14.85
		RECON2	12.06	8.06	15.71	16.95
		RECON3	12.70	12.01	15.41	10.92
14	R	INTACT	19.81	17.97	9.03	10.01
		RECON1	22.90	15.64	8.96	15.39
		RECON2	21.97	16.33	10.27	15.41
		RECON3	22.83	15.58	8.68	14.74
15	R	INTACT	23.52	15.47	12.30	20.02
		RECON1	19.88	4.81	18.71	20.01
		RECON2	19.11	4.05	18.33	18.64
		RECON3	20.58	4.91	19.08	18.86
16	R	INTACT	16.33	13.00	13.61	16.15
		RECON1	16.77	14.21	15.01	14.22
		RECON2	16.54	14.99	14.88	16.26
		RECON3	16.23	14.77	14.78	15.80

Table 24. Location of center of pressure [mm] for 30 degrees of flexion

Sample Number	Knee	State	Lateral		Medial	
			x [mm]	y [mm]	x [mm]	y [mm]
5	L	INTACT	17.58	26.62	19.17	22.19
		RECON1	18.94	26.97	19.53	24.19
		RECON2	18.48	25.30	19.10	23.59
		RECON3	17.26	25.14	18.71	19.02
6	L	INTACT	13.54	14.85	16.27	14.69
		RECON1	11.48	15.14	16.38	21.07
		RECON2	11.23	14.07	16.56	21.60
		RECON3	11.39	15.80	16.82	20.04
7	L	INTACT	18.60	17.47	20.52	12.78
		RECON1	18.06	18.60	21.64	16.90
		RECON2	18.85	23.86	21.26	12.90
		RECON3	17.31	18.30	21.55	14.42
8	L	INTACT	20.90	19.24	22.38	20.43
		RECON1	18.42	14.99	21.32	20.01
		RECON2	18.81	15.82	21.65	21.29
		RECON3	19.11	15.56	21.79	20.63
9	L	INTACT	16.28	19.96	11.54	18.71
		RECON1	17.29	21.35	12.49	16.98
		RECON2	17.08	13.24	10.89	16.61
		RECON3	16.80	17.02	11.37	18.61
10	L	INTACT	15.29	20.57	13.97	21.30
		RECON1	16.86	18.40	12.72	20.43
		RECON2	12.31	21.52	12.30	22.84
		RECON3	14.71	19.69	12.94	21.95
11	R	INTACT	18.10	17.77	11.55	18.19
		RECON1	18.06	21.38	12.17	17.50
		RECON2	18.03	18.67	10.09	17.39
		RECON3	17.82	15.16	8.99	16.72
12	R	INTACT	15.48	21.84	7.40	20.35
		RECON1	14.99	18.95	8.22	21.47
		RECON2	14.42	20.59	8.10	21.81
		RECON3	14.32	19.75	8.08	21.55
13	R	INTACT	10.38	16.19	15.81	15.60
		RECON1	7.67	11.33	16.93	19.92
		RECON2	10.52	11.00	17.18	18.90
		RECON3	8.64	11.70	15.49	15.40
14	R	INTACT	19.20	21.73	12.70	13.58
		RECON1	24.15	24.33	12.85	23.16
		RECON2	22.58	23.93	13.94	23.97
		RECON3	23.11	24.36	11.92	21.01
15	R	INTACT	22.44	22.86	13.56	21.95
		RECON1	20.10	5.09	15.67	23.37
		RECON2	20.21	4.70	13.90	23.71
		RECON3	20.58	5.08	15.27	23.58
16	R	INTACT	15.94	15.45	15.08	20.50
		RECON1	14.50	17.68	15.84	18.27
		RECON2	14.43	18.21	15.42	19.54
		RECON3	13.77	18.69	15.22	19.63

Table 25. Location of center of pressure [mm] for 45 degrees of flexion

Sample Number	Knee	State	Lateral		Medial	
			x_loc	y_loc	x_loc	y_loc
5	L	INTACT	17.79	27.58	19.39	22.84
		RECON1	19.71	28.41	20.22	26.47
		RECON2	18.26	27.20	19.68	25.36
		RECON3	16.74	26.27	18.71	19.84
6	L	INTACT	12.48	17.92	14.78	16.29
		RECON1	11.28	20.47	14.71	21.40
		RECON2	10.56	19.10	14.81	22.20
		RECON3	11.10	19.93	14.69	21.53
7	L	INTACT	16.58	19.35	20.75	16.05
		RECON1	21.03	25.59	21.63	16.07
		RECON2	20.38	26.10	21.55	16.11
		RECON3	19.45	23.50	21.57	15.73
8	L	INTACT	22.18	19.80	23.68	21.06
		RECON1	20.34	17.55	24.23	21.43
		RECON2	19.67	17.18	23.49	22.02
		RECON3	20.19	16.96	23.90	21.35
9	L	INTACT	16.81	23.13	12.42	17.93
		RECON1	16.76	22.63	12.45	18.11
		RECON2	17.03	22.23	12.30	18.40
		RECON3	15.95	22.35	12.19	18.93
10	L	INTACT	13.76	21.76	14.09	22.37
		RECON1	11.62	22.92	11.93	25.19
		RECON2	11.23	23.08	11.57	25.71
		RECON3	13.39	21.75	12.87	24.74
11	R	INTACT	17.28	20.66	12.09	19.62
		RECON1	19.17	23.70	14.10	22.94
		RECON2	18.87	22.34	13.36	23.20
		RECON3	17.95	18.57	10.80	19.67
12	R	INTACT	14.37	23.53	6.97	21.65
		RECON1	13.83	21.52	8.04	22.81
		RECON2	13.67	22.68	7.90	22.92
		RECON3	13.51	21.91	8.54	22.86
13	R	INTACT	10.24	18.81	16.14	16.36
		RECON1	9.43	16.10	16.27	20.91
		RECON2	9.72	12.56	16.52	22.19
		RECON3	8.51	14.98	15.93	15.43
14	R	INTACT	18.83	23.18	14.73	17.63
		RECON1	21.98	28.37	14.98	25.68
		RECON2	21.98	27.76	15.27	25.91
		RECON3	22.14	28.95	14.50	25.73
15	R	INTACT	22.91	24.28	13.46	22.74
		RECON1	24.02	16.92	12.94	22.45
		RECON2	20.66	5.55	10.53	25.32
		RECON3	24.29	15.28	12.48	22.31
16	R	INTACT	15.20	16.89	15.30	20.47
		RECON1	12.20	18.42	15.01	18.56
		RECON2	12.67	19.30	15.04	19.73
		RECON3	13.06	19.33	14.92	19.95

The peak pressure and the location of peak pressure is given below for 0, 15, 30, and 45 degrees of flexion.

Table 26. Peak pressure [MPa] and the location of peak pressure [mm] for 0 degrees of flexion

Sample Number	Knee	State	Lateral	Medial	Lateral		Medial	
			Peak Pressure	Peak Pressure	x [mm]	y [mm]	x [mm]	y [mm]
5	L	INTACT	3.25	5.07	22.89	10.79	5.14	3.17
		RECON_1	2.97	4.40	22.89	14.60	7.68	3.17
		RECON_2	2.73	3.95	22.89	13.33	7.68	3.17
		RECON_3	3.33	4.66	15.28	9.52	8.94	3.17
6	L	INTACT	3.75	4.72	24.16	3.17	15.28	5.71
		RECON_1	2.78	4.60	24.16	4.44	14.02	5.71
		RECON_2	2.18	3.26	27.97	5.71	14.02	5.71
		RECON_3	3.27	4.03	27.33	5.71	19.09	12.06
7	L	INTACT	3.36	5.04	27.97	12.06	17.82	4.44
		RECON_1	3.55	4.57	27.97	12.06	19.09	3.17
		RECON_2	2.01	2.75	27.97	12.06	19.09	3.17
		RECON_3	3.00	3.02	27.97	12.06	19.09	3.17
8	L	INTACT	2.19	8.67	24.16	6.98	24.16	11.42
		RECON_1	2.27	6.56	24.80	5.71	27.97	6.98
		RECON_2	2.70	6.14	21.63	3.17	27.97	6.98
		RECON_3	2.81	6.56	22.89	4.44	27.97	6.98
9	L	INTACT	2.38	9.94	15.28	13.33	3.87	9.52
		RECON_1	2.62	7.84	15.92	10.79	5.77	3.81
		RECON_2	0.85	2.92	16.55	10.79	5.77	3.81
		RECON_3	0.85	3.14	15.92	11.42	5.56	5.71
10	L	INTACT	1.40	2.01	25.43	10.79	5.14	5.71
		RECON_1	1.16	1.90	25.43	15.23	8.94	5.71
		RECON_2	1.15	1.97	17.82	15.23	2.60	5.71
		RECON_3	1.32	2.18	17.82	14.60	8.94	3.17
11	R	INTACT	4.66	1.81	23.46	5.08	14.58	4.44
		RECON_1	3.22	1.39	24.73	4.44	13.95	3.81
		RECON_2	2.92	1.45	24.73	5.71	13.32	3.17
		RECON_3	2.98	1.58	24.73	4.44	12.81	2.67
12	R	INTACT	4.63	1.86	20.93	4.44	0.63	4.44
		RECON_1	3.15	1.71	22.19	4.44	0.63	4.44
		RECON_2	2.90	1.74	22.19	4.44	0.63	4.44
		RECON_3	5.33	2.01	22.19	4.44	0.63	5.08
13	R	INTACT	1.42	1.53	9.51	4.44	5.71	0.63
		RECON_1	1.39	1.42	8.88	4.44	0.63	0.63
		RECON_2	1.28	1.46	9.51	3.17	0.63	0.63
		RECON_3	1.54	1.49	8.24	3.17	13.32	4.44
14	R	INTACT	3.18	1.67	24.73	14.60	0.63	0.63
		RECON_1	2.36	0.85	24.73	12.06	5.28	8.67
		RECON_2	2.27	0.65	24.73	12.06	5.71	8.25
		RECON_3	2.22	0.82	24.73	12.06	5.71	8.25
15	R	INTACT	6.71	3.92	19.66	4.44	13.32	17.13
		RECON_1	3.30	5.87	19.02	4.44	20.93	6.98
		RECON_2	2.59	6.20	16.70	2.75	19.66	5.71
		RECON_3	2.84	5.78	19.66	4.44	20.93	6.98
16	R	INTACT	2.21	1.85	24.73	4.44	14.58	4.44
		RECON_1	2.08	1.55	24.73	4.44	14.58	4.44
		RECON_2	2.06	1.11	24.73	5.71	6.98	2.75
		RECON_3	2.14	1.59	24.73	5.71	15.85	4.44

Table 27. Peak pressure [MPa] and the location of peak pressure [mm] for 15 degrees of flexion

Sample Number	Knee	State	Lateral	Medial	Lateral		Medial	
			Peak Pressure	Peak Pressure	x [mm]	y [mm]	x [mm]	y [mm]
5	L	INTACT	2.98	2.10	24.16	24.75	17.40	20.10
		RECON_1	2.60	2.20	25.43	24.75	19.09	15.87
		RECON_2	2.59	2.24	24.80	24.75	16.55	18.40
		RECON_3	2.68	1.97	24.58	23.06	19.09	14.60
6	L	INTACT	2.32	2.03	21.63	6.98	20.36	10.79
		RECON_1	1.20	0.94	10.21	19.04	21.63	24.75
		RECON_2	2.63	2.15	24.16	5.71	19.09	13.33
		RECON_3	1.53	1.26	25.43	6.35	19.09	12.06
7	L	INTACT	3.32	1.52	27.97	15.87	17.82	5.71
		RECON_1	3.28	1.52	27.97	14.60	19.09	5.71
		RECON_2	3.22	1.48	11.48	13.33	19.09	5.71
		RECON_3	3.29	1.28	27.97	15.23	19.09	5.71
8	L	INTACT	2.65	3.18	27.97	14.60	21.63	15.87
		RECON_1	2.14	5.07	24.16	7.62	18.45	18.40
		RECON_2	2.67	4.78	25.43	10.79	19.09	18.40
		RECON_3	2.41	5.36	24.16	8.25	19.09	18.40
9	L	INTACT	2.81	8.32	15.28	12.69	4.50	10.79
		RECON_1	2.35	5.99	14.65	12.06	5.14	6.98
		RECON_2	0.94	3.16	15.28	12.06	5.14	6.98
		RECON_3	0.49	1.51	15.28	12.06	5.14	7.83
10	L	INTACT	1.42	1.12	16.55	23.48	11.48	20.94
		RECON_1	1.43	0.87	19.09	15.23	15.28	24.75
		RECON_2	1.47	0.82	13.38	20.31	5.14	23.48
		RECON_3	1.22	0.99	17.82	15.87	11.48	18.40
11	R	INTACT	2.22	2.41	23.46	7.62	10.78	9.52
		RECON_1	1.74	2.00	23.46	8.25	4.44	11.42
		RECON_2	1.90	1.99	27.27	8.25	3.17	9.52
		RECON_3	1.84	2.28	26.00	6.98	11.03	4.44
12	R	INTACT	1.67	2.21	23.46	17.13	6.98	9.52
		RECON_1	1.51	1.86	22.19	15.23	5.71	13.96
		RECON_2	1.60	1.70	22.19	15.23	5.71	13.33
		RECON_3	1.62	1.79	22.83	14.60	3.17	9.52
13	R	INTACT	1.70	1.84	5.71	9.52	17.75	20.94
		RECON_1	1.06	1.58	8.88	5.71	17.12	23.48
		RECON_2	1.40	2.06	8.24	4.44	15.85	23.48
		RECON_3	1.59	1.96	5.71	9.52	13.32	5.71
14	R	INTACT	2.38	1.88	26.00	17.13	0.63	0.63
		RECON_1	3.15	1.74	27.27	14.60	4.76	13.64
		RECON_2	2.58	1.90	27.27	14.60	8.24	16.50
		RECON_3	3.16	2.14	27.27	13.33	7.61	16.50
15	R	INTACT	4.84	6.11	23.46	14.60	12.05	18.40
		RECON_1	4.12	6.71	23.46	6.35	18.39	19.67
		RECON_2	4.02	8.95	17.97	3.17	18.39	18.40
		RECON_3	3.92	6.71	27.27	8.25	18.39	18.40
16	R	INTACT	1.17	2.00	17.12	10.79	14.58	17.13
		RECON_1	1.24	1.84	10.78	19.67	19.66	18.40
		RECON_2	1.31	2.41	10.78	19.67	10.36	9.10
		RECON_3	1.12	2.08	10.78	19.67	18.39	19.67

Table 28. Peak pressure [MPa] and the location of peak pressure [mm] for 30 degrees of flexion

Sample Number	Knee	State	Lateral	Medial	Lateral		Medial	
			Peak Pressure	Peak Pressure	x [mm]	y[mm]	x [mm]	y [mm]
5	L	INTACT	5.24	3.03	27.97	29.83	18.24	21.36
		RECON_1	5.63	3.33	27.97	29.83	21.63	24.75
		RECON_2	5.27	3.14	26.06	26.02	20.36	24.75
		RECON_3	4.57	2.59	25.43	24.75	20.36	19.67
6	L	INTACT	3.34	1.79	10.21	6.98	19.09	13.33
		RECON_1	1.49	1.46	10.85	11.42	17.82	14.60
		RECON_2	1.77	1.29	12.75	1.90	21.63	0.63
		RECON_3	1.54	1.49	19.09	5.08	21.63	0.63
7	L	INTACT	5.30	1.58	27.97	20.94	21.63	14.60
		RECON_1	6.59	2.70	27.97	19.67	22.89	17.13
		RECON_2	5.48	2.41	27.97	24.11	22.89	15.87
		RECON_3	6.44	2.54	27.97	17.77	22.89	15.87
8	L	INTACT	4.43	5.04	25.43	18.40	26.06	15.87
		RECON_1	2.82	3.31	25.43	10.15	18.45	19.67
		RECON_2	3.19	4.37	25.43	14.60	19.09	19.67
		RECON_3	3.36	4.26	26.06	14.60	19.09	19.67
9	L	INTACT	7.84	16.32	14.02	17.13	7.04	18.40
		RECON_1	7.84	11.72	14.65	15.87	12.11	24.75
		RECON_2	2.32	8.39	15.28	12.06	5.14	7.62
		RECON_3	2.19	5.27	14.65	13.33	5.56	13.75
10	L	INTACT	2.10	1.19	11.48	14.60	11.48	28.56
		RECON_1	3.02	1.82	19.09	15.23	15.28	24.75
		RECON_2	2.32	1.19	14.65	15.23	8.31	27.92
		RECON_3	2.15	1.33	11.48	14.60	9.58	28.56
11	R	INTACT	1.64	3.03	22.83	10.15	12.05	13.33
		RECON_1	1.10	3.26	23.04	12.48	8.24	15.87
		RECON_2	1.10	3.08	24.73	19.67	10.78	18.40
		RECON_3	0.99	2.99	27.27	13.33	12.30	6.22
12	R	INTACT	1.63	2.48	25.15	19.25	4.44	14.60
		RECON_1	1.35	2.58	23.46	17.77	9.51	27.92
		RECON_2	1.37	2.66	12.05	16.50	8.88	28.56
		RECON_3	1.35	2.60	12.68	13.96	4.44	17.13
13	R	INTACT	1.73	1.99	6.98	14.60	17.12	21.89
		RECON_1	1.41	2.13	6.98	6.98	6.98	27.29
		RECON_2	1.02	2.14	6.98	5.71	24.73	5.71
		RECON_3	1.37	1.55	4.44	10.15	12.68	12.37
14	R	INTACT	2.17	2.03	27.27	20.94	14.58	15.87
		RECON_1	1.52	2.29	27.27	27.29	6.34	17.13
		RECON_2	1.56	2.62	27.27	27.29	9.51	21.58
		RECON_3	1.68	2.34	27.27	27.29	7.61	19.67
15	R	INTACT	5.27	6.62	26.00	20.94	15.85	19.67
		RECON_1	5.27	6.53	23.46	6.35	17.12	19.67
		RECON_2	5.16	6.02	20.93	4.87	15.85	20.94
		RECON_3	5.45	6.38	27.27	8.25	17.12	19.67
16	R	INTACT	1.32	2.80	14.58	15.87	14.58	23.48
		RECON_1	1.16	2.95	9.51	10.79	17.12	19.67
		RECON_2	1.12	3.28	9.51	13.33	9.51	10.37
		RECON_3	1.12	2.98	9.51	13.33	14.58	22.85

Table 29. Peak pressure [MPa] and the location of peak pressure [mm] for 45 degrees of flexion

Sample Number	Knee	State	Lateral	Medial	Lateral		Medial	
			Peak Pressure	Peak Pressure	x [mm]	y [mm]	x [mm]	y [mm]
5	L	INTACT	5.78	3.22	27.97	29.83	18.24	21.36
		RECON_1	6.65	3.08	27.97	29.83	21.63	26.02
		RECON_2	5.99	3.14	26.06	26.65	21.63	24.75
		RECON_3	4.69	2.84	25.85	26.02	20.36	19.67
6	L	INTACT	5.51	1.91	8.94	9.52	17.82	14.60
		RECON_1	2.15	1.47	8.31	17.13	15.28	18.40
		RECON_2	2.25	1.13	8.94	9.52	5.14	31.10
		RECON_3	2.06	1.25	16.55	9.52	16.55	15.23
7	L	INTACT	6.74	0.85	12.75	19.67	21.63	17.13
		RECON_1	8.25	3.25	27.97	24.75	22.26	16.50
		RECON_2	6.59	2.59	27.97	24.75	21.63	17.13
		RECON_3	8.12	2.44	27.97	19.67	22.89	15.87
8	L	INTACT	6.20	5.16	24.16	19.67	26.06	15.87
		RECON_1	5.10	4.95	23.53	11.42	22.89	20.31
		RECON_2	5.54	5.78	21.63	17.13	27.97	20.94
		RECON_3	5.16	5.01	24.16	15.87	27.97	20.94
9	L	INTACT	8.60	13.89	14.65	18.40	7.68	17.77
		RECON_1	14.62	15.36	15.28	17.13	10.85	24.75
		RECON_2	3.05	4.26	15.28	23.48	7.68	14.60
		RECON_3	3.11	4.23	15.28	17.13	6.41	13.33
10	L	INTACT	2.56	1.37	11.48	19.04	10.85	28.56
		RECON_1	2.87	1.29	16.55	19.67	17.19	24.11
		RECON_2	2.80	1.33	12.75	19.67	10.21	27.29
		RECON_3	2.86	1.33	8.94	20.94	13.38	26.02
11	R	INTACT	1.25	3.16	10.21	12.69	16.55	15.23
		RECON_1	1.33	6.20	6.41	16.29	19.09	18.40
		RECON_2	1.23	5.60	3.87	18.40	15.28	23.48
		RECON_3	1.13	5.24	3.87	18.40	16.30	10.28
12	R	INTACT	1.96	2.90	11.48	19.25	21.63	19.67
		RECON_1	1.84	2.73	16.55	17.13	19.72	25.38
		RECON_2	1.77	2.90	15.92	17.77	20.36	26.02
		RECON_3	1.99	2.76	15.92	16.50	24.16	16.50
13	R	INTACT	1.99	2.68	21.63	18.40	11.16	19.99
		RECON_1	0.70	2.50	21.63	10.79	3.87	18.40
		RECON_2	0.60	2.90	24.16	9.52	3.87	18.40
		RECON_3	1.08	2.80	23.53	11.42	14.33	13.96
14	R	INTACT	2.27	2.62	1.97	28.56	11.48	19.67
		RECON_1	0.95	1.17	1.33	29.83	21.63	17.45
		RECON_2	0.95	1.29	1.33	29.83	19.09	22.21
		RECON_3	1.97	2.31	1.33	29.83	19.72	22.21
15	R	INTACT	5.46	8.81	2.60	22.21	11.48	22.21
		RECON_1	5.19	6.08	5.14	10.15	12.75	19.67
		RECON_2	6.17	5.45	7.68	4.87	21.63	23.48
		RECON_3	5.54	6.17	2.60	15.87	15.28	19.67
16	R	INTACT	1.37	3.13	17.82	16.50	14.02	23.48
		RECON_1	1.04	2.92	19.09	15.87	14.02	20.94
		RECON_2	1.10	3.32	18.67	17.98	19.51	9.94
		RECON_3	1.04	3.22	18.24	18.83	14.65	23.48

C.2 GRAFT FIXATION (NO AXIAL LOADING)

The peak pressure during graft fixation is given below.

Table 30. Peak pressure [MPa] for 30 degrees of flexion with no graft

Sample Number	Knee	State	Side A	Side B
			Peak Pressure	Peak Pressure
5	L	RECON_1	0.0025	0.0844
		RECON_2	0.0025	0.0658
		RECON_3	0.0000	0.0658
6	L	RECON_1	0.0608	0.1789
		RECON_2	0.0157	0.0776
		RECON_3	0.0235	0.1276
7	L	RECON_1	0.0964	0.1016
		RECON_2	0.0097	0.1102
		RECON_3	0.0591	0.0709
8	L	RECON_1	0.0053	0.0097
		RECON_2	0.0053	0.0362
		RECON_3	0.0053	0.0362
9	L	RECON_1	0.0314	0.0591
		RECON_2	0.0314	0.0591
		RECON_3	0.0025	0.0053
10	L	RECON_1	0.0692	0.0235
		RECON_2	0.1861	0.0692
		RECON_3	0.1067	0.0558
11	R	RECON_1	0.1102	0.0314
		RECON_2	0.1171	0.0112
		RECON_3	0.0642	0.0025
12	R	RECON_1	0.0330	0.0097
		RECON_2	0.0330	0.0235
		RECON_3	0.1825	0.0298
13	R	RECON_1	0.3904	0.0476
		RECON_2	0.3717	0.0525
		RECON_3	0.3306	0.0625
14	R	RECON_1	0.0642	0.0219
		RECON_2	0.0595	0.0198
		RECON_3	0.0525	0.0127
15	R	RECON_1	0.0427	0.0250
		RECON_2	0.0298	0.0282
		RECON_3	0.0235	0.0250
16	R	RECON_1	0.0142	0.0827
		RECON_2	0.0575	0.2005
		RECON_3	0.0492	0.0575

Table 31. Peak pressure [MPa] at 0 degrees of flexion no graft

Sample Number	Knee	State	Side A	Side B
			Peak Pressure	Peak Pressure
5	L	RECON_1	0.0930	0.1085
		RECON_2	0.0793	0.4206
		RECON_3	0.0776	0.1050
6	L	RECON_1	0.2077	0.3586
		RECON_2	0.0759	0.1434
		RECON_3	0.1085	0.1933
7	L	RECON_1	0.3530	0.1682
		RECON_2	0.2077	0.0895
		RECON_3	0.1951	0.0709
8	L	RECON_1	0.0861	0.0658
		RECON_2	0.0558	0.2494
		RECON_3	0.0827	0.0266
9	L	RECON_1	0.0591	0.4528
		RECON_2	0.0097	0.4528
		RECON_3	0.0742	0.4471
10	L	RECON_1	0.3792	0.0282
		RECON_2	0.4452	0.2059
		RECON_3	0.4093	0.0459
11	R	RECON_1	0.3717	0.0861
		RECON_2	0.2059	0.0625
		RECON_3	0.1915	0.0575
12	R	RECON_1	0.2203	0.0188
		RECON_2	0.3380	0.0250
		RECON_3	0.2440	0.1364
13	R	RECON_1	0.2733	0.1753
		RECON_2	0.3287	0.1629
		RECON_3	0.4282	0.1879
14	R	RECON_1	0.1879	0.0203
		RECON_2	0.1813	0.2489
		RECON_3	0.1753	0.0509
15	R	RECON_1	0.3999	0.1807
		RECON_2	0.2549	0.4433
		RECON_3	0.3266	0.1250
16	R	RECON_1	0.0142	0.4490
		RECON_2	0.1013	0.5759
		RECON_3	0.0827	0.4263

Table 32. Peak pressure [MPa] at 0 degrees of flexion with PL graft inserted

Sample Number	Knee	State	Side A	Side B
			Peak Pressure	Peak Pressure
5	L	RECON_1	0.0127	0.0692
		RECON_2	0.1593	0.3324
		RECON_3	0.1861	0.1771
6	L	RECON_1	0.2294	0.3343
		RECON_2	0.1102	0.1647
		RECON_3	0.1682	0.1915
7	L	RECON_1	0.3287	0.1576
		RECON_2	0.2843	0.1171
		RECON_3	0.1700	0.0742
8	L	RECON_1	0.1050	0.2458
		RECON_2	0.0709	0.1682
		RECON_3	0.0394	0.2549
9	L	RECON_1	0.1879	0.4414
		RECON_2	0.1259	0.4395
		RECON_3	0.1879	0.4414
10	L	RECON_1	0.3679	0.0330
		RECON_2	0.4376	0.1487
		RECON_3	0.4395	0.0558
11	R	RECON_1	0.4093	0.0827
		RECON_2	0.2861	0.0266
		RECON_3	0.2330	0.0575
12	R	RECON_1	0.3623	0.0188
		RECON_2	0.2972	0.0172
		RECON_3	0.3083	0.0330
13	R	RECON_1	0.2825	0.2240
		RECON_2	0.3567	0.2041
		RECON_3	0.4112	0.1879
14	R	RECON_1	0.2023	0.0314
		RECON_2	0.2113	0.0266
		RECON_3	0.1540	0.0250
15	R	RECON_1	0.2861	0.1540
		RECON_2	0.2167	0.4263
		RECON_3	0.2400	0.1761
16	R	RECON_1	0.0219	0.4395
		RECON_2	0.1280	0.6527
		RECON_3	0.2005	0.4301

Table 33. Peak pressure [MPa] at 0 degrees of flexion with PL graft fixed

Sample Number	Knee	State	Side A	Side B
			Peak Pressure	Peak Pressure
5	L	RECON_1	0.2861	0.1294
		RECON_2	0.2494	0.1505
		RECON_3	0.2185	0.2221
6	L	RECON_1	0.2843	0.2935
		RECON_2	0.1381	0.1789
		RECON_3	0.2041	0.2095
7	L	RECON_1	0.1346	0.1364
		RECON_2	0.1505	0.0964
		RECON_3	0.4301	0.1593
8	L	RECON_1	0.0726	0.2861
		RECON_2	0.0427	0.1399
		RECON_3	0.0558	0.2403
9	L	RECON_1	0.0720	0.6174
		RECON_2	0.0542	0.4395
		RECON_3	0.1381	0.4528
10	L	RECON_1	0.3961	0.0591
		RECON_2	0.4168	0.1085
		RECON_3	0.3474	0.1137
11	R	RECON_1	0.1861	0.0793
		RECON_2	0.2494	0.0188
		RECON_3	0.3046	0.0793
12	R	RECON_1	0.3287	0.0443
		RECON_2	0.3980	0.0282
		RECON_3	0.3604	0.0362
13	R	RECON_1	0.3867	0.1505
		RECON_2	0.3829	0.1294
		RECON_3	0.3754	0.1137
14	R	RECON_1	0.2898	0.0394
		RECON_2	0.2312	0.0575
		RECON_3	0.3028	0.1329
15	R	RECON_1	0.3548	0.2494
		RECON_2	0.3717	0.2005
		RECON_3	0.3578	0.3985
16	R	RECON_1	0.0608	0.4395
		RECON_2	0.0691	0.6174
		RECON_3	0.1469	0.4357

Table 34. Peak pressure [MPa] at 30 degrees with PL graft fixed

Sample Number	Knee	State	Side A	Side B
			Peak Pressure	Peak Pressure
5	L	RECON_1	0.0157	0.0298
		RECON_2	0.0053	0.0625
		RECON_3	0.0082	0.0492
6	L	RECON_1	0.0410	0.1753
		RECON_2	0.0082	0.1033
		RECON_3	0.0282	0.1505
7	L	RECON_1	0.0726	0.0759
		RECON_2	0.0394	0.0827
		RECON_3	0.0314	0.0509
8	L	RECON_1	0.0172	0.0142
		RECON_2	0.0378	0.0097
		RECON_3	0.0525	0.0000
9	L	RECON_1	0.0410	0.1224
		RECON_2	0.0188	0.1294
		RECON_3	0.0443	0.0053
10	L	RECON_1	0.0608	0.0112
		RECON_2	0.1771	0.0625
		RECON_3	0.1171	0.0235
11	R	RECON_1	0.0878	0.0219
		RECON_2	0.0861	0.0097
		RECON_3	0.0912	0.0039
12	R	RECON_1	0.0203	0.0142
		RECON_2	0.0492	0.0298
		RECON_3	0.0542	0.0314
13	R	RECON_1	0.4206	0.0709
		RECON_2	0.4414	0.0625
		RECON_3	0.4995	0.0634
14	R	RECON_1	0.0235	0.0266
		RECON_2	0.0692	0.1016
		RECON_3	0.0378	0.0127
15	R	RECON_1	0.0142	0.0362
		RECON_2	0.0172	0.0330
		RECON_3	0.0182	0.0320
16	R	RECON_1	0.0142	0.0947
		RECON_2	0.0608	0.0250
		RECON_3	0.0157	0.1206

Table 35. Peak pressure [MPa] at 30 degrees with AM graft inserted and PL graft fixed

Sample Number	Knee	State	Side A	Side B
			Peak Pressure	Peak Pressure
5	L	RECON_1	0.0203	0.0575
		RECON_2	0.0053	0.0591
		RECON_3	0.0625	0.0250
6	L	RECON_1	0.0575	0.1933
		RECON_2	0.0188	0.0912
		RECON_3	0.0203	0.1311
7	L	RECON_1	0.1119	0.0726
		RECON_2	0.0330	0.0692
		RECON_3	0.0981	0.1381
8	L	RECON_1	0.0053	0.0127
		RECON_2	0.0266	0.0025
		RECON_3	0.0188	0.0053
9	L	RECON_1	0.0861	0.0127
		RECON_2	0.0525	0.0082
		RECON_3	0.0675	0.0188
10	L	RECON_1	0.1189	0.0097
		RECON_2	0.1399	0.0459
		RECON_3	0.1434	0.0250
11	R	RECON_1	0.1171	0.0112
		RECON_2	0.0692	0.0053
		RECON_3	0.0575	0.0039
12	R	RECON_1	0.0082	0.0097
		RECON_2	0.0157	0.0142
		RECON_3	0.0427	0.0314
13	R	RECON_1	0.4773	0.0837
		RECON_2	0.3999	0.0427
		RECON_3	0.5599	0.0720
14	R	RECON_1	0.0509	0.0188
		RECON_2	0.0810	0.0427
		RECON_3	0.0492	0.0127
15	R	RECON_1	0.0298	0.0330
		RECON_2	0.0266	0.0314
		RECON_3	0.0235	0.0282
16	R	RECON_1	0.0203	0.0625
		RECON_2	0.0749	0.1220
		RECON_3	0.0157	0.0625

Table 36. Peak pressure [MPa] at 30 degrees with AM graft fixed and PL graft fixed

Sample Number	Knee	State	Side A	Side B
			Peak Pressure	Peak Pressure
5	L	RECON_1	0.0427	0.0410
		RECON_2	0.0509	0.0642
		RECON_3	0.0298	0.0642
6	L	RECON_1	0.0709	0.1807
		RECON_2	0.0235	0.1067
		RECON_3	0.0314	0.1452
7	L	RECON_1	0.1119	0.0844
		RECON_2	0.0142	0.1346
		RECON_3	0.0558	0.1033
8	L	RECON_1	0.0082	0.0068
		RECON_2	0.0025	0.0188
		RECON_3	0.0068	0.0053
9	L	RECON_1	0.0658	0.0127
		RECON_2	0.0142	0.2421
		RECON_3	0.0097	0.1469
10	L	RECON_1	0.0947	0.0266
		RECON_2	0.1294	0.0314
		RECON_3	0.1399	0.2861
11	R	RECON_1	0.1736	0.0188
		RECON_2	0.1276	0.0082
		RECON_3	0.1558	0.0039
12	R	RECON_1	0.0298	0.0142
		RECON_2	0.1259	0.0298
		RECON_3	0.0330	0.0235
13	R	RECON_1	0.4963	0.1191
		RECON_2	0.4055	0.1016
		RECON_3	0.3735	0.0844
14	R	RECON_1	0.1593	0.0157
		RECON_2	0.1154	0.0203
		RECON_3	0.3604	0.0172
15	R	RECON_1	0.0591	0.0895
		RECON_2	0.0427	0.0443
		RECON_3	0.0427	0.0282
16	R	RECON_1	0.0810	0.1189
		RECON_2	0.1085	0.0575
		RECON_3	0.1753	0.0947

The location of peak pressure for 0, 15, 30, and 45 degrees of flexion during graft fixation is given below.

Table 37. Location of peak pressure [mm] for 30 degrees of flexion with no graft

Sample Number	Knee	State	Lateral		Medial	
			x location [mm]	y location	x location	y location [mm]
5	L	RECON_1	8.51	6.54	21.12	18.66
		RECON_2	7.20	7.94	22.66	18.63
		RECON_3	7.68	6.79	28.60	0.00
6	L	RECON_1	7.38	12.98	23.55	10.78
		RECON_2	6.91	13.82	24.17	8.14
		RECON_3	6.80	13.90	24.36	10.10
7	L	RECON_1	9.16	6.34	12.58	12.83
		RECON_2	10.80	6.59	19.25	20.24
		RECON_3	9.51	4.84	12.98	6.07
8	L	RECON_1	4.46	7.89	9.09	31.99
		RECON_2	5.41	7.78	3.93	25.12
		RECON_3	2.70	6.06	6.49	22.09
9	L	RECON_1	7.82	17.07	12.75	12.71
		RECON_2	11.85	14.83	8.07	12.14
		RECON_3	1.92	27.11	12.40	10.10
10	L	RECON_1	12.78	7.18	3.36	7.96
		RECON_2	11.07	10.24	5.75	9.60
		RECON_3	13.42	6.49	4.08	7.13
11	R	RECON_1	11.26	10.85	17.17	15.11
		RECON_2	11.62	11.41	19.39	27.14
		RECON_3	10.29	9.52	9.75	21.74
12	R	RECON_1	4.34	8.55	22.75	15.58
		RECON_2	5.22	7.11	21.66	17.43
		RECON_3	3.33	7.21	18.77	16.55
13	R	RECON_1	16.92	19.27	16.76	20.83
		RECON_2	18.44	17.46	21.52	22.91
		RECON_3	16.38	20.07	18.72	22.38
14	R	RECON_1	11.34	12.23	25.19	19.64
		RECON_2	11.58	14.52	25.63	19.42
		RECON_3	11.96	9.95	26.01	19.12
15	R	RECON_1	14.40	9.86	13.45	20.63
		RECON_2	17.55	13.25	10.77	21.83
		RECON_3	16.58	13.57	11.05	21.68
16	R	RECON_1	12.09	11.68	5.42	4.56
		RECON_2	10.22	9.56	8.66	8.19
		RECON_3	13.13	8.27	5.53	5.01

Table 38. Location of peak pressure [mm] for 0 degrees of flexion with no graft

Sample Number	Knee	State	Lateral		Medial	
			x location [mm]	y location [mm]	x location [mm]	y location [mm]
5	L	RECON_1	17.23	9.05	8.78	2.26
		RECON_2	19.74	8.69	5.04	3.22
		RECON_3	15.04	9.57	10.25	1.43
6	L	RECON_1	9.93	10.22	21.15	18.98
		RECON_2	9.31	11.11	21.43	16.79
		RECON_3	9.48	11.21	21.70	17.28
7	L	RECON_1	17.01	6.43	18.50	15.81
		RECON_2	18.07	6.80	20.08	16.28
		RECON_3	15.54	6.45	17.70	10.53
8	L	RECON_1	23.09	2.72	11.77	5.41
		RECON_2	20.25	5.94	7.64	9.43
		RECON_3	18.56	3.50	11.11	6.50
9	L	RECON_1	15.15	14.14	15.66	12.01
		RECON_2	15.38	13.66	13.76	13.68
		RECON_3	16.12	12.70	5.78	5.74
10	L	RECON_1	18.00	10.05	5.81	6.68
		RECON_2	16.76	11.11	7.80	8.41
		RECON_3	19.82	11.43	6.19	6.95
11	R	RECON_1	19.36	7.75	11.48	8.89
		RECON_2	19.19	8.49	9.28	6.65
		RECON_3	19.77	7.23	4.97	7.98
12	R	RECON_1	13.19	7.11	22.12	15.51
		RECON_2	14.84	6.63	20.57	16.12
		RECON_3	5.30	11.37	10.84	14.52
13	R	RECON_1	13.85	16.00	16.53	14.73
		RECON_2	16.51	14.50	18.58	14.68
		RECON_3	14.15	15.88	15.19	13.49
14	R	RECON_1	17.14	10.59	21.31	12.44
		RECON_2	17.28	9.56	17.59	11.08
		RECON_3	17.36	8.52	13.71	9.57
15	R	RECON_1	13.41	5.35	16.76	9.98
		RECON_2	14.79	6.30	18.32	6.87
		RECON_3	13.61	4.94	17.36	8.44
16	R	RECON_1	13.36	13.03	9.51	3.91
		RECON_2	10.31	11.42	9.84	5.62
		RECON_3	21.70	7.29	12.54	12.77

Table 39. Location of peak pressure [mm] at 0 degrees of flexion with PL graft inserted

Sample Number	Knee	State	Lateral		Medial	
			x location [mm]	y location [mm]	x location [mm]	y location [mm]
5	L	RECON_1	8.45	7.42	17.91	14.17
		RECON_2	19.07	9.79	6.50	2.77
		RECON_3	18.43	9.59	9.56	1.78
6	L	RECON_1	9.58	10.13	21.23	19.03
		RECON_2	9.93	10.19	20.95	16.52
		RECON_3	11.47	9.07	19.79	14.69
7	L	RECON_1	15.84	6.78	18.54	12.40
		RECON_2	17.76	6.13	18.34	10.48
		RECON_3	13.54	7.04	18.40	10.82
8	L	RECON_1	21.35	2.33	14.50	3.89
		RECON_2	16.29	4.01	21.92	2.54
		RECON_3	17.43	2.28	17.54	4.44
9	L	RECON_1	14.97	13.26	11.36	7.89
		RECON_2	17.10	12.04	7.10	5.94
		RECON_3	16.18	13.37	5.42	4.30
10	L	RECON_1	18.61	11.72	6.17	6.25
		RECON_2	18.08	10.63	7.32	6.99
		RECON_3	19.13	10.80	6.83	6.31
11	R	RECON_1	20.35	6.76	13.12	9.95
		RECON_2	20.13	7.33	12.96	10.88
		RECON_3	20.59	7.03	5.05	8.60
12	R	RECON_1	14.71	6.65	23.14	14.84
		RECON_2	14.42	6.89	17.48	10.67
		RECON_3	10.39	10.20	21.15	14.78
13	R	RECON_1	13.85	16.13	15.50	13.77
		RECON_2	16.56	14.55	15.86	13.00
		RECON_3	14.06	16.10	16.24	13.28
14	R	RECON_1	17.27	9.89	18.72	10.34
		RECON_2	15.73	11.21	17.98	20.59
		RECON_3	16.65	9.57	14.12	10.58
15	R	RECON_1	13.47	5.67	17.15	11.41
		RECON_2	14.59	6.71	18.33	6.71
		RECON_3	13.48	5.29	17.16	7.47
16	R	RECON_1	15.30	11.76	9.75	3.92
		RECON_2	11.78	10.65	10.60	5.16
		RECON_3	22.84	4.95	12.48	13.44

Table 40. Location of peak pressure [mm] at 0 degrees of flexion with PL graft fixed

Sample Number	Knee	State	Lateral		Medial	
			x location [mm]	y location [mm]	x location [mm]	y location [mm]
5	L	RECON_1	18.34	10.26	9.91	2.10
		RECON_2	16.42	11.23	10.05	2.06
		RECON_3	19.13	10.38	10.01	1.62
6	L	RECON_1	9.44	10.06	21.73	17.37
		RECON_2	10.45	9.63	20.38	12.86
		RECON_3	10.43	9.37	19.55	13.46
7	L	RECON_1	12.99	7.16	19.24	11.34
		RECON_2	15.10	7.66	20.50	10.59
		RECON_3	18.56	7.55	19.83	7.54
8	L	RECON_1	20.75	2.45	16.78	3.45
		RECON_2	17.77	4.77	19.59	3.03
		RECON_3	18.11	2.09	20.10	3.49
9	L	RECON_1	14.80	14.82	16.19	9.60
		RECON_2	15.76	14.69	10.49	8.68
		RECON_3	15.35	14.01	6.87	5.75
10	L	RECON_1	19.72	12.40	6.44	6.36
		RECON_2	16.76	9.80	7.29	5.88
		RECON_3	19.69	12.29	7.52	5.96
11	R	RECON_1	16.80	10.08	7.40	7.96
		RECON_2	17.52	9.30	11.16	10.96
		RECON_3	19.00	8.00	3.97	4.53
12	R	RECON_1	10.35	5.86	9.23	6.43
		RECON_2	13.37	5.94	16.59	11.90
		RECON_3	12.41	7.64	20.72	14.05
13	R	RECON_1	14.08	15.28	20.34	15.49
		RECON_2	17.04	14.47	22.35	16.20
		RECON_3	13.75	15.85	19.10	14.06
14	R	RECON_1	17.58	9.39	18.52	9.63
		RECON_2	14.68	10.76	15.96	14.80
		RECON_3	16.51	10.35	11.20	8.91
15	R	RECON_1	13.16	4.62	18.27	8.11
		RECON_2	14.09	4.37	16.40	11.04
		RECON_3	13.22	3.95	18.83	5.62
16	R	RECON_1	16.32	9.68	11.08	4.37
		RECON_2	16.60	9.07	10.19	3.96
		RECON_3	21.02	6.56	13.29	14.09

Table 41. Location of peak pressure [mm] at 30 degrees of flexion with PL graft fixed

Sample Number	Knee	State	Lateral		Medial	
			x location [mm]	y location [mm]	x location [mm]	y location [mm]
5	L	RECON_1	7.94	7.96	11.22	8.38
		RECON_2	6.96	7.18	20.10	20.50
		RECON_3	7.86	6.67	9.03	14.38
6	L	RECON_1	6.94	13.00	23.76	8.81
		RECON_2	6.91	12.69	23.98	7.13
		RECON_3	6.95	12.89	20.92	9.87
7	L	RECON_1	8.56	7.84	13.11	13.14
		RECON_2	9.23	7.49	16.23	13.15
		RECON_3	8.76	4.94	18.24	15.47
8	L	RECON_1	6.69	9.43	9.65	24.36
		RECON_2	5.65	4.04	6.81	9.04
		RECON_3	28.60	0.00	8.19	7.83
9	L	RECON_1	11.93	16.49	13.58	16.00
		RECON_2	12.57	14.82	18.52	18.14
		RECON_3	2.48	27.41	12.54	13.49
10	L	RECON_1	12.56	6.34	3.52	8.65
		RECON_2	11.94	8.63	4.85	7.51
		RECON_3	13.20	5.52	4.26	8.36
11	R	RECON_1	11.84	11.03	19.73	28.39
		RECON_2	14.31	11.37	22.49	18.71
		RECON_3	14.70	10.82	9.11	19.37
12	R	RECON_1	4.09	7.28	23.50	19.11
		RECON_2	10.07	7.14	22.33	16.43
		RECON_3	6.44	7.82	20.90	13.65
13	R	RECON_1	15.65	18.16	20.37	22.88
		RECON_2	18.04	16.32	20.87	23.06
		RECON_3	16.29	18.78	21.22	22.94
14	R	RECON_1	6.07	11.55	12.24	12.62
		RECON_2	8.69	9.79	8.89	8.91
		RECON_3	12.13	10.28	25.40	19.75
15	R	RECON_1	18.52	15.22	14.02	23.36
		RECON_2	20.86	17.26	11.30	22.57
		RECON_3	21.20	15.77	8.57	20.59
16	R	RECON_1	3.24	23.13	4.86	5.75
		RECON_2	13.39	7.71	6.17	9.77
		RECON_3	9.39	10.69	5.93	4.97

Table 42. Location of peak pressure [mm] with 30 degrees of flexion with AM graft inserted and PL graft fixed

Sample Number	Knee	State	Lateral		Medial	
			x location [mm]	y location [mm]	x location [mm]	y location [mm]
5	L	RECON_1	8.37	6.35	8.81	8.97
		RECON_2	6.78	8.85	24.74	4.24
		RECON_3	7.61	8.54	9.63	10.44
6	L	RECON_1	7.69	13.03	22.67	13.35
		RECON_2	7.17	12.82	23.99	8.66
		RECON_3	6.74	13.09	23.98	9.61
7	L	RECON_1	7.74	8.70	13.87	11.19
		RECON_2	9.14	7.05	10.46	12.35
		RECON_3	11.32	8.17	18.88	7.00
8	L	RECON_1	6.10	6.91	8.28	28.82
		RECON_2	1.33	23.48	8.25	7.27
		RECON_3	16.93	4.60	8.10	7.56
9	L	RECON_1	9.67	15.36	11.78	12.15
		RECON_2	5.40	19.83	10.99	11.49
		RECON_3	8.03	17.59	11.16	12.53
10	L	RECON_1	12.97	5.06	3.56	7.61
		RECON_2	10.87	8.60	4.65	8.54
		RECON_3	11.25	7.15	3.84	7.73
11	R	RECON_1	12.30	10.02	18.36	27.83
		RECON_2	13.00	10.97	22.85	16.06
		RECON_3	13.61	10.92	14.57	19.40
12	R	RECON_1	7.58	5.19	21.08	14.69
		RECON_2	7.76	7.07	17.44	11.63
		RECON_3	4.51	8.76	21.55	15.52
13	R	RECON_1	16.55	18.58	22.53	21.11
		RECON_2	18.76	17.79	14.31	15.33
		RECON_3	15.85	18.50	20.84	23.28
14	R	RECON_1	7.50	10.34	25.61	21.30
		RECON_2	8.90	10.78	11.51	10.44
		RECON_3	9.26	9.52	25.39	20.56
15	R	RECON_1	16.19	12.50	12.93	22.90
		RECON_2	16.97	14.91	10.77	22.51
		RECON_3	16.89	13.04	11.55	20.94
16	R	RECON_1	12.92	9.94	5.54	4.52
		RECON_2	12.98	7.82	7.07	4.07
		RECON_3	9.45	26.71	9.10	24.19

Table 43. Location of peak pressure [mm] at 30 degrees of flexion with PL graft and AM graft fixed

Sample Number	Knee	State	Lateral		Medial	
			x location [mm]	y location [mm]	x location [mm]	y location [mm]
5	L	RECON_1	8.65	6.65	17.03	3.53
		RECON_2	11.72	9.71	21.29	5.70
		RECON_3	11.79	10.11	23.88	10.03
6	L	RECON_1	7.76	12.60	22.62	13.85
		RECON_2	7.61	12.17	23.85	11.09
		RECON_3	7.30	12.95	20.29	18.50
7	L	RECON_1	8.49	6.38	12.59	11.07
		RECON_2	10.98	5.09	21.43	17.97
		RECON_3	9.66	6.71	17.49	10.13
8	L	RECON_1	9.54	5.65	11.51	30.69
		RECON_2	4.24	7.02	7.04	24.75
		RECON_3	3.71	6.75	14.84	13.96
9	L	RECON_1	8.90	15.25	16.11	11.69
		RECON_2	16.84	14.89	20.69	22.87
		RECON_3	14.14	13.99	16.43	24.16
10	L	RECON_1	16.12	10.95	4.88	9.08
		RECON_2	11.35	8.38	8.59	15.33
		RECON_3	18.46	13.61	8.38	9.97
11	R	RECON_1	14.13	9.31	19.74	30.18
		RECON_2	14.35	10.01	21.60	25.79
		RECON_3	15.07	9.79	17.21	26.32
12	R	RECON_1	3.28	7.43	20.38	16.38
		RECON_2	12.64	6.46	22.97	18.47
		RECON_3	5.87	7.38	19.66	14.47
13	R	RECON_1	15.39	17.33	20.42	23.13
		RECON_2	17.45	16.50	21.87	22.23
		RECON_3	14.55	17.69	21.03	22.82
14	R	RECON_1	13.97	11.04	24.26	19.75
		RECON_2	9.98	9.76	24.03	18.67
		RECON_3	16.51	11.32	23.99	17.36
15	R	RECON_1	13.16	9.75	15.93	14.83
		RECON_2	16.71	10.73	11.72	19.50
		RECON_3	14.31	10.40	10.76	21.96
16	R	RECON_1	17.34	7.26	7.77	6.31
		RECON_2	13.72	7.28	9.38	5.73
		RECON_3	15.42	6.99	11.63	3.39

The location of the center of pressure during graft fixation is given below for 0, 15, 30, and 45 degrees of flexion.

Table 44. Location of center of pressure [mm] at 30 degrees with no graft

Sample Number	Knee	State	Lateral		Medial	
			x location [mm]	y location	x location	y location [mm]
5	L	RECON_1	8.51	6.54	21.12	18.66
		RECON_2	7.20	7.94	22.66	18.63
		RECON_3	7.68	6.79	28.60	0.00
6	L	RECON_1	7.38	12.98	23.55	10.78
		RECON_2	6.91	13.82	24.17	8.14
		RECON_3	6.80	13.90	24.36	10.10
7	L	RECON_1	9.16	6.34	12.58	12.83
		RECON_2	10.80	6.59	19.25	20.24
		RECON_3	9.51	4.84	12.98	6.07
8	L	RECON_1	4.46	7.89	9.09	31.99
		RECON_2	5.41	7.78	3.93	25.12
		RECON_3	2.70	6.06	6.49	22.09
9	L	RECON_1	7.82	17.07	12.75	12.71
		RECON_2	11.85	14.83	8.07	12.14
		RECON_3	1.92	27.11	12.40	10.10
10	L	RECON_1	12.78	7.18	3.36	7.96
		RECON_2	11.07	10.24	5.75	9.60
		RECON_3	13.42	6.49	4.08	7.13
11	R	RECON_1	11.26	10.85	17.17	15.11
		RECON_2	11.62	11.41	19.39	27.14
		RECON_3	10.29	9.52	9.75	21.74
12	R	RECON_1	4.34	8.55	22.75	15.58
		RECON_2	5.22	7.11	21.66	17.43
		RECON_3	3.33	7.21	18.77	16.55
13	R	RECON_1	16.92	19.27	16.76	20.83
		RECON_2	18.44	17.46	21.52	22.91
		RECON_3	16.38	20.07	18.72	22.38
14	R	RECON_1	11.34	12.23	25.19	19.64
		RECON_2	11.58	14.52	25.63	19.42
		RECON_3	11.96	9.95	26.01	19.12
15	R	RECON_1	14.40	9.86	13.45	20.63
		RECON_2	17.55	13.25	10.77	21.83
		RECON_3	16.58	13.57	11.05	21.68
16	R	RECON_1	12.09	11.68	5.42	4.56
		RECON_2	10.22	9.56	8.66	8.19
		RECON_3	13.13	8.27	5.53	5.01

Table 45. Location of center of pressure [mm] at 0 degrees with no graft

Sample Number	Knee	State	Lateral		Medial	
			x location [mm]	y location [mm]	x location [mm]	y location [mm]
5	L	RECON_1	17.23	9.05	8.78	2.26
		RECON_2	19.74	8.69	5.04	3.22
		RECON_3	15.04	9.57	10.25	1.43
6	L	RECON_1	9.93	10.22	21.15	18.98
		RECON_2	9.31	11.11	21.43	16.79
		RECON_3	9.48	11.21	21.70	17.28
7	L	RECON_1	17.01	6.43	18.50	15.81
		RECON_2	18.07	6.80	20.08	16.28
		RECON_3	15.54	6.45	17.70	10.53
8	L	RECON_1	23.09	2.72	11.77	5.41
		RECON_2	20.25	5.94	7.64	9.43
		RECON_3	18.56	3.50	11.11	6.50
9	L	RECON_1	15.15	14.14	15.66	12.01
		RECON_2	15.38	13.66	13.76	13.68
		RECON_3	16.12	12.70	5.78	5.74
10	L	RECON_1	18.00	10.05	5.81	6.68
		RECON_2	16.76	11.11	7.80	8.41
		RECON_3	19.82	11.43	6.19	6.95
11	R	RECON_1	19.36	7.75	11.48	8.89
		RECON_2	19.19	8.49	9.28	6.65
		RECON_3	19.77	7.23	4.97	7.98
12	R	RECON_1	13.19	7.11	22.12	15.51
		RECON_2	14.84	6.63	20.57	16.12
		RECON_3	5.30	11.37	10.84	14.52
13	R	RECON_1	13.85	16.00	16.53	14.73
		RECON_2	16.51	14.50	18.58	14.68
		RECON_3	14.15	15.88	15.19	13.49
14	R	RECON_1	17.14	10.59	21.31	12.44
		RECON_2	17.28	9.56	17.59	11.08
		RECON_3	17.36	8.52	13.71	9.57
15	R	RECON_1	13.41	5.35	16.76	9.98
		RECON_2	14.79	6.30	18.32	6.87
		RECON_3	13.61	4.94	17.36	8.44
16	R	RECON_1	13.36	13.03	9.51	3.91
		RECON_2	10.31	11.42	9.84	5.62
		RECON_3	21.70	7.29	12.54	12.77

Table 46. Location of center of pressure [mm] at 0 degrees with PL graft inserted

Sample Number	Knee	State	Lateral		Medial	
			x location [mm]	y location [mm]	x location [mm]	y location [mm]
5	L	RECON_1	8.45	7.42	17.91	14.17
		RECON_2	19.07	9.79	6.50	2.77
		RECON_3	18.43	9.59	9.56	1.78
6	L	RECON_1	9.58	10.13	21.23	19.03
		RECON_2	9.93	10.19	20.95	16.52
		RECON_3	11.47	9.07	19.79	14.69
7	L	RECON_1	15.84	6.78	18.54	12.40
		RECON_2	17.76	6.13	18.34	10.48
		RECON_3	13.54	7.04	18.40	10.82
8	L	RECON_1	21.35	2.33	14.50	3.89
		RECON_2	16.29	4.01	21.92	2.54
		RECON_3	17.43	2.28	17.54	4.44
9	L	RECON_1	14.97	13.26	11.36	7.89
		RECON_2	17.10	12.04	7.10	5.94
		RECON_3	16.18	13.37	5.42	4.30
10	L	RECON_1	18.61	11.72	6.17	6.25
		RECON_2	18.08	10.63	7.32	6.99
		RECON_3	19.13	10.80	6.83	6.31
11	R	RECON_1	20.35	6.76	13.12	9.95
		RECON_2	20.13	7.33	12.96	10.88
		RECON_3	20.59	7.03	5.05	8.60
12	R	RECON_1	14.71	6.65	23.14	14.84
		RECON_2	14.42	6.89	17.48	10.67
		RECON_3	10.39	10.20	21.15	14.78
13	R	RECON_1	13.85	16.13	15.50	13.77
		RECON_2	16.56	14.55	15.86	13.00
		RECON_3	14.06	16.10	16.24	13.28
14	R	RECON_1	17.27	9.89	18.72	10.34
		RECON_2	15.73	11.21	17.98	20.59
		RECON_3	16.65	9.57	14.12	10.58
15	R	RECON_1	13.47	5.67	17.15	11.41
		RECON_2	14.59	6.71	18.33	6.71
		RECON_3	13.48	5.29	17.16	7.47
16	R	RECON_1	15.30	11.76	9.75	3.92
		RECON_2	11.78	10.65	10.60	5.16
		RECON_3	22.84	4.95	12.48	13.44

Table 47. Location of center of pressure [mm] at 0 degrees with PL graft fixed

Sample Number	Knee	State	Lateral		Medial	
			x location [mm]	y location [mm]	x location [mm]	y location [mm]
5	L	RECON_1	18.34	10.26	9.91	2.10
		RECON_2	16.42	11.23	10.05	2.06
		RECON_3	19.13	10.38	10.01	1.62
6	L	RECON_1	9.44	10.06	21.73	17.37
		RECON_2	10.45	9.63	20.38	12.86
		RECON_3	10.43	9.37	19.55	13.46
7	L	RECON_1	12.99	7.16	19.24	11.34
		RECON_2	15.10	7.66	20.50	10.59
		RECON_3	18.56	7.55	19.83	7.54
8	L	RECON_1	20.75	2.45	16.78	3.45
		RECON_2	17.77	4.77	19.59	3.03
		RECON_3	18.11	2.09	20.10	3.49
9	L	RECON_1	14.80	14.82	16.19	9.60
		RECON_2	15.76	14.69	10.49	8.68
		RECON_3	15.35	14.01	6.87	5.75
10	L	RECON_1	19.72	12.40	6.44	6.36
		RECON_2	16.76	9.80	7.29	5.88
		RECON_3	19.69	12.29	7.52	5.96
11	R	RECON_1	16.80	10.08	7.40	7.96
		RECON_2	17.52	9.30	11.16	10.96
		RECON_3	19.00	8.00	3.97	4.53
12	R	RECON_1	10.35	5.86	9.23	6.43
		RECON_2	13.37	5.94	16.59	11.90
		RECON_3	12.41	7.64	20.72	14.05
13	R	RECON_1	14.08	15.28	20.34	15.49
		RECON_2	17.04	14.47	22.35	16.20
		RECON_3	13.75	15.85	19.10	14.06
14	R	RECON_1	17.58	9.39	18.52	9.63
		RECON_2	14.68	10.76	15.96	14.80
		RECON_3	16.51	10.35	11.20	8.91
15	R	RECON_1	13.16	4.62	18.27	8.11
		RECON_2	14.09	4.37	16.40	11.04
		RECON_3	13.22	3.95	18.83	5.62
16	R	RECON_1	16.32	9.68	11.08	4.37
		RECON_2	16.60	9.07	10.19	3.96
		RECON_3	21.02	6.56	13.29	14.09

Table 48. Location of center of pressure [mm] at 30 degrees and PL graft fixed

Sample Number	Knee	State	Lateral		Medial	
			x location [mm]	y location [mm]	x location [mm]	y location [mm]
5	L	RECON_1	7.94	7.96	11.22	8.38
		RECON_2	6.96	7.18	20.10	20.50
		RECON_3	7.86	6.67	9.03	14.38
6	L	RECON_1	6.94	13.00	23.76	8.81
		RECON_2	6.91	12.69	23.98	7.13
		RECON_3	6.95	12.89	20.92	9.87
7	L	RECON_1	8.56	7.84	13.11	13.14
		RECON_2	9.23	7.49	16.23	13.15
		RECON_3	8.76	4.94	18.24	15.47
8	L	RECON_1	6.69	9.43	9.65	24.36
		RECON_2	5.65	4.04	6.81	9.04
		RECON_3	28.60	0.00	8.19	7.83
9	L	RECON_1	11.93	16.49	13.58	16.00
		RECON_2	12.57	14.82	18.52	18.14
		RECON_3	2.48	27.41	12.54	13.49
10	L	RECON_1	12.56	6.34	3.52	8.65
		RECON_2	11.94	8.63	4.85	7.51
		RECON_3	13.20	5.52	4.26	8.36
11	R	RECON_1	11.84	11.03	19.73	28.39
		RECON_2	14.31	11.37	22.49	18.71
		RECON_3	14.70	10.82	9.11	19.37
12	R	RECON_1	4.09	7.28	23.50	19.11
		RECON_2	10.07	7.14	22.33	16.43
		RECON_3	6.44	7.82	20.90	13.65
13	R	RECON_1	15.65	18.16	20.37	22.88
		RECON_2	18.04	16.32	20.87	23.06
		RECON_3	16.29	18.78	21.22	22.94
14	R	RECON_1	6.07	11.55	12.24	12.62
		RECON_2	8.69	9.79	8.89	8.91
		RECON_3	12.13	10.28	25.40	19.75
15	R	RECON_1	18.52	15.22	14.02	23.36
		RECON_2	20.86	17.26	11.30	22.57
		RECON_3	21.20	15.77	8.57	20.59
16	R	RECON_1	3.24	23.13	4.86	5.75
		RECON_2	13.39	7.71	6.17	9.77
		RECON_3	9.39	10.69	5.93	4.97

Table 49. Location of center of pressure [mm] at 30 degrees with AM graft inserted and PL graft fixed

Sample Number	Knee	State	Lateral		Medial	
			x location [mm]	y location [mm]	x location [mm]	y location [mm]
5	L	RECON_1	8.37	6.35	8.81	8.97
		RECON_2	6.78	8.85	24.74	4.24
		RECON_3	7.61	8.54	9.63	10.44
6	L	RECON_1	7.69	13.03	22.67	13.35
		RECON_2	7.17	12.82	23.99	8.66
		RECON_3	6.74	13.09	23.98	9.61
7	L	RECON_1	7.74	8.70	13.87	11.19
		RECON_2	9.14	7.05	10.46	12.35
		RECON_3	11.32	8.17	18.88	7.00
8	L	RECON_1	6.10	6.91	8.28	28.82
		RECON_2	1.33	23.48	8.25	7.27
		RECON_3	16.93	4.60	8.10	7.56
9	L	RECON_1	9.67	15.36	11.78	12.15
		RECON_2	5.40	19.83	10.99	11.49
		RECON_3	8.03	17.59	11.16	12.53
10	L	RECON_1	12.97	5.06	3.56	7.61
		RECON_2	10.87	8.60	4.65	8.54
		RECON_3	11.25	7.15	3.84	7.73
11	R	RECON_1	12.30	10.02	18.36	27.83
		RECON_2	13.00	10.97	22.85	16.06
		RECON_3	13.61	10.92	14.57	19.40
12	R	RECON_1	7.58	5.19	21.08	14.69
		RECON_2	7.76	7.07	17.44	11.63
		RECON_3	4.51	8.76	21.55	15.52
13	R	RECON_1	16.55	18.58	22.53	21.11
		RECON_2	18.76	17.79	14.31	15.33
		RECON_3	15.85	18.50	20.84	23.28
14	R	RECON_1	7.50	10.34	25.61	21.30
		RECON_2	8.90	10.78	11.51	10.44
		RECON_3	9.26	9.52	25.39	20.56
15	R	RECON_1	16.19	12.50	12.93	22.90
		RECON_2	16.97	14.91	10.77	22.51
		RECON_3	16.89	13.04	11.55	20.94
16	R	RECON_1	12.92	9.94	5.54	4.52
		RECON_2	12.98	7.82	7.07	4.07
		RECON_3	9.45	26.71	9.10	24.19

Table 50. Location of center of pressure [mm] at 30 degrees with AM graft fixed and PL graft fixed

Sample Number	Knee	State	Lateral		Medial	
			x location [mm]	y location [mm]	x location [mm]	y location [mm]
5	L	RECON_1	8.65	6.65	17.03	3.53
		RECON_2	11.72	9.71	21.29	5.70
		RECON_3	11.79	10.11	23.88	10.03
6	L	RECON_1	7.76	12.60	22.62	13.85
		RECON_2	7.61	12.17	23.85	11.09
		RECON_3	7.30	12.95	20.29	18.50
7	L	RECON_1	8.49	6.38	12.59	11.07
		RECON_2	10.98	5.09	21.43	17.97
		RECON_3	9.66	6.71	17.49	10.13
8	L	RECON_1	9.54	5.65	11.51	30.69
		RECON_2	4.24	7.02	7.04	24.75
		RECON_3	3.71	6.75	14.84	13.96
9	L	RECON_1	8.90	15.25	16.11	11.69
		RECON_2	16.84	14.89	20.69	22.87
		RECON_3	14.14	13.99	16.43	24.16
10	L	RECON_1	16.12	10.95	4.88	9.08
		RECON_2	11.35	8.38	8.59	15.33
		RECON_3	18.46	13.61	8.38	9.97
11	R	RECON_1	14.13	9.31	19.74	30.18
		RECON_2	14.35	10.01	21.60	25.79
		RECON_3	15.07	9.79	17.21	26.32
12	R	RECON_1	3.28	7.43	20.38	16.38
		RECON_2	12.64	6.46	22.97	18.47
		RECON_3	5.87	7.38	19.66	14.47
13	R	RECON_1	15.39	17.33	20.42	23.13
		RECON_2	17.45	16.50	21.87	22.23
		RECON_3	14.55	17.69	21.03	22.82
14	R	RECON_1	13.97	11.04	24.26	19.75
		RECON_2	9.98	9.76	24.03	18.67
		RECON_3	16.51	11.32	23.99	17.36
15	R	RECON_1	13.16	9.75	15.93	14.83
		RECON_2	16.71	10.73	11.72	19.50
		RECON_3	14.31	10.40	10.76	21.96
16	R	RECON_1	17.34	7.26	7.77	6.31
		RECON_2	13.72	7.28	9.38	5.73
		RECON_3	15.42	6.99	11.63	3.39

BIBLIOGRAPHY

[1] Robert Allarie, Muturi Muriuki, Lars Gilbertson, and Christopher Harner, "Biomechanical Consequences of a Tear of the Posterior Root of the Medial Meniscus Similar to Total Meniscectomy," *The Journal of Bone and Joint Surgery, Incorporated*, pp. 1922-1931, 90: 2008.

[2] Kent N. Bachus, Alyssa L. DeMarco, Kyle T. Judd, Daniel S. Horwitz, and Brodke S. Darrel, "Measuring contact area, force, and pressure for bioengineering applicaitons: Using Fuji Film and TekScan systems," *Medical Engineering & Physics*, vol. 28, pp. 483-488, 2006.

[3] T. E. Baer et al., "Calibrating and Monitoring Sheet Array Pressure Sensors for Intra-Articular Load Measurement," , Banff, Alberta, Canada, 2004.

[4] Asheesh Bedi et al., "Dynamic Contact Mechanics of the Medial Meniscus as a Function of Radial Tear, Repair, and Partial Meniscectomy," *The Journal of Bone and Joint Surgery*, vol. 92, pp. 1398-1408, June 2010.

[5] Mark F. Brady et al., "Effects of Initial Graft Tension on the Tibiofemoral Compressive Forces and Joint Position Follwoing ACL Reconstruction," vol. 25, no. 3, 2007.

[6] Jill M. Brimacombe, Carolyn Anglin, Anthony J. Hodgson, and David R. Wilson, "Validation of Calibration Techniques for Tekscan Pressure Sensors," , Vancouver, BC, Canada, 2005.

[7] Jill M. Brimacombe, David R. Wilson, Anthony J. Hodgson, Karen C.T. Ho, and Carolyn Anglin, "Effect of Calibration Method on Tekscan Sensor Accuracy," *Journal of Biomechanical Engineering*, vol. 131, 2009.

[8] Thomas D. Brown, James M. Rudert, and Nicole M. Grosland, "New Methods for Assessing Cartilage Contact Stress after Articular Fracture," no. 423, 2004.

[9] Anikar Chhabra et al., "Anatomic, Radiographic, Biomechanical, and Kinematic Evaluation of the Anterior Cruciate Ligament and Its Two Functional Bundles," *The Journal of Bone and Joint Surgery*, pp. 2-10, 88-A: 2006.

[10] Jonathan Cluett. Meniscus Tear. [Online]. http://orthopedics.about.com/cs/meniscusinjuries1/a/meniscusrepair.htm

[11] Nimesh Dayal et al., "The Natural History of Anteroposterior Laxity and Its Role in Knee Osteoarthritis Progression," *Arthritis and Rheumatology*, pp. 23-33, 52: 2005.

[12] Richard S. Figliola and Donald E. Beasley, *Theory and Design for Mechanical Measurements*. New York: Wiley, 2006.

[13] Clare K. Fitzpatrick, Mark A. Baldwin, and Paul J. Rullkoetter, "Computationally Efficient Finite Element Evaluation of Natural Patellofemoral Mechanics," vol. 132, no. 121013-1, 2010.

[14] Daniel C. Fitzpatrick, Jason K. Otto, Todd O. McKinley, Lawrence Marsh, and Thomas D. Brown, "Kinematic and Contact Stress Analysis of Posterior Malleolus Fractures of the Ankle," vol. 18, 2004.

[15] Braden C. Fleming et al., "Tibiofemoral Compression Force Differences Using Laxity-and Force-Based Initial Graft Tensioning Techniques in the ACL-Reconstructed Knee," vol. 24, no. 9, 2008.

[16] Benjamin J. Fregly and Gregory W. Sawyer, "Estimation of Discretization Errors in Contact Pressure Measurement," vol. 36, 2002.

[17] T. Fukubayashi and H. Kurosawa, "The contact are and pressure distribution pattern of the knee. A study of normal and osteoarthrotic knee joints," *Acta Orthop Scand*, vol. 51, pp. 871-879, 1980.

[18] Henry Gray, *Anatomy of the Human Body*. Philadelphia: Lea & Febiger, 1918.

[19] Jordan M. Hartmann et al., "Compliance-Dependent Load Allocation Between Sensing versus Non-sensing Portions of a Sheet-Array Contact Stress Sensor," vol. 29, 2009.

[20] Tammy L. Haut Donahue, M. L. Hull, Mark M. Rashid, and Christopher R. Jacobs, "The Sensitivity of Tibiofemoral Contact Pressure to the Size and Shape of the Lateral Medial Menisci," vol. 22, 2004.

[21] Lu Kang, Thomas E. Baer, James M. Rudert, Douglas R. Pedersen, and Thomas D. Brown, "Traveling-Load Calibraton of Grid-Array Transient Contact Stress Sensors," vol. 43, no. 11, 2010.

[22] Stephen Kishner. Knee Joint Anatomy. [Online]. http://emedicine.medscape.com/article/1898986-overview#aw2aab6b3

[23] Stephen J. Lee et al., "Tibiofemoral Contact Mechanics After Serial Medial Meniscectomies in the Human Cadaveric Knee".

[24] Augustus D. Mazzocca et al., "Biomechanical Evaluation of Arthroscopic Rotator Cuff Reparis Over Time," vol. 26, no. 5.

[25] Todd O. McKinley, Yuki Tochigi, M. James Rudert, and Thomas D. Brown, "Instability-Associated Changes in Contact Stress and Contact Stress Rates in Human Cadaveric Ankles," vol. 90, no. 2, 2008.

[26] Yusuke Morimoto, Mario Ferretti, Max Ekdahl, Patrick Smolinski, and Fu Freddie, "Tibiofemoral Joint Contact Area and Pressure After Signle- and Double-Bundle Anterior Cruciate Ligament Reconstruction," *Arthroscopy: The Journal of Arthroscopic and Related Surgery*, pp. 62-69, 25: 2009.

[27] J. K. Otto, T. D. Brown, and J. J. Callaghan, "Static and Dynamic Response of a Multiplexed-array Piezoresistive Contact Sensor," 1999.

[28] James M. Paci et al., "Knee Medial Compartment Contact Pressure Increases with Release of the Type I Anterior Intermeinscal Ligament," vol. 37, no. 7, 2009.

[29] George Papaioannou et al., "A New Method For Pressure Sensor Equillibration and Conditioning," vol. 2, no. 003, 2008.

[30] M. J. Rudert et al., "A New Sensor for Measurement of Dynamic Contact Stress in the Hip," vol. 136, 2014.

[31] Andreas Martin Seitz, Anja Lubomierski, Benedikt Friemert, Anita Ignatius, and Lutz Durselen, "Effect of Partial Meniscectomy at the Medial Posterior Horn on Tibiofemoral Contact Mechanics and Mensical Hoop Strains in Human Knees," vol. 30, 2012.

[32] Tekscan.. [Online]. http://www.tekscan.com/tekscan-technology

[33] Tekscan. [Online]. http://www.tekscan.com/pdf/Sensor-Catalog-Introduction.pdf

[34] Tekscan. [Online]. http://www.tekscan.com/sensor-technology#hardware

[35] *Tekscan: I-Scan & High Speed I-Scan User Manual*. South Boston, 2009.

[36] A. Wilharm, Ch. Hurschler, T. Dermitas, and M. Bohnsack, "Use of Tekscan K-Scan Sensors for Retropatellar Pressure Measurement Avoiding Errors During Implantation and the Effects of Shear Forces on the Measurement Precision," 2013.

[37] D. R. Wilson, Maria V. Apreleva, Mark J. Eichler, and Fraser R. Harrold, "Accuracy and Repeatibility of a Pressure Measurement system in the Patellofemoral Joint," vol. 36, 2003.

[38] Derek C. Wilson, Christina A. Niosi, and Qingan A. Zhu, "Accuracy and repeatibility of a New Method for Measuring Facet Loads in the Lumbar Spine," *Journal of Biomechanics*, pp. 348-353, December 2004.

[39] Changfu Wu, Sabrina Noorani, Vercillo Fabio, and Woo Savio L-Y., "Tension Patterns of The Anteromedial and Posterolateral Grafts in a Double-Bundle Anterior Cruciate Ligament Reconstruction," *Journal of Orthopaedic Research*, pp. 879-884, 27: 2008.

[40] Xiaoyan Zhang, Guotai Jiang, and Savio L.Y. Woo, "A Subject Specific Finite Element Model of the Anterior Cruciate Ligament," in *IEEE EMBS*, Vancouver, British Columbia, Canada, 2008, pp. 891-894.